

Symmetry-related effects of optical metamaterials



Dissertation
zur Erlangung des akademischen Grades
doctor rerum naturalium (Dr. rer. nat.)

vorgelegt dem Rat der Physikalisch-Astronomischen Fakultät
der Friedrich-Schiller-Universität Jena

von Diplom-Physiker Christian Helgert
geboren am 29.06.1980 in Gera

1. Gutachter: Prof. Dr. Thomas Pertsch, Friedrich-Schiller-Universität Jena
2. Gutachter: Prof. Dr. Stefan Linden, Rheinische Friedrich-Wilhelm-Universität Bonn
3. Gutachter: Prof. Dr. Costas Soukoulis, Iowa State University, USA

Tag der Disputation: 28.04.2011

Contents

1	Introduction	3
1.1	Metamaterials and symmetry	3
1.2	Current state of knowledge	4
1.3	Aim and structure of this thesis	6
2	Fundamental concepts and methods	9
2.1	Electromagnetic wave propagation	9
2.2	The concept of optical metamaterials	14
2.3	Effective optical properties of metamaterials	18
2.4	Alternative optical target functions	21
2.5	Computational treatment of metamaterials	26
2.6	Fabrication of nanostructured optical materials	28
2.7	Experimental characterization of optical metamaterials	37
3	High-symmetry metaatoms for polarization insensitivity	41
3.1	Metamaterial designs for a negative refractive index	41
3.2	Single layer nanofabrication technology	44
3.3	Experimental investigation of the Swiss cross	47
4	Three-dimensional chiral metaatoms for huge optical activity	55
4.1	Optical activity from chiral metaatoms	55
4.2	Multilayer nanofabrication technology	58
4.3	Experimental characterization of the loop-wire metamaterial	60
4.4	Optical activity of the loop-wire metamaterial	63
4.5	Visualization of polarization eigenstates	68
5	Low-symmetry metaatoms for asymmetric transmission	71
5.1	Design of low-symmetry metaatoms	71
5.2	Experimental observation of asymmetric transmission	73
6	Disorder and amorphization of high-symmetry metaatoms	77
6.1	Transition from periodic to amorphous arrangements	77

6.2	Plasmonic modes in cut-wire pair metaatoms	80
6.3	Sensitivity of plasmonic modes to positional disorder	81
6.4	Top-down and bottom-up amorphous metamaterials	85
6.5	Symmetry reduction by anisotropic positional disorder	86
7	Summary and outlook	91
8	Zusammenfassung	96
A	Bibliography	I
B	List of Abbreviations	XIX
C	List of symbols and conventions	XX
D	Publications	XXIII
E	Acknowledgements	XXX
	Short Curriculum Vitae	XXXII
	Ehrenwörtliche Erklärung	XXXIII

1 Introduction

1.1 Metamaterials and symmetry

The subject of this thesis “Symmetry-related effects of optical metamaterials” is embedded in the research topic of modern nanooptics. It comes along with the recently evoked great interest in developing artificial materials which are expected to control the flow of electromagnetic waves in unprecedented ways. The fabrication of nano-sized structures has provided us means to create artificial materials that have no natural counterparts. The subclass of these materials which probably attracted the most scientific attention are the so-called metamaterials. These man-made media are composed of their nanostructured elements in the same sense as natural matter consists of atoms. Therefore these structural elements will be termed metaatoms throughout this thesis. Ideally, they are supposed to be considerably smaller than the wavelength of the interacting electromagnetic fields. However, as it will be shown later on, it is challenging to meet this requirement for practical implementations of metamaterials in the optical spectral domain. The metaatoms themselves are made of conventional materials such as noble metals, but their specifically tailored shapes and arrangements promote their constituting ensembles to a superior level of structural organization of matter. Most metaatoms are made of metallo-dielectric composites in order to support resonant surface plasmon polaritonic eigenmodes. Since nanofabrication technology practically facilitates to create metaatoms according to predefined designs, their electromagnetic response can be tailored on purpose. In this thesis we primarily focus on the interaction of such artificial matter with light from the near-infrared and visible part of the electromagnetic spectrum, restricting our attention to so-called optical metamaterials.

Symmetry is of general and fundamental relevance in physics, since almost every microscopic or macroscopic system exhibits symmetric relations between its constituents. More specifically, structured matter has inherent symmetric properties with respect to space, like, e.g., the famous crystallographic lattices. In order to describe a complex system, the investigation of its symmetry properties can yield immediate insight into the underlying physical principles. Furthermore, some very general statements may even be deducible without a deep mathematical analysis.

In this thesis, we will study how the spatial symmetries of nanoscaled, three-dimensional metaatoms, the building-blocks of optical metamaterials, can be utilized to design their op-

tical response. In particular, the reduction of the degree of spatial symmetry of a metaatom, commonly referred to as symmetry breaking, will be shown to be a decisive means to foster extended or even completely novel optical material properties that may be unavailable in nature.

1.2 Current state of knowledge

At a first glance, any attempt to review the state of knowledge about metamaterials appears as a Sisyphean task due to the daily and almost exponentially increasing number of scientific publications dedicated to the topic. However, without making a claim to completeness of information, it is attempted to classify the state of the art in a historical context and to provide an overview of a selection of contributions with high impact on the field. By general opinion, two seminal papers have predominantly stimulated the field of research. Already in 1968, the Russian scientist Victor Veselago hypothetically considered the interaction of a medium with a negative index of refraction and electromagnetic radiation [1], even though there was no adequate experimental platform in sight. However, systematic literature investigations attribute his basic statements to earlier reports from the 1940s [2], which are not commonly recognized and hence rarely quoted by contemporary authors. Further decades had passed until in 1999 Sir John Pendry ignited the concept of modern metamaterials by introducing sub-wavelength metal inclusions in artificial media, whose electric and, most notably, magnetic properties could be modified by design [3]. Retrospectively, this is commonly considered as the starting point for a boost of publications devoted to artificially engineered and resonance supporting electromagnetic media which are unattainable in nature. Following the original material science paradigm of Veselago, the pursuit for a negative refractive index at any range of the electromagnetic spectrum [4]-[6] was initially inseparably connected to the notion of metamaterials itself.

In the course of time, the generalization of the concept paved the way for a much broader context to access other exotic electromagnetic effects like, e.g., artificial magnetism at optical frequencies [7, 8], enhanced optical activity [9, 10], tunable plasmonic Fano resonances [11, 12], directional asymmetry in the transmission of light [13, 14] and the excitation of toroidal dipoles [15]. Hand in hand with the interest in the investigation of such fundamental properties of metamaterials the perspective of their great potential for application devices emerged. Now and after more than a decade of intensive research, it is fair enough to bring some of the overrated expectations of metamaterials into balance. Exemplarily, metamaterial based super- and hyperlenses [16]-[18] still face fundamental physical restrictions. For direct comparison it shall be noted that stimuli from other fields have demonstrated imaging beyond the diffraction limit in a more established [19, 20] or more convenient way [21, 22]

under specific assumptions. The concept of electromagnetic invisibility cloaking, maybe the most advertised and fascinating promise of metamaterials, was experimentally demonstrated for some particular configurations [23]-[28], while its transfer into an application oriented environment is still considered a huge challenge. In turn, metamaterials have addressed other topics where their true potential can unfold. Among them, active terahertz metamaterial devices [29], active optical nanocircuits [30, 31], perfect optical absorbers [32, 33], memory devices [34] and polarizers for circularly polarized light [35] have made remarkable progress. Later on we will further specify the state of knowledge regarding metamaterials that are strongly associated to the respective parts of this thesis. At long sight the prospective of the general transformation of optical space via metamaterials [36]-[38] will nourish the ongoing public interest in the study of artificially structured electromagnetic media.

When the work for this thesis started in 2007, there was still much room for improvement of the conceptual understanding of optical metamaterials. Maybe the most prominent goal was the compensation of their optical losses that arise from damping of the resonant oscillations of electrons and light. Current approaches try to combine metamaterials with active gain media and hold promise to resolve this issue in the near future [39, 40]. On a more fundamental level, a systematic classification of metaatoms that could be used to derive generalized design guidelines to address a specific optical property was still lacking in 2007. In particular, a comprehensive understanding of the connection between the spatial symmetries and the consequential optical properties of a metamaterial was just developing [41]-[44]. In the following, a selection of open questions related to this missing link which will be specifically addressed in this thesis are listed:

- State-of-the-art demonstrations of a negative index of refraction were restricted to a predefined orientation of the respective metamaterials with a low degree of spatial symmetry relative to the polarization state of the incoming illumination. Furthermore, angularly resolved optical measurements had not been reported for this important subclass, apart from one notable exception [45]. This fact exhibited a substantial vacancy in the state of knowledge, since angular resolved spectroscopy can deliver a clear signature of the presence or absence of spatial dispersion in metamaterials.
- Chiral metamaterials aiming at the maximization of optical activity were demonstrated for the optical regime in the form of single- or bi-layered thin films. By contrast, truly single-block, three-dimensional chiral metaatoms operating at optical wavelengths had not been fabricated due to the associated challenges in nanofabrication technology. This state of the art suggested that the true potential of chiral metamaterials with respect to optical activity for visible light was not fully explored yet.
- There had been no investigation of metaatoms with almost no inherent spatial symmetries. Particularly, metaatoms which show a strong symmetry breaking in the direction

of light propagation were not considered for design purposes. As a result and since no natural medium shows this property (though there is no physical objection against it), the effect of asymmetric transmission of linearly polarized light had never been consciously observed.

- The vast majority of contemporary metamaterials was investigated with their constituting metaatoms ordered on a periodic lattice. It remained rather unclear whether their optical properties could be retained when the symmetry of this lattice was broken and the metaatoms were put in an amorphous arrangement. The solution of this issue is of primary importance for the advancement of bottom-up fabricated amorphous metamaterials.

Furthermore, in 2007 only very few research groups possessed the technological means to fabricate high-quality metamaterials consisting of sub-wavelength metaatoms for the optical regime, i.e. nanoscaled structures with feature sizes of less than 100 nm. As a result, the majority of experiments concentrated on metamaterials that were resonantly operated at gigahertz or terahertz frequencies. In the optical range of the spectrum, being considered as the more challenging task, experimental evidence of accordingly down-scaled metamaterials was comparably rare. This was also due to the fact that, as far as metals were involved, they do no longer behave as perfect conductors at high frequencies. In addition, most experiments were performed in a proof-of-principle manner and on small nanostructured areas of the order of $100\ \mu\text{m} \times 100\ \mu\text{m}$, which barely met the requirements of future optical applications.

1.3 Aim and structure of this thesis

Based on the final statements of the previous section, this work deals with the technological realization and experimental evaluation of metamaterials, their characteristic resonant responses at optical wavelengths and the optical properties and effects that can be deduced from the experiments. To fabricate metaatoms with feature sizes smaller than 100 nm, a reliable nanofabrication technology with a reproducible, high-quality throughput had to be established in the first place. This technology should be demonstrated to be transferable to large-scale metamaterial fabrication, aiming at areas of several square millimeters. As a next step, the metamaterials fabricated with this technique were characterized by polarization-resolved far-field spectroscopy in the visible and near-infrared spectral domain. Other experimental methods like angular resolved transmission spectroscopy and white-light Fourier-transform interferometry could be applied as complementary techniques to access additional observables of interest. To validate the measured quantities they were complemented with the results of numerical calculations taking into account the material and geometry properties of the respective metamaterials with an appropriate accuracy.

The choice of metamaterial designs that were actually investigated in this thesis followed the principle of the transition from high-symmetry and geometrically simple to low-symmetry and geometrically complex metaatoms. Their properties will be expressed in terms of an individual “optical target function”. Throughout this thesis this expression will denote a precisely defined optical quantity or property which evidences the functionality of the metamaterial at best. It will be argued that the reduction of the degree of spatial symmetry of metamaterials is the pivotal key to access optical properties that either outperform currently existing natural and artificial optical media or even provide effects that are entirely novel. In any case, the optical target function to support these statements has to be chosen from case to case. Then the individual design of a metaatom that is supposed to fulfill this property is introduced. Consequently, a prototypical metamaterial composed of such metaatoms is fabricated and the optical target function is demonstrated as a proof of principle. The implications of the experimental results are discussed in a comprehensive physical manner and put in the context of the current state of literature.

This thesis is structured as follows: In chapter 2 the theoretical, technological and experimental basics relevant to the description, fabrication and characterization of optical metamaterials are recapitulated. We start with the principles of optics in media exhibiting plasmonic resonances. Using metallic nanoparticles as the key building blocks of engineered artificial media, i.e. as their metaatoms, leads to the concept and design of optical metamaterials. A concise overview of the spatial symmetries of metamaterials and the mathematical means to describe their optical responses is provided. Next, the state of the art of nanos-structure technology with particular emphasis on optical metamaterials is summarized and the experimental tools for their optical characterization are briefly described. In the chapters 3-6 the actual results of this work are presented. The two leitmotifs that guide the reader through the thesis are the metaatoms and their spatial symmetries. Chapters 3-5 deal with experimental examples of metaatoms with a stepwise decreasing degree of symmetry. In detail, a Swiss cross metamaterial (chapter 3), a metamaterial composed of loop-wires (chapter 4) and a metamaterial with the lowest possible symmetry (chapter 5) are presented. For each of them the respective optical target functions the metaatoms were designed for will be discussed. They are, namely, a polarization-independent negative index of refraction (chapter 3), a record-breaking optical activity expressed in terms of the rotation of the polarization azimuth (chapter 4) and the asymmetric transmission of linearly polarized light (chapter 5). Chapter 6 considers the case when the symmetry of certain metaatoms is sustained, while the periodic lattice in which they are usually assembled is destroyed in a controlled way. The influence of positional disorder of metaatoms will lead us to the transition from perfectly periodic to amorphous metamaterials. This study establishes a missing link between bottom-up and top-down fabricated metamaterials. Finally, in the last chapter

the key results of this thesis are summarized and an outlook on further research activities is given.

As already indicated, this thesis contains contributions of technological, experimental and theoretical value which have considerably benefited from the close cooperation between different people. This is emphasized as a positive aspect here, since networking and unbiased intellectual exchange between researchers with different backgrounds may promote the overall scientific output. In the following I will specify the main sources of help and all contributions that were made in cooperation with others. The technological issues associated with optical metamaterial fabrication were addressed by means of the facilities and long-term experience of the technical staff of the Institute of Applied Physics (IAP) at the Friedrich-Schiller-Universität and the Fraunhofer Institute for Applied Optics and Precision Engineering (IOF) in Jena. I was directly responsible for the fabrication of every metamaterial reported in this thesis. After the technological recipes were evaluated and fixed, the support from the technical staff associated to the IAP assured a continuous flow of samples. In addition, external technological support was provided by Birger Steinbach (Institute of Photonic Technology Jena), Kevin Fücksel (IOF Jena) and Maria Oliva (IOF Jena) in terms of gold and magnesia thin films, indium tin oxide thin films and atomic force microscopy measurements, respectively. The subsequent optical characterization of the fabricated samples was mostly performed by means of existing experimental setups at the IAP Jena. The white-light interferometer was developed and operated by Ekaterina Pshenay-Severin and Matthias Falkner. The latter setup was modified in 2010, improving its overall sensitivity, extending the spectral bandwidth and enabling phase measurements of the off-diagonal elements of the Jones matrix. These modifications contribute to the results reported in Sec. 4.3. The measured data presented in Sec. 3.3.3 was recorded with a spectroscopy setup built by Andreas Bielawny and Johannes Üpping from the Institute of Physics at the Martin-Luther-Universität Halle-Wittenberg, where Johannes Üpping and I did the measurements together. The theoretical part of this thesis took great advantage from my close cooperation with the Institute of Condensed Matter Theory and Solid State Optics (IFTO) at the Friedrich-Schiller-Universität Jena. Particularly, many of the metamaterial designs reported here followed suggestions from Christoph Menzel, who simultaneously worked on a thesis focusing on the theoretical aspects of the treatment of optical metamaterials. He also provided Fourier modal method simulations for the metamaterials reported in chapters 3-5. As for the investigation in chapter 6, Christoph Etrich (IFTO Jena) did the finite-difference time-domain simulations. Additionally, the conceptual and practical input of many senior scientists contributed to this work.

2 Fundamental concepts and methods

This chapter gives an introduction to optical metamaterials in terms of the physical, technological and experimental concepts and methods dedicated to their treatment. Despite the clearly experimental nature of this thesis, a concise coverage of the relevant basic mathematical framework is needed. After the introduction of the basic equations of classical electrodynamics, the focus is put on the interaction of electromagnetic fields and matter with particular emphasis on metal nanoparticles. Based on a criterion for plasmonic resonances in such particles, the concept of metamaterials consisting of arrangements of strongly scattering metaatoms with different degrees of symmetry is introduced. After a critical discussion of the description of optical metamaterials in terms of effective optical properties, alternative optical target functions such as asymmetric transmission or chirality-related phenomenological quantities are defined. A brief overview of the two types of numerical methods whose results were compared to the main experimental results of this thesis is given. Then the state of the art of nanofabrication technology will be reviewed with particular emphasis on planar optical metamaterials. The chapter is closed with a concise description of the utilized experimental characterization techniques which were, namely, normal-incidence transmittance and reflectance spectroscopy, angular resolved transmission spectroscopy and measurements with a Jamin-Lebedeff interferometer.

2.1 Electromagnetic wave propagation

2.1.1 Maxwell's and material equations

The propagation of electromagnetic waves is classically described by the macroscopic Maxwell equations:

$$\nabla \cdot \mathbf{D}(\mathbf{r}, t) = \rho_0(\mathbf{r}, t), \quad (2.1)$$

$$\nabla \cdot \mathbf{B}(\mathbf{r}, t) = 0, \quad (2.2)$$

$$\nabla \times \mathbf{E}(\mathbf{r}, t) = -\frac{\partial}{\partial t} \mathbf{B}(\mathbf{r}, t), \quad (2.3)$$

$$\nabla \times \mathbf{H}(\mathbf{r}, t) = \mathbf{j}_0(\mathbf{r}, t) + \frac{\partial}{\partial t} \mathbf{D}(\mathbf{r}, t), \quad (2.4)$$

while the free charge density $\rho_0(\mathbf{r}, t) = \rho_{\text{ext}}(\mathbf{r}, t)$ and the density of the external currents $\mathbf{j}_{\text{ext}}(\mathbf{r}, t)$, being part of the free electric current density $\mathbf{j}_0(\mathbf{r}, t) = \mathbf{j}_{\text{ext}}(\mathbf{r}, t) + \mathbf{j}_{\text{cond}}(\mathbf{r}, t)$ are connected by the continuity equation

$$\nabla \cdot \mathbf{j}_{\text{ext}}(\mathbf{r}, t) + \frac{\partial}{\partial t} \rho_0(\mathbf{r}, t) = 0. \quad (2.5)$$

Inside a medium, the dielectric displacement $\mathbf{D}(\mathbf{r}, t)$ and the magnetic field strength $\mathbf{H}(\mathbf{r}, t)$ differ from the electric field $\mathbf{E}(\mathbf{r}, t)$ and the magnetic induction $\mathbf{B}(\mathbf{r}, t)$ according to

$$\mathbf{D}(\mathbf{r}, t) = \epsilon_0 \mathbf{E}(\mathbf{r}, t) + \mathbf{P}(\mathbf{r}, t), \quad (2.6)$$

$$\mathbf{H}(\mathbf{r}, t) = \frac{1}{\mu_0} [\mathbf{B}(\mathbf{r}, t) - \mathbf{M}(\mathbf{r}, t)]. \quad (2.7)$$

Here, the dielectric polarization $\mathbf{P}(\mathbf{r}, t)$ and the magnetization $\mathbf{M}(\mathbf{r}, t)$ account for the influence of the material. The constants ϵ_0 and μ_0 are the electric permittivity and the magnetic permeability of the vacuum, respectively. The principal task of electrodynamics including optics is to solve Eqs. 2.1-2.7 (together with appropriate boundary conditions) in a self-consistent manner. Since the temporal and spatial evolution of electromagnetic fields in the presence of matter can in general be arbitrarily complex, further simplifications are usually made. Methodically, the angular frequency space ω of each field is accessed by a Fourier transformation with respect to time

$$\mathbf{E}(\mathbf{r}, t) = \int_{-\infty}^{\infty} \bar{\mathbf{E}}(\mathbf{r}, \omega) e^{-i\omega t} d\omega, \quad (2.8)$$

$$\bar{\mathbf{E}}(\mathbf{r}, \omega) = \frac{1}{2\pi} \int_{-\infty}^{\infty} \mathbf{E}(\mathbf{r}, t) e^{i\omega t} dt. \quad (2.9)$$

Assuming a homogeneous, linear and isotropic material, two linear relations of the Fourier-transforms of the electric field $\mathbf{E}(\mathbf{r}, t)$ and the magnetic field $\mathbf{H}(\mathbf{r}, t)$ can be derived

$$\bar{\mathbf{P}}(\mathbf{r}, \omega) = \epsilon_0 \chi_{\text{el}}(\omega) \bar{\mathbf{E}}(\mathbf{r}, \omega), \quad (2.10)$$

$$\bar{\mathbf{M}}(\mathbf{r}, \omega) = \chi_{\text{mag}}(\omega) \bar{\mathbf{H}}(\mathbf{r}, \omega), \quad (2.11)$$

where $\chi_{\text{el}}(\omega)$ and $\chi_{\text{mag}}(\omega)$ are the frequency-dependent electric and magnetic susceptibilities, respectively. The Eqs. 2.10 and 2.11 are the so-called linear material equations. Alternatively,

the material response can be described by the electric permittivity $\epsilon(\omega)$ and the magnetic permeability $\mu(\omega)$ of the medium¹ :

$$\bar{\mathbf{D}}(\mathbf{r}, \omega) = \epsilon_0[1 + \chi_{\text{el}(\omega)}]\bar{\mathbf{E}}(\mathbf{r}, \omega) = \epsilon_0\epsilon(\omega)\bar{\mathbf{E}}(\mathbf{r}, \omega), \quad (2.12)$$

$$\bar{\mathbf{B}}(\mathbf{r}, \omega) = \mu_0[1 + \chi_{\text{mag}(\omega)}]\bar{\mathbf{H}}(\mathbf{r}, \omega) = \mu_0\mu(\omega)\bar{\mathbf{H}}(\mathbf{r}, \omega). \quad (2.13)$$

More generally, Eqs. 2.10-2.13 (and other, more involved variations of them) are referred to as the constitutive relations of a medium. One particular class of solutions for the electric field $\mathbf{E}(\mathbf{r}, t)$ (and for $\mathbf{B}(\mathbf{r}, t)$ accordingly) are plane waves in time and space described by

$$\mathbf{E}(\mathbf{r}, t) = \mathbf{E}_0 e^{i(\mathbf{k}(n, \omega)\mathbf{r} - \omega t)}, \quad (2.14)$$

with the wave vector $\mathbf{k}(n, \omega)$, which is connected to the angular frequency ω by the speed of light in vacuum $c_0 = 1/\sqrt{\epsilon_0\mu_0}$ via

$$\mathbf{k}^2(n, \omega) = k_x^2 + k_y^2 + k_z^2 = \frac{\omega^2}{c_0^2}n^2(\omega). \quad (2.15)$$

Equation 2.15 is the so-called dispersion relation and is considered in more detail with focus on metamaterials in Sec. 2.4.1. Note that the wave vector $\mathbf{k}(n, \omega)$ is of fundamental importance, since it carries the full information about the principal propagation properties of the optical wave field through the medium. The refractive index $n(\omega)$ and the wave impedance $Z(\omega)$ of the medium are related to $\epsilon(\omega)$ and $\mu(\omega)$ as

$$n^2(\omega) = \epsilon(\omega)\mu(\omega), \quad (2.16)$$

$$Z^2(\omega) = \epsilon(\omega)/\mu(\omega). \quad (2.17)$$

These two quantities should be kept in mind as the natural counterparts of the effective refractive index n_{eff} and the effective wave impedance Z_{eff} which will be introduced in Sec. 2.3.1. In optics and throughout this thesis, the vacuum wavelength $\lambda = 2\pi c_0/\omega$ is commonly used to characterize a spectral range instead of the angular frequency ω . Next we will discuss the permittivity functions of bulk metals and the resonance conditions for small particles because they play an important role for the design of metamaterials.

¹In the more general anisotropic case, $\chi_{\text{el}(\omega)}$, $\chi_{\text{mag}(\omega)}$ and likewise $\epsilon(\omega)$, $\mu(\omega)$ become tensors.

2.1.2 Optical properties of metals

The material properties needed for the electrodynamic calculations are provided by solid state theory. Among others, the Drude-Sommerfeld model is a common approach to describe the response of free electrons in a metal to an external electromagnetic field. Assuming independent and free electrons in the partially filled conduction band with a common relaxation time, the optical properties of metals (in this thesis, gold is of primary relevance) are successfully described in many cases². The model considers a motion of a free electron with a charge e and an effective mass m_e^* under the influence of an external electric field³, where a damping constant γ_0 accounts for scattering events with different collision centers (lattice ions, other electrons, phonons, lattice defects, etc.)⁴. The resulting differential equation (for details, see e.g. [46]) describes a quasi-free electron as a damped harmonic oscillator without feedback and without resonance frequencies for $\omega > 0$. Introducing the electron density n_e , its solution can be summarized in form of a (Drude) permittivity function

$$\epsilon_{\text{Drude}}(\omega) = 1 - \frac{\omega_{\text{pl}}}{\omega^2 + i\gamma_0\omega}, \quad (2.18)$$

with the (Drude) plasma frequency $\omega_{\text{pl}} = \sqrt{n_e e^2 / \epsilon_0 m_e^*}$ as a characteristic material constant [$\epsilon_{\text{Drude}}(\omega_{\text{pl}}) = 0$]. Above its plasma frequency, a metal behaves like an ordinary dielectric. $\epsilon_{\text{Drude}}(\omega)$ describes most optical properties of metals surprisingly well, despite of the drastic simplifications of the Drude-Sommerfeld model. In practice, ω_{pl} and γ_0 are used as fit parameters to match empirical bulk values, e.g. for the noble metals gold, silver and copper [47].

It can be deduced that electromagnetically excited quasi-free electrons perform a collective motion relative to the fixed crystal lattice in a metal. This collective and coherent excitation of a large number of electrons is called a plasmon⁵. In the most general case the term plasmon describes a collective oscillation of the electron gas relative to the lattice. In particular, if spatial boundary conditions are imposed on the system as it is the case for metallic nanoparticles, the electromagnetic modes at these boundaries are of combined plasmonic and polaritonic nature.

2.1.3 Plasmonic resonances in metallic nanoparticles

The interaction of a single nanoparticle with the electromagnetic field can be analyzed using the quasi-static approximation method provided that the particle is much smaller than the

²At optical frequencies, additional terms are added to $\epsilon(\omega)$, accounting for interband transitions.

³In general, the effective mass m_e^* is different from the free-electron mass m_e , since only electrons near the Fermi level can contribute to the motion [46].

⁴ γ_0 is the inverse of the so-called electron relaxation time.

⁵In quantum mechanical systems, the energy quanta of plasmonic oscillations are called plasmons.

wavelength of light in the surrounding medium. In this case, the phase and amplitude of the harmonically oscillating electromagnetic field are almost constant over the particle volume, so that one can calculate the spatial field distribution by assuming the simplified problem of a particle in an electrostatic field. The harmonic time dependence can then be added to the solution once the field distributions are known. This lowest-order approximation of the full scattering problem describes the optical properties of nanoparticles adequately for many purposes, given that the ratio between the wavelength and the particle dimensions is sufficiently large. It should be mentioned that for very small particles (diameters smaller than roughly 10 nm) intrinsic effects like changes in the volume and surface properties dramatically change the optical response [46]. In that case, size-dependent permittivity functions are more suitable [48].

Concerning a small, sub-wavelength, metallic nanoparticle in an oscillating electromagnetic field, the boundaries of the particle provide an effective confinement of the electrons. In analogy to a cavity of finite length, the oscillation evokes an electronic resonance, leading to field amplification in the optical near-field of the particle. The resonance is called a localized surface plasmon polariton (in short and throughout this thesis: plasmonic resonance). Contrary to propagating surface plasmon polaritons (SPPs) on extended metal-dielectric interfaces, plasmonic resonances can be directly excited by light illumination from free space. Already in 1908 Gustav Mie developed an analytical theory for calculating the polarizability of spherical particles [49]. Following a modern textbook [50] and slightly more generally, we consider here an ellipsoidal particle with the semiaxes d_x , d_y , d_z and with an electric permittivity $\epsilon(\omega)$. It shall be placed in a surrounding dielectric medium with a permittivity constant of ϵ_m . The main axes are aligned with respect to the coordinate system. In this case the complex polarizability $\hat{\alpha}(\omega)$ is a diagonal tensor, which relates the macroscopic polarization $\bar{\mathbf{P}}(\mathbf{r}, \omega)$ to an external electric field $\bar{\mathbf{E}}(\mathbf{r}, \omega)$ via $\bar{\mathbf{P}}(\mathbf{r}, \omega) = \epsilon_0 \epsilon_m \hat{\alpha}(\omega) \bar{\mathbf{E}}(\mathbf{r}, \omega)$. For the principal axes $i = x, y, z$, the respective diagonal elements of the polarizability tensor $\alpha_{ii}(\omega)$ can be directly calculated as

$$\alpha_{ii}(\omega) = 4\pi d_x d_y d_z \frac{\epsilon(\omega) - \epsilon_m}{\epsilon_m + L_i [\epsilon(\omega) - \epsilon_m]}, \quad (2.19)$$

where L_i denotes a geometrical depolarization factor which depends on the particle shape and particle aspect ratio ($0 \leq L_i \leq 1$) [50]. Resonant enhancement of the polarizability $\alpha_{ii}(\omega)$ is obtained under the condition that $|\epsilon_m + [\epsilon(\omega) - \epsilon_m] L_i|$ is minimal. Assuming a small or slowly varying imaginary part of $\epsilon(\omega)$ this happens for

$$\Re[\epsilon(\omega = \omega_{\text{res}})] = \epsilon_m - \frac{\epsilon_m}{L_i}. \quad (2.20)$$

From Eqs. 2.19 and 2.20 immediate conclusions with respect to all parameters that affect

the nature of plasmonic resonances can be drawn:

- **Material:** Since $0 \leq L_i \leq 1$, Eq. 2.20 can be fulfilled only for media with $\Re[\epsilon(\omega)] < 0$. In the optical spectral range⁶, this holds for gold, silver, copper and aluminum. In turn, the smaller $\Im[\epsilon(\omega = \omega_{\text{res}})]$, the higher and sharper is the resonance curve.
- **Surrounding dielectric:** The resonance wavelength is red-shifted, if ϵ_m is increased with respect to vacuum.
- **Geometry:** Controlling L_i allows to tune the resonance frequency of the plasmonic resonance. An increase of L_i (higher aspect ratio) leads to a red-shift of the resonance wavelength.
- **Input polarization:** If the particle is held at a fixed position in space, changing the polarization of the incoming field can access another principal axis of the particle and thus excite another plasmonic resonance. Mathematically, this corresponds to a different depolarization factor L_i .

To summarize this section, the possibility to excite localized surface plasmon polaritons in metallic nanoparticles enables a broadly tunable optical response to an external electromagnetic field. Unfortunately, the analytical derivation of the resonance condition is restricted to few geometrical shapes (spheres, ellipsoids, spherical shells [46]). Nevertheless, the principal conclusions and some physical design guidelines can be transferred to particles with a more complex shape as well. If we were able to tailor complexly shaped metallic inclusions at will, purposefully targeted electromagnetic properties and devices with completely novel optical functionalities that are unavailable in nature could be accessed. This thought is the key to the concept of modern optical metamaterials. Its practical implementation can be achieved by the state-of-the-art nanostructure technology.

2.2 The concept of optical metamaterials

Artificial electromagnetic metamaterials are loosely defined as man-made media in which the propagation of electromagnetic radiation is significantly governed by their artificially structured geometry rather than by the natural materials they are composed of. The invention of the word is most probably attributed to Rodger Walser [51]. If the electromagnetic waves interacting with such media stem from the optical or near-infrared spectral domain, we will use the term optical metamaterials. The concept implies that one wishes to access and to control the principal propagation properties of an optical wave field. Thus, the knowledge of

⁶The optical spectral range is usually equated with visible light, i.e. $\lambda=400\dots700$ nm. In the context of this thesis, we will expand this definition of the optical spectral range by also including near-infrared wavelengths up to $\lambda=1800$ nm.

the control mechanisms allows the realization of artificial matter with potentially novel optical functionalities. Moreover, by means of metamaterials, the properties of light propagation can be extended into domains where nature does not provide any equivalent. Therefore they represent a material class that permits the control of light propagation beyond that in natural media⁷. Accordingly, although still at the stage of fundamental research from many perspectives, the concept of optical metamaterials has elicited a boost in the field of modern optics due to its promise to permit groundbreaking applications such as sub-wavelength imaging [16], cloaking devices [52] and transformation optics [36, 53].

2.2.1 Design of metaatoms

On a microscopic level, natural solids and crystals show an atomic lattice. When visible light passes through such media, the light wavelength is thousands of times larger than this lattice. Hence the atomic details are not resolved by the light and lose importance in describing how the lattice interacts with it. Drawing an analogy, metamaterials are obtained by assembling sub-wavelength unit cells. Referring to atoms in a crystal, these unit cells are called metaatoms⁸. This conceptual approach was first introduced in a clear form to distinguish between “electric” and “magnetic” metaatoms in 1999 [3]. In order to exhibit truly sub-wavelength unit cells for the optical spectral range, the metaatoms must be engineered on the nanoscale. Their arrangement can be both periodic or aperiodic, as will be detailed in chapter 6. Following the above definition of optical metamaterials, it is implied that their macroscopic properties are dominated by the specific geometric shapes of their metaatoms rather than by the natural constituents they consist of.

Accordingly the question arises which natural materials should be the appropriate basis to form such artificial metaatoms. As it was shown in Sec. 2.1.3, metallic nanoparticles offer a strong scattering mechanism of electromagnetic radiation in general and a conveniently tunable resonance condition for localized surface plasmon polaritons in particular. Accordingly, the utilization of metallic nanoparticles with artificially engineered shapes as metaatoms is an ideal platform to tailor the optical response of a metamaterial. It should be emphasized that finite metallic structures can differ dramatically in their optical response from bulk metals. To be precise, only when driven in resonance a plasmonic metamaterial provides dispersive regimes beyond those achievable by a mere averaging of its constituents. It is mentioned for completeness that (few) alternative concepts of non-metallic metamaterials are based on Mie-resonances in high index dielectric particles [54]-[56].

⁷The word “meta” translates as “beyond” in Greek, and in this sense the name “metamaterials” means “beyond conventional materials”.

⁸Although some authors may alternatively use the term “metamolecules” for some elements described in this thesis, we will consistently refer to them as metaatoms for convenience.

The possibility to really design metaatoms and metamaterials has considerably changed the notion of the working strategy in this field during the past decade. The design of metamaterials is recognized as a “creative act” on a physical and material scientific platform. An exemplary strategy of optical metamaterial research in the year 2011 can be formulated as follows:

1. An optical target function or, in a broader sense, an innovative physical idea to be demonstrated, should be identified.
2. A design of a metaatom that fulfills this optical target function must be extracted. The necessary design guidelines for this metaatom should be based on a profound understanding of the scattering properties of the individual metaatom.
3. It must be assured that the optical response of a single metaatom is not hampered when put in a huge ensemble that will deliver a collective response.
4. The potential limitations of current nanotechnology may pose additional side conditions for the practical realization and must be taken into account.
5. At last and in the context of this thesis, an experimental proof is needed to verify the design-related predictions. If necessary, the theoretical predictions have to be refined.

Following this reasoning, numerous plasmonic metaatoms like, e.g., split-ring resonators [57], cut-wire pairs [58, 59], fishnet unit-cells [60] and Swiss crosses (see chapter 3) have been designed and thoroughly investigated.

2.2.2 Symmetry classification and symmetry breaking of metaatoms

Since any real metaatom can be considered as a nanoscale, yet finite three-dimensional object, it is straightforward to explore its spatial symmetries. Such an investigation can help to gain immediate preliminary insight into the physics of any structure, anticipating its very general properties even without a deep theoretical or numerical analysis [41, 43]. A spatial symmetry is present, if an object can be imaged onto itself either upon a mirroring operation with respect to a plane or upon a rotation with respect to an axis. The image of the object is then indistinguishable from its original. Commonly, spatial symmetries are classified into mirror, rotational and translational symmetries. In accordance to literature [61], we will denote a mirror (or inversion) symmetry with respect to the ij -plane with M_{ij} and an n -fold rotational symmetry with respect to the i -axis with $C_{n,i}$ ($i, j = x, y, z$). Optical metaatoms are usually repetitively assembled on a periodic lattice in one or two directions in order to form a metamaterial, which can be regarded to have additional translation symmetries in one or two dimensions.

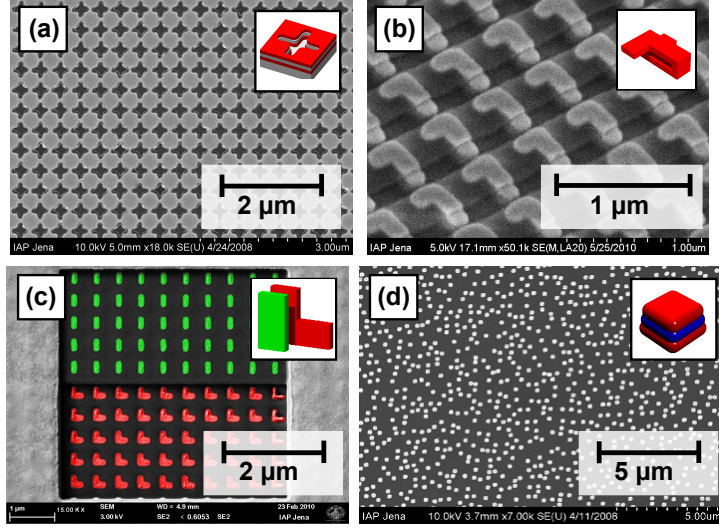


Fig. 2.1: Scanning electron micrographs of optical metamaterials presented in this thesis with a decreasing degree of symmetry from the left to the right. The insets show schematics of the respective metaatoms in an ideal case, i.e. if no symmetry violations due to fabrication imperfections were present. a) Swiss cross metamaterial with $C_{4,z}$ symmetry (see chapter 3). There are additional M_{xy} , M_{xz} and M_{yz} symmetries if the substrate was neglected and the structure was ideal. b) Loop-wire particle with $C_{2,y}$ symmetry (see chapter 4). c) Metamaterial consisting of metaatoms without spatial symmetries (see chapter 5). d) Cut-wire pair metamaterial with $C_{4,z}$ symmetry if the metaatoms were arranged on a periodic lattice (see chapter 6). There are additional M_{xy} , M_{xz} and M_{yz} symmetries if the substrate was neglected and the structure was ideal. Complete and deterministic symmetry breaking occurs with respect to the lattice period.

Common thin film metamaterials composed of “planar” metaatoms are essentially two-dimensional with respect to the direction of light propagation. If a structural variation along this axis was enforced, it can have a dramatic impact on their optical response, as it will be shown in the chapters 4 and 5. This highlighted axis is parallel to the direction of light and will be denoted as the z -axis throughout this thesis. On the other hand, the x - and y -axes are always meant to be parallel to the plane of the main extension of planar metamaterials and therefore parallel to their supporting substrates. We will explicitly include mirroring operations with respect to the xy -plane and consider truly three-dimensional metaatoms without loss of generality. Furthermore, it is important to note that all symmetry operations applied to a metaatom have to be consistent with the symmetry of the lattice and its dielectric surrounding. In fact, it will be shown in chapter 6 how the overall symmetry in a metamaterial can be broken by a positional disarrangement of the lattice while leaving the symmetry of the respective metaatoms untouched.

Recently, a symmetry classification scheme of metamaterials relying on very basic physical assumptions and the classical Jones calculus was established [44]. On the basis of pure symmetry considerations, it was demonstrated that all periodic metamaterials may be divided into five different classes only. Each of these classes is characterized by unique relations that

connect the entries of the Jones matrix and hence sustain specific polarization phenomena directly linked to the symmetry of the respective structure. Symmetry breaking, or with other words, the reduction of the degree of symmetry of a particular metaatom, turned out to be a key feature to access extended or even novel material functionalities. Some selected examples from recent literature are the excitability of additional resonant modes that are otherwise optically inactive [62, 63], the enhancement of an existing magneto-optical response [64], the emergence of tunable Fano resonances in plasmonic nanostructures [12, 65] and asymmetric transmission of light through optical metamaterials (see chapter 5). The notion of metamaterial design in terms of symmetry breaking has fostered the design of metaatoms during the past four years and should also be understood as the leitmotif of this thesis (Fig. 2.1).

2.3 Effective optical properties of metamaterials

According to Sec. 2.2.1, metaatoms are considered to be man-made counterparts of classical atoms in, e.g., usual crystals. In natural media, one can average over the atomic scale, conceptually replacing the otherwise inhomogeneous medium by a homogeneous material characterized by few macroscopic electromagnetic parameters like $\epsilon(\omega)$ and $\mu(\omega)$ (see Eqs. 2.12 and 2.13). As a first approximation, this reasoning can be straightforwardly applied to metamaterials. Under the assumption that electromagnetic waves do not resolve the fine structure of a metamaterial but experience an effective homogeneous material, the interaction can be conveniently described by introducing just two macroscopic properties as optical target functions: an effective electric permittivity $\epsilon_{\text{eff}}(\omega)$ and an effective magnetic permeability $\mu_{\text{eff}}(\omega)$. This assumption will be critically analyzed in Sec. 2.3.2. In case it was valid, it simplifies the theoretical treatment of metamaterials because all details of spatial inhomogeneities on the nanoscale could be neglected in favor of the functions $\epsilon_{\text{eff}}(\omega)$ and $\mu_{\text{eff}}(\omega)$ only. We prefer to reflect the fundamental differences that distinguish $\epsilon(\omega)$ and $\mu(\omega)$ of natural media from their effective counterparts in metamaterials by a careful choice of terminology throughout this thesis: $\epsilon(\omega)$ and $\mu(\omega)$ are denoted as true material parameters while $\epsilon_{\text{eff}}(\omega)$ and $\mu_{\text{eff}}(\omega)$ will be referred to as effective optical properties. We note that this distinction is based to some extent on our personal preference since the terminology is not coherently used in the current literature.

2.3.1 Retrieval procedure for effective optical properties

The mathematical framework to obtain $\epsilon_{\text{eff}}(\omega)$ and $\mu_{\text{eff}}(\omega)$ in practice was proposed by Smith et al. [66]. In the following, we consider a single frequency ω and therefore omit all explicit frequency dependencies for brevity. The principal idea is to replace the metamaterial by an

isotropic homogeneous slab with thickness s , and to calculate its effective optical properties from the measured or simulated complex transmission and reflection coefficients T and R for normal incidence by using the theoretical formulas for the slab. In a vacuum surrounding they are correlated to the index of refraction n_{eff} and to the wave impedance Z_{eff} of the slab via

$$\frac{1}{T} = \cos(n_{\text{eff}}ks) - \frac{i}{2}\left[Z_{\text{eff}} + \frac{1}{Z_{\text{eff}}}\sin(n_{\text{eff}}ks)\right], \quad (2.21)$$

$$\frac{R}{T} = -\frac{i}{2}\left(Z_{\text{eff}} - \frac{1}{Z_{\text{eff}}}\right)\sin(n_{\text{eff}}ks), \quad (2.22)$$

where $k = |\mathbf{k}|$ is the modulus of the wave vector from Eq. 2.15. Both equations can be inverted to calculate n_{eff} and Z_{eff} from T and R . This inversion reads as

$$Z_{\text{eff}} = \pm \sqrt{\frac{(1+R)^2 - T^2}{(1-R)^2 - T^2}}, \quad (2.23)$$

$$\cos(n_{\text{eff}}ks) = \frac{1}{2T}(1 + T^2 - R^2). \quad (2.24)$$

Although Eqs. 2.23 and 2.24 have a relatively simple form, both are complex functions with multiple branches, which may lead to ambiguities in determining the final expressions that can only be resolved if additional information is known: In a passive medium, the real part of the effective wave impedance $\Re(Z_{\text{eff}}) > 0$, which fixes the sign in Eq. 2.23. For the same reason, requiring $\Im(n_{\text{eff}}) < 0$ determines the signs of both real and imaginary part of n_{eff} . Furthermore, since the cosine function has multiple branches, there are still multiple solutions for the real part of n_{eff} . A common way to choose the correct branch is to calculate all solutions of n_{eff} in a non-dispersive regime far below any resonance, where n_{eff} must be close to one, and calculate it successively by assuming the continuity of n_{eff} as the frequency ω increases. At last, the target functions ϵ_{eff} and μ_{eff} can be obtained by $\epsilon_{\text{eff}} = n_{\text{eff}}/Z_{\text{eff}}$ and $\mu_{\text{eff}} = n_{\text{eff}}Z_{\text{eff}}$.

This retrieval procedure works under the assumption that the metamaterial can be viewed as a homogeneous medium. It is implied that the metaatoms of the metamaterial are symmetric along the light propagating direction. However, real metamaterials are mostly prepared on a substrate, which leads to non-identical reflections from both sides of the fictitious slab. In that case, a modification of the standard retrieval procedure yields physically reasonable values for the retrieved electromagnetic parameters [67]. Many extensions and variations of the general retrieval algorithm are existent [68]-[71], among them a method applicable to the situation of obliquely incident waves on a metamaterial [72].

2.3.2 Limits of validity for optical metamaterials

The embodiment of the electromagnetic response of metamaterials in effective optical properties like $\epsilon_{\text{eff}}(\omega)$ and $\mu_{\text{eff}}(\omega)$ is only approximate, as spatial dispersion is always present to some degree in metamaterials. Spatial dispersion phenomena denote a wave vector dependence of the effective properties [73], i.e. $\epsilon_{\text{eff}}=\epsilon_{\text{eff}}(\omega, \mathbf{k})$ and $\mu_{\text{eff}}=\mu_{\text{eff}}(\omega, \mathbf{k})$. They can be observed in electromagnetic media if the characteristic sizes of its constituents (the metaatoms in the present case) are comparable to the wavelength of the interacting radiation [74]. Regrettably, this is the case for the majority of today's optical metamaterials which are intrinsically mesoscopic. Typically, the vacuum wavelength is only a few times larger than their constituting metaatoms. If the particular optical response of such metaatoms relies on resonant plasmonic eigenmodes as described in Sec. 2.1.3, the induced currents depend nonlocally on the electric field. In frequency space, this fact transforms into a spatially dispersive conductivity. At this point, the distinction between weak and strong spatial dispersion is usually applied [74]. Only in the case of weak spatial dispersion an averaging procedure aiming at the introduction of effective optical properties in the sense above is meaningful. In a recent work, Menzel et al. established a validity criterion for the regime of weak spatial dispersion [75]. It was shown that this criterion is rarely met by contemporary optical metamaterials, in particular in the spectral regions close to the targeted plasmonic resonances. These findings clearly indicated that the mesoscopic nature of contemporary optical metamaterials prohibits the meaningful introduction of effective material properties in a conventional sense. Though the retrieval procedure from Sec. 2.3.1 is always mathematically applicable, the physical meaning of its results must be considered with care.

As a resort, the retrieved properties can still be regarded as partially valuable quantities if not only the metamaterial but also its orientation to the incoming light wave and the respective polarization state are taken into account [76]. In that case and according to Rockstuhl et al. [77], the effective optical properties of mesoscopic metamaterials can be understood as wave parameters that accurately describe the medium only in synthesis with a precisely specified illumination scheme. Practically, an experimentally accessible indication for the regime of strong spatial dispersion is the check of the angular dependence the optical response. Exemplarily, for the metamaterial reported in chapter 3 the effects of spatial dispersion are discussed in Sec. 3.3.3.

It is emphasized that the rating of the limited validity of effective properties of optical metamaterials is subject to an ongoing debate in the research community, where such properties have been calculated regularly for years. However, numerous experimental observations confirming strong spatial dispersion in optical metamaterials [78]-[84] have suggested that the concept of effective optical properties may not accurately reflect the complicated constitutive relations (see Eqs. 2.10-2.13) of mesoscopic and complexly shaped nanostructures. Now in

2011, the assignment of effective optical properties is utilized with increasing reluctance [85]-[92]. This initiated paradigm shift indicates that alternative optical target functions will be essential for the future of this field of research. In a chronological context and within this thesis, effective optical properties were attributed to the metamaterials presented in chapters 3 and 6. For completeness they will be shown and discussed, implying that they are understood here as wave parameters in the sense above. Effective optical properties have proven to be a convenient means to describe the light-matter interaction in a simplified way in order to gain preliminary insight into the underlying physics. Nevertheless, the limits of their validity must always be carefully borne in mind.

2.4 Alternative optical target functions

Despite the fact that the assignment of effective material properties is doubtful in some cases, the attractiveness of the concept of optical metamaterials itself is not diminished. On the contrary, the emerging challenge is to define physically meaningful optical target functions that can be optimized by appropriate metamaterial designs. Recalling our definition from Sec. 1.3, an optical target function is an individually chosen quantity that gives clear physical evidence of the aspired optical functionality of a particular metamaterial. In the following, a few examples that may constitute potential guidelines for future metamaterial research are briefly introduced.

2.4.1 The dispersion relation

The characterization of the properties of artificial bulk materials in terms of their dispersion relation is a well-established technique, e.g., for photonic crystals [93, 94]. For such systems, the so-called Floquet-Bloch analysis is applied to obtain a complete set of eigen-solutions (Floquet-Bloch modes) of periodic structures. Therein, the frequency-dependent wave vector $\mathbf{k}(n, \omega)$ (see Eq. 2.15) is decomposed into its transverse (k_x, k_y) and longitudinal (k_z) components, where the latter is frequently termed propagation constant. The approach predicts that the propagation constants k_z of the eigenmodes form a band structure versus the transverse wave vectors k_x and k_y , where the individual bands are separated by gaps in which propagating modes do not exist. Assuming a linear superposition of the optical fields, their evolution can be described by a decomposition into these eigenmodes. The variation of the propagation constant with respect to the optical frequency ω governs dispersive effects and is accordingly called the dispersion relation. As an alternative notation to Eq. 2.15 it is often written as

$$\omega = \omega(k_x, k_y, k_z), \quad (2.25)$$

relating the frequency to the wave vector of the eigenmodes⁹. Equation 2.25 describes the interaction of any optical medium with light completely and without approximations, given that the eigenmodes of the system are known. Therefore, if this quantity is at hand, an optical system can be evaluated thoroughly and bare of physical misinterpretations, like they may be associated with the assignment of effective properties to optical metamaterials. On the down-side, obtaining the full dispersion relation is normally linked to huge computational and experimental efforts as they were established for the treatment of photonic crystals. However, the transfer of this concept to mesoscopic metamaterials leads to the conclusion that the dispersion relation itself could be an ideal optical target function which has to be optimized with respect to free geometry parameters and spatial symmetries of metamaterials [42, 85]. More specifically, if evaluated at a fixed frequency ω_0 it yields the so-called isofrequency contours $k_z = k_z(k_x, k_y, \omega_0)$. Shaping these contours practically enables the design of, e.g., optically isotropic [95, 96] or non-diffracting metamaterials [85] for limited frequency bands. For comparison, the exploration of effective optical properties on its own has failed to provide design guidelines for such sophisticated optical functions so far.

2.4.2 Transmission coefficients and Jones calculus

If both the effective optical properties and the dispersion relation are not suitable for a specific metamaterial characterization (the further may not be physically meaningful and the latter may be too complex to obtain), the optical response itself is the primary target function to address. This optical response is encoded in the response functions, namely the complex transmission and reflection coefficients T and R , for a given input illumination. Ideally, those quantities are directly accessible by an experiment such that no further computational effort is required. This argumentation holds particularly in the case when the symmetry of the involved metaatoms is very low and the associated constitutive relation of the metamaterial gets too complex [74, 97].

To prove that a metamaterial shows a desired optical response, further phenomenological quantities may be defined. In contrast to effective optical properties, they must be directly deducible from T and R without further physical assumptions¹⁰. Here, focus is put exclu-

⁹It is noteworthy that if the dispersion relation is given, a refractive index can be derived straightforwardly as $n = c/\omega\sqrt{k_x^2 + k_y^2 + k_z^2}$, assuming that the light propagation inside the structure is governed by the properties of a single Floquet-Bloch mode only.

¹⁰In fact, in the following the medium is assumed to be linear, reciprocal and non-depolarizing. However, these assumptions do not exhibit considerable constraints but are rather needed to correctly exclude very exotic material classes that are of no importance for this work.

sively on quantities that depend on the transmission coefficients only. In accordance with Eq. 2.14, we suppose that a medium is illuminated by a plane wave propagating in the positive z -direction

$$\mathbf{E}_{\text{inc}}(\mathbf{r}, t) = \begin{pmatrix} E_x \\ E_y \end{pmatrix} e^{i(k_z z - \omega t)}, \quad (2.26)$$

where E_x and E_y are the complex amplitudes in the linear (Cartesian) polarization base. Accordingly, the field transmitted through the material is characterized by the complex amplitudes T_x and T_y via

$$\mathbf{E}_{\text{trans}}(\mathbf{r}, t) = \begin{pmatrix} T_x \\ T_y \end{pmatrix} e^{i(k_z z - \omega t)}. \quad (2.27)$$

The transmission properties of coherent light through a linear, reciprocal and non-depolarizing optical medium are completely determined on the basis of the classical Jones calculus [98]. Generally, the so-called Jones matrix \hat{T} contains 2×2 complex and dispersive quantities T_{ij} which connect the incident field (E_x, E_y) with the transmitted field (T_x, T_y) . The entries T_{ij} represent the complex amplitudes of the zeroth diffraction order in transmission

$$\begin{pmatrix} T_x \\ T_y \end{pmatrix} = \begin{pmatrix} T_{xx} & T_{xy} \\ T_{yx} & T_{yy} \end{pmatrix} \begin{pmatrix} E_x \\ E_y \end{pmatrix} = \hat{T}_{\text{lin}}^{\text{f}} \begin{pmatrix} E_x \\ E_y \end{pmatrix}. \quad (2.28)$$

The superscript f and the subscript lin indicate propagation in forward direction (corresponding to the z -direction throughout this thesis) and a linear (Cartesian) base with base vectors parallel to the coordinate axes, i.e. decomposing the field into x - and y -polarized light. For completeness it is mentioned that the classical Jones calculus inherently neglects spatial dispersion, since the matrix $\hat{T}_{\text{lin}}^{\text{f}}$ is defined for one specific illumination direction only. Its entries T_{ij} would generally have to be modified if the light incidence deviated from this preferential optical axis.

2.4.3 Polarization conversion dichroism and asymmetric transmission

Now we will consider the effect that the fraction of the power transmitted through a device differs for illumination with a fixed polarization from opposite sides. This effect is called asymmetric transmission and is experimentally accessed with the optical metamaterial reported in chapter 5. To elaborate an analytical definition, the Jones matrices for forward and backward propagation through the medium must be distinguished. In the following we assume our medium to be reciprocal, explicitly excluding Faraday magneto-optic me-

dia [99]. Applying the reciprocity theorem yields the Jones matrix \hat{T}^b for propagation in $-z$ or backward direction simply by sign reversal and interchange of the off-diagonal elements

$$\hat{T}_{\text{lin}}^b = \begin{pmatrix} T_{xx} & -T_{yx} \\ -T_{xy} & T_{yy} \end{pmatrix}, \quad (2.29)$$

characterizing the transmission in a fixed coordinate system with the sample being rotated by 180° with respect to either the x - or the y -axis. At this stage, we shall have a look on the polarization conversion efficiency at the example of linearly polarized light. When an x - or y -linearly polarized wave is incident onto an optically active medium, a fraction of light is converted into its orthogonal polarization state. The efficiency of this polarization conversion is directly expressed by the difference between the off-diagonal elements of the Jones matrix T_{xy} and T_{yx} . If this efficiency is dependent on the propagation direction, namely forward and backward direction, we speak of linear polarization conversion dichroism Ψ_{lin} . From a comparison of the Jones matrices for forward and backward propagation direction (Eqs. 2.28 and 2.29), we see that the off-diagonal matrix elements are interchanged. Hence, Ψ_{lin} reads as

$$\Psi_{\text{lin}}^{(x)} = T_{xy} - T_{yx} = -\Psi_{\text{lin}}^{(y)}. \quad (2.30)$$

Now we introduce the total transmission in a linear polarization base with the normalized and linearly independent base vectors \mathbf{e}_x and \mathbf{e}_y . If linearly polarized light passes forward or backward through a medium and is detected by a non-polarization-sensitive sensor, the measured quantity corresponds to the total transmission $\mathbf{T}_{\text{lin}}^{\text{f,b}}$. It is written in dependence of the base vectors \mathbf{e}_x and \mathbf{e}_y as

$$\mathbf{T}_{\text{lin}}^{\text{f,b}} = T_x^{\text{f,b}} \mathbf{e}_x + T_y^{\text{f,b}} \mathbf{e}_y = \hat{T}_{\text{lin}}^{\text{f,b}} (E_x \mathbf{e}_x + E_y \mathbf{e}_y). \quad (2.31)$$

Finally we can define asymmetric transmission $\Delta^{(i)}$ for a given base vector as the difference between the transmitted intensities for different propagation directions. In particular for the linear base ($i = x, y$) we obtain

$$\Delta_{\text{lin}}^{(x)} = |\mathbf{T}_{\text{lin}}^{\text{f}}|^2 - |\mathbf{T}_{\text{lin}}^{\text{b}}|^2 = |T_{yx}|^2 - |T_{xy}|^2 = -\Delta_{\text{lin}}^{(y)}. \quad (2.32)$$

It is noteworthy, that both $\Psi_{\text{lin}}^{(x,y)} \neq 0$ and $\Delta_{\text{lin}}^{(x,y)} \neq 0$ if and only if $T_{xy} \neq T_{yx}$. It is useful for our purposes to transform the Jones matrix of the linear polarization base $\hat{T}_{\text{lin}}^{\text{f}}$ from Eq. 2.28 into the circular polarization base $\hat{T}_{\text{circ}}^{\text{f}}$. This transformation is given by

$$\hat{T}_{\text{circ}}^{\text{f}} = \hat{\Lambda}^{-1} \hat{T}_{\text{lin}}^{\text{f}} \hat{\Lambda}, \quad (2.33)$$

with the transformation matrix

$$\hat{\Lambda} = \frac{1}{\sqrt{2}} \begin{pmatrix} 1 & 1 \\ i & -i \end{pmatrix}. \quad (2.34)$$

In analogy to Eq. 2.28, the matrix $\hat{T}_{\text{circ}}^{\text{f}}$ connects the amplitudes of circularly polarized incident light with those of circularly polarized transmitted light

$$\begin{pmatrix} T_+ \\ T_- \end{pmatrix} = T_{\text{circ}}^{\text{f}} \begin{pmatrix} E_+ \\ E_- \end{pmatrix} = \begin{pmatrix} T_{++} & T_{+-} \\ T_{-+} & T_{--} \end{pmatrix} \begin{pmatrix} E_+ \\ E_- \end{pmatrix}, \quad (2.35)$$

where the entries of $\hat{T}_{\text{circ}}^{\text{f}}$ can be directly calculated from the entries of $\hat{T}_{\text{lin}}^{\text{f}}$ (and vice versa) according to Eq. 2.35 as

$$T_{++} = [T_{xx} + T_{yy} + i(T_{xy} - T_{yx})]/2, \quad (2.36)$$

$$T_{+-} = [T_{xx} - T_{yy} - i(T_{xy} + T_{yx})]/2, \quad (2.37)$$

$$T_{-+} = [T_{xx} - T_{yy} + i(T_{xy} + T_{yx})]/2, \quad (2.38)$$

$$T_{--} = [T_{xx} + T_{yy} - i(T_{xy} - T_{yx})]/2. \quad (2.39)$$

Having these quantities at hand, asymmetric transmission for the circular polarization base is derived as

$$\Delta_{\text{circ}}^{(+)} = |\mathbf{T}_{\text{circ}}^{\text{f}}|^2 - |\mathbf{T}_{\text{circ}}^{\text{b}}|^2 = |T_{-+}|^2 - |T_{+-}|^2 = -\Delta_{\text{circ}}^{(-)}, \quad (2.40)$$

where T_{-+} and T_{+-} are the off-diagonal entries of the Jones matrix defined by circular base vectors. Comparing Eqs. 2.32 and 2.40 immediately yields that the absolute value of $\Delta^{(i)}$ depends on the choice of the polarization base vectors. Note that both polarization conversion dichroism and asymmetric transmission are optical target functions that can be directly calculated from the optical response of the metamaterial itself. This response is experimentally accessible, e.g., by a combined spectroscopic and interferometric investigation as it will be demonstrated in Sec. 4.3.

2.4.4 Circular dichroism and circular birefringence

The optical target functions that are addressed in this section are related to chiral metaatoms (see chapter 4). More than one century ago [100], chirality was defined by Lord Kelvin as follows: “I call any geometrical figure, or group of points, chiral, and say it has chirality, if its image in a plane mirror, ideally realized, cannot be brought to coincide with itself.”

The two mirror image objects are now commonly known as enantiomers. This famous definition of enantiomorphism is inherently linked to three-dimensional space, where it applies to natural objects like helices, proteins, snails or seashells as well as manufactured articles such as screws, springs and golf clubs. In optics, materials made of three-dimensional chiral metaatoms show two important polarization phenomena that are jointly referred to as optical activity. In particular, we consider circular dichroism, which corresponds to different direct transmission (or reflection) levels for left-handed and right-handed circularly polarized waves. The second phenomenological quantity is called circular birefringence and refers to a rotation of the plane of polarization of light. Note that both effects are, in contrast to asymmetric transmission, identical for opposite directions of wave propagation, i.e. forward and backward propagating waves.

In classical bulk media optical activity is often assigned to different refractive indices for left-handed and right-handed circularly polarized waves. In that sense, circular birefringence arises from different real parts of these refractive indices, which result in different phase delays for left-handed and right-handed components of an electromagnetic wave and thus a polarization rotation. On the other hand, circular dichroism in bulk media is evoked by different imaginary parts of these indices, which cause different absorption losses for circularly polarized waves of opposite handedness. However, since the introduction of a meaningful refractive index is problematic for optical metamaterials, here we will use the more general phenomenological definitions shown above which are directly amenable from the response of an optical metamaterial itself. In order to obtain analytical expressions, we rely on the derivation of the Jones matrix in the circular polarization base $\hat{T}_{\text{circ}}^{\text{f}}$ from the previous section (see Eq. 2.35). Accordingly, circular dichroism δ and circular birefringence Σ are calculated directly from the measured optical response as

$$\delta = |T_{++}|^2 - |T_{--}|^2, \quad (2.41)$$

$$\Sigma = -\frac{1}{2}[\arg(T_{++}) - \arg(T_{--})]. \quad (2.42)$$

2.5 Computational treatment of metamaterials

In general, the computational treatment of nanoscale electromagnetic systems can be done either analytically or numerically. Currently, analytical and semi-analytical approaches to describe the linear and nonlinear response of optical metamaterials are exploited only for a limited number of systems [101]-[106]. To study the nanostructures considered in this thesis, we relied exclusively on numerical methods. The numerical treatment of such systems is

a broad field of modern optics, for which a variety of computational techniques have been widely tested and are partly commercially available. The numerical simulations of metamaterials corresponding to the experiments reported in this thesis were done by Christoph Menzel, Carsten Rockstuhl and Christoph Etrich from the IFTO Jena. Here the two methods of interest are briefly sketched, while the technical details will be omitted for reasons of brevity.

2.5.1 The Fourier modal method

Being a subcategory of the Rigorous Coupled Wave Analysis (RCWA), the Fourier modal method (FMM) is most suitable for optical systems with a periodic repetition of a structure (the unit cell) in one or more dimensions [107]-[109]. It makes use of periodic boundaries, meaning that the structure is considered to extend periodically over an infinite distance. The FMM computation is twofold. First, the Fourier expansion of the field inside the unit cell translates the respective system of Maxwell's equations into a set of algebraic equations. To decrease computational effort, this expansion and hence the number of equations is truncated to a finite length. Second, once the eigenvalues and the eigenvectors of this system are found, the boundary conditions at the interfaces of the unit cell are matched to compute the diffraction efficiencies.

In our case, the FMM was implemented in a home-made *Matlab* code originally written by Jari Turunen. For the calculations performed by Christoph Menzel, the full dispersion of noble metals was properly taken into account according to documented values [47]. In practice, the spectral features of resonant nanostructures reproduced by the FMM can be very sensitive to the input parameters regarding their topography. Thus, the input geometry parameters were varied within the limits of realistic fabrication tolerances, which resulted mostly in good agreement with the experimental spectra of a fabricated sample. No corrections of the imaginary part of the electric permittivity were applied¹¹.

2.5.2 The finite-difference time-domain method

In the case of non-periodic optical systems, the method of choice to solve Maxwell's equations rigorously is the finite-difference time-domain (FDTD) method [112]. A differential equation system comprising Maxwell's equation in the temporal domain and relations connecting polarization and conduction with the electric field are directly discretized in space

¹¹In some related publications, a "wavelength-dependent loss factor" with a seemingly arbitrary value larger than one is multiplied with the imaginary part of the electric permittivity to account for additional losses and to match experimental results [110, 111]. Naturally, such permittivity functions are not necessarily consistent with the Kramers-Kronig relations.

and time on the so-called Yee-grid. Nowadays, the FDTD method can also handle nanoscale heterogeneous structures in the optical domain by a proper subpixel smoothing [113].

For the system described in chapter 6, Christoph Etrich discretized comparably large supercells ($7\ \mu\text{m} \times 7\ \mu\text{m}$) using a resolution of 5 nm. These supercells were truncated by periodic boundaries in the lateral dimensions whereas perfectly matched layers were used along the light propagation direction. A Drude model with adjusted plasma frequency and damping constant was implemented to simulate induced currents. Then, this adapted FDTD method solves the wave equations in the time domain, meaning that each wavelength has to be treated separately. The temporal evolution of a system must be computed sufficiently long to obtain the steady-state field. From the transmitted locally resolved amplitudes the complex transmission can be extracted by imposing a spatial Fourier-transform on the complex field. Subtracting the incident field, the equivalent treatment is applied to the reflected field. In order to obtain a spectral response, this procedure is repeated for a finite number of discrete wavelengths. Besides the transmission and reflection spectra, which are mainly investigated in this thesis, this treatment provides also the spatially resolved optical near-fields of the system under consideration. Details of this numerical technique are outlined in [114].

2.6 Fabrication of nanostructured optical materials

This section deals with the fabrication of nanostructured materials whose unique properties attracted mankind's interest since the time of the Roman empire [115]. However, the big part of modern nanofabrication technology has its roots in the standardized methods developed for the semiconductor industry of the late 20th century [116]. A short summary of the current state of the art is accompanied by pivotal examples from literature that evidence the relevance of the individual methods for the fabrication of optical metamaterials. We will restrict the considerations on essentially planar metallo-dielectric films with characteristic thicknesses of less than $2\ \mu\text{m}$ placed on a supporting substrate. For our purposes concerning optical metamaterials, only methods reaching a sub-100 nm spatial resolution are of interest¹². A comprehensive overview of nanostructure fabrication in general can be found in [117], while a recent review article by Boltasseva et al. was devoted to negative-index optical metamaterial fabrication in particular [118].

¹²This section is not intended to provide a comprehensive state of the art of nanostructure technology, but a practical classification of tools which are suitable for the current (and in some cases future) fabrication of optical metamaterials. In order to deepen his or her understanding for practical purposes, the gentle reader may conveniently resort to the referenced literature.

2.6.1 Nanolithography

In most general terms, lithography is a technique to transfer a generated pattern into a medium. The recording medium must be sensitive to a local interaction with an illuminating particle (or wave) source. The physical nature of these particles yields a straightforward classification scheme into electron-, photon-¹³ and ion-based lithography. Within the context of this thesis, lithography will denote the transfer of a pattern into a resist. The resist is mostly a polymer that changes its solubility in a developer solution upon local interaction with electrons, photons or ions in comparison to the non-illuminated polymer (Fig. 2.2). By this means, a spatially heterogeneous exposure leads to a solubility pattern that is memorized as a fixed structure in the resist. Two different kinds of resists are available: positive and negative. In a positive resist, the exposed areas will be dissolved in the subsequent development stage (Fig. 2.2c), whereas in a negative resist, the exposed areas will remain intact after the development (Fig. 2.2d). Note that in addition to ion beam lithography, purely physical ion beam nanostructuring requires neither a resist medium nor a development step.

Electron beam lithography

In electron beam lithography (EBL), a beam of electrons is used to generate a pattern in a resist. Since electron beam widths can be on the order of nanometers, EBL gives rise to a nanoscale resolution. The serial nature of the process is manifested in a scanning procedure across the surface to be patterned. EBL is most versatile at the point of initial design and preliminary experimental studies since it offers sub-wavelength resolution and almost complete pattern flexibility. These advantages outbalance the principal restriction of EBL application to limited areas, as long as no mass production is required. To date, it is the first

¹³The denotation of photons as particles pays reference to their well-known wave-particle duality.

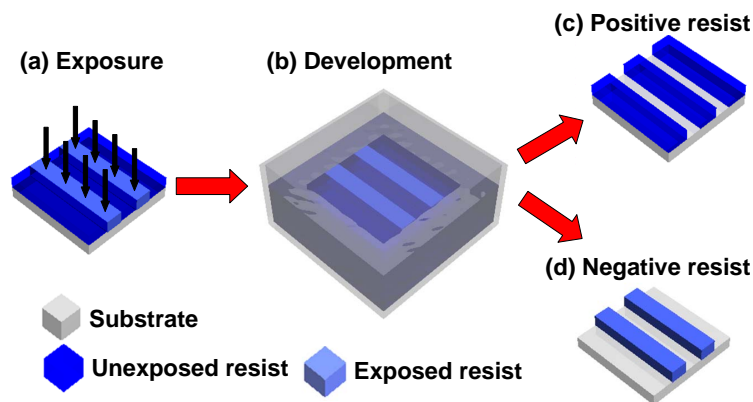


Fig. 2.2: Schematic view of a) exposure and b) development of c) a positive and d) a negative resist.

choice for the fabrication of nanostructured metamaterials [118]. EBL-based nanofabrication procedures including transfer technologies can be achieved on sub-10 nm scales [119, 120].

Optical lithography

Any optical lithography (OL) method uses one or several optical beams or waves to expose a photosensitive resist. To obtain high resolutions, light with short wavelengths and lens systems with large numerical apertures are integrated. OL is routinely applied to produce large micro- and nanostructured areas of up to square meters in size while its resolution limit can be driven down to the nanoscale [121]. Note that the concepts of OL are likewise applied in X-ray- and extreme ultraviolet (EUV)-lithography. Here, only established OL methods capable of achieving sub-100 nm resolution are briefly mentioned.

- Interference lithography (IL): This fabrication technique is based on the superposition of two or more coherent optical waves forming a standing pattern. Alternatively, the wave pattern can be generated using a phase mask. Being a parallel process, IL provides a low-cost, large-area and mass production capability. Though the pattern flexibility is limited, a huge variety of interference patterns can be created by adjusting the relative directions, intensities, polarizations and relative phases of the waves. The resolution limit of IL can ultimately be extended to below 20 nm [122] such that optical metamaterial fabrication was routinely demonstrated [60, 123].
- Multi-photon photopolymerization: In this technique, also referred to as direct laser writing, a photoresist is illuminated by laser light at a frequency below the single-photon polymerization threshold of the resist. When the laser is tightly focused inside the photoresist, the light intensity inside the focus may exceed the threshold for initiating multi-photon photopolymerization [124]. Three-dimensional scanning of the beam over the sample (or vice versa) enables the generation of three-dimensional polymer nanostructures down to about 100 nm lateral feature sizes [125]. Incorporating the concept of stimulated emission depletion [126] holds solid promise to decrease the spatial resolution of multi-photon photopolymerization down to 10 nm [127].

Ion beam lithography and ion beam nanostructuring

Apart from ion beam lithography, which can be considered as an ion-based analogon to EBL, ion beam nanostructuring has gained increasing importance with respect to prototypical high resolution patterning. A focused ion beam (FIB) can be used to remove (or deposit, see Sec. 2.6.2) material in a small region with a footprint of typically less than $100\ \mu\text{m} \times 100\ \mu\text{m}$. Though the ion selectivity depends slightly on the material to be structured, virtually any surface can be patterned by purely physical means. In particular, FIB requires no develop-

ment step. Hence, the writing of a pattern can be monitored *in situ* by a scanning electron microscope (SEM), which is a clear advantage of FIB over EBL. A related aspect is the consequent cycle time, i.e. the time between fabrication and investigation of a test sample and a subsequent sample fabrication with modified process parameters. The shorter cycle time of FIB in comparison to EBL makes the former an attractive and cost-effective tool for rapid prototyping of small nanostructured areas [128], though it is possibly accompanied by an unwanted deposition of ions. This shortcoming can substantially decrease the optical performance of an optical metamaterial [6, 129].

2.6.2 Thin film deposition

As outlined in Sec. 2.1.3, nanostructured noble metals are indispensable to the design of plasmonic metamaterials¹⁴. Regardless of the chosen method defining the nanometric pattern, metallic and non-metallic films must be deposited either before or after the patterning process. Today, numerous materials can be processed as thin films with high homogeneity on a nanometric scale. In principle, a thin film can be deposited from the liquid or the gaseous phase. In the first case, a liquid wets the surface of the substrate and is supported to form a solid film. In the latter case, we can distinguish between chemical and physical gaseous phase deposition, which is the most relevant technique with respect to nowadays metamaterial fabrication.

Liquid phase deposition

- Spin coating: In this three step process, a drop of a liquid material is placed on the substrate. Rotating the substrate at speeds of typically several 1000 revolutions per minute (rpm) leads to a uniform covering of the substrate with the liquid. The last step is the hardening of the film by volatilizing excessive solvents in an oven or on a hot plate. Spin coating is the standard method to prepare thin films sensitive to EBL or OL. Additionally, it can be exploited for the planarization of rough or structured surfaces [132], which allows, e.g., for multiple stacking of single structured layers [133, 134].
- Electroplating (or electrodeposition): The achieved target heights of metals films obtained with this method are typically in the order of tens of micrometers. The substrate is introduced in a solution containing a reducible form of the ion of the desired material and is maintained at a negative potential (cathode) relative to the anode. While the ions are reduced at the substrate surface, the insoluble metal atoms form a solid film.

¹⁴In a broader context, recent reviews attempted to explore the potential of alternative plasmonic materials for specific purposes [130, 131].

Relevant to the field of metamaterials, this technique was shown to be suitable to coat three-dimensional micro- and nanostructures with noble metals [35, 135, 136]. Very recently, the electrochemical postprocessing of a plasmonic metamaterial and the consequential reduction of its plasmonic damping characteristics were demonstrated [137].

Chemical vapor deposition and atomic layer deposition

Chemical vapor deposition (CVD) involves the reaction of chemicals in a gas phase to form a solid film. The needed energy is usually supplied by maintaining the substrate at elevated temperatures. CVD processes offer excellent conformal coverage of three-dimensionally structured surfaces, even at the nanoscale [138, 139]. Most noteworthy, the chemical synthesis of single-crystalline metal films offers superior optical properties for future plasmonic nanostructures [140].

- Atomic layer deposition (ALD): The characteristic feature of this CVD-related technology is the ability the control of the thickness of the deposited material with a sub-nanometer precision. The method is based on sequential self-saturated surface reactions, leading to the controlled atomic (or molecular) layer-by-layer growth of thin films. An ALD cycle comprises the subsequent injection of two material components into the reaction chamber, each followed by a purging pulse or an evacuation step. Self-saturated growth is attained when the highly reactive precursors are kept separate from each other in the gas phase [141]. For instance, three-dimensional patterns obtained by multi-photon photopolymerization [142, 143] or by OL [144] were coated by means of noble metal ALD to form plasmonic structures. Thus, ALD is considered to be a promising candidate to enable the precisely controlled functionalization of almost arbitrary nanopatterns, e.g., by a conformal metallization of their surfaces.
- Focused ion/electron beam deposition: This process denotes the ion or electron beam assisted decomposition of a gas precursor of the specific material that has to be deposited. When, e.g., metalorganic precursors are injected in the beam path, they can be dissociated and parts of them will be deposited on the surface of the substrate. In general, the deposits are nanocomposites containing the (metallic) target material [145]. When at the same time the beam is scanned across the surface, a pattern can be generated. This feature makes focused beam deposition an independent nanolithography tool on its own [146]. As such, it has similar advantages (*in situ* observability, rapid prototyping, short cycle times) and drawbacks (small pattern areas, undesired impurities such as carbon and oxygen [147]) as FIB in comparison to EBL. The potential of focused beam deposition techniques to fabricate nanostructures with sufficiently good optical and/or plasmonic properties is currently under investigation [148, 149].

Physical vapor deposition

The term “physical” indicates that the material to be deposited exists in the desired stoichiometric composition, is sublimated or vaporised and transferred to the substrate without chemical reaction under ultra high vacuum conditions [150]. Any diminishment of the vacuum conditions in the process chamber causes potential reactions with remnant gases and may degrade the purity of the films. The deposited material condensates on the surface of the substrate and gradually changes from a film consisting of isolated particles and clusters to an “infinite” cluster spanning over the whole substrate. The transition point between the two regimes is called the percolation threshold [151]. The deposition rate and the straightness of the incoming beam are mainly governed by the distance between source and substrate and the directness of the incoming particle beam. By subsequent deposition from two or more different sources multilayer stacks can be fabricated.

- Thermal evaporation: The source material is placed in a small container called crucible and heated up to a temperature at which it evaporates. Among other means, the temperature rise can be reached by passing a large current through the resistive crucible.
- Electron beam evaporation: In contrast to thermal evaporation, the surface of the material in the crucible is heated by a bombardment with an electron beam. This method is typically used if the evaporation temperature of the deposition material is higher than the melting point of the crucible. Thus the evaporation of the material is enabled, while the temperature of the crucible holding the material is only marginally raised.
- Sputtering: A target of the material to be deposited is bombarded with high energy inert ions like argon. As a result individual clusters are removed from the surface and almost isotropically ejected into the half-space above the target. Due to the physical nature of this process, it can be applied to almost any material.

Thermal and electron beam evaporation are currently the standard techniques to integrate metal thin films in metamaterials. They have mostly been combined with the lift-off method (see Sec. 2.6.3) for the fabrication of the vast majority of contemporary optical metamaterials including the structures considered in this thesis. It should be mentioned that all thin films produced by physical vapor deposition techniques consist of randomly oriented crystal grains with typical diameters of up to 50 nm. This multicrystallinity impedes the fabrication of structures containing features of comparable size and introduces an intrinsic surface roughness for larger structures. From the optical point of view, grain structures in metal films lead to additional scattering and increased dephasing of surface plasmon polaritons [152], both resulting in undesired broadening of plasmonic resonances. Recently, Nagpal

et al. demonstrated an elegant way to circumvent this issue at least at the surfaces of the involved metallic films by a template stripping technique [153].

2.6.3 Nanopattern transfer methods

A nanopattern generated by lithography is usually written in a resist with high sensitivity to the applied illumination. In most cases, the resist is dissimilar to the desired functional materials that are to bear to final pattern. Therefore the initial resist pattern must subsequently be transferred into the functional material(s). Nanopattern transfer techniques can be distinguished with respect to their either subtractive or additive interaction with the functional material, as it is schematically shown in Fig. 2.3. The first case comprises etching techniques, while the most relevant version of the latter case is the lift-off method.

Subtractive nanopattern transfer

The subtractive interaction with a functional material, i.e. its removal (Fig. 2.3a-e), is mostly achieved by etching. A specific etching method is primarily chosen with respect to its material selectivity, etch rate and directionality (isotropic or anisotropic). In principle, we distinguish between wet and dry etching. Wet etching methods make use of liquid acids or bases to contact an etchable material and to dissolve its surface. If the material itself shows no inherently anisotropic properties, these liquids etch rather isotropically and perform a lateral undercut¹⁵ which limits the smallest feasible feature sizes. More favorable, dry etching methods allow to tune the directionality of the etching. Practically, a higher anisotropy of the applied etching method enables higher aspect ratio vertical structures and smaller undercuts, which in turn can lead to smaller lateral feature sizes. Here, three types of dry-etching processes are briefly mentioned.

- Ion beam etching (IBE, also called ion milling) is a purely physical process that utilizes accelerated inert ions (mostly argon). The process is equivalent to sputtering described above with the difference that the removed material from the target is not recollected. IBE offers high directionality but poor material selectivity. IBE was shown to be a suitable tool to etch thin gold films for optical metamaterials by Liu et al. [134, 155].
- Reactive ion etching (RIE, also called ion-assisted etching) and reactive ion beam etching (RIBE) are mixtures of physical and chemical etching techniques. Instead of or in addition to inert gas ions, reactive gases in the process chamber can support the desired selective material removal. The reaction initiates only if the surface is

¹⁵Lateral undercut is present if the effective angle between the sidewalls of a pattern and the supporting substrate is smaller than 90° [154].

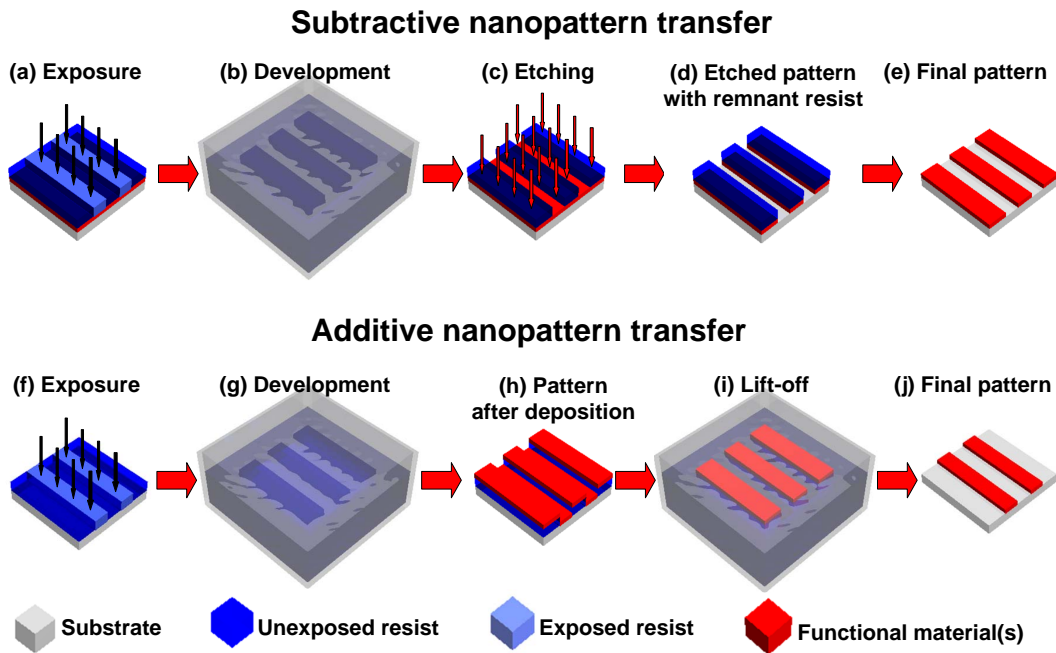


Fig. 2.3: Schematic view of the transfer of a nanopattern written in a positive resist a)-e) by a subtractive transfer method such as etching and f)-j) by an additive transfer method such as lift-off. Note that when a positive resist is used, the final pattern made of the functional material(s) corresponds to the unexposed resist areas for the subtractive transfer method and to the exposed resist areas for the additive transfer method, respectively.

“activated” by the collision of incident ions supplying an activation energy. Since the directionality of the accelerated ions favors collisions on surfaces which are normal to the ion beam, the etching rate is higher in the direction parallel to the ion acceleration. To the best of my knowledge, no RIE or RIBE process for structuring noble metals in optical metamaterials has been reported so far.

- Inductively coupled plasma (ICP) etching is a version of RIE assisted by a plasma ignition. In addition to RIE, a high frequency voltage is inductively coupled into the reaction chamber. The ions generated by the ignited plasma contribute to breaking chemical bonds at the etchable surface.

Additive nanopattern transfer

If a directional physical vapor deposition technique (see Sec. 2.6.2) is applied on a binary resist pattern placed on a substrate, the material will be deposited on the substrate in the cleared areas and on the non-dissolved resist of all other parts. This classifies this step as an additive nanopattern transfer method (see Fig. 2.3f-j). By “lifting off” the remaining resist including the deposited material on top of it, one ends up with the inverse pattern - a thin film of the deposited material at the formerly cleared areas. If the resist is polymer-based,

the lift-off step can be performed in, e.g., acetone, and may be supported by ultrasonication. For this method, a sufficient adhesion of the thin film to the substrate surface is crucial. Therefore, an adhesion promoter like an ultrathin layer of titanium or chromium is usually applied. Although it is known that such adhesion layers are detrimental to the performance of optical films [156], their indispensability for a sufficient yield of adhering nanostructures is commonly recognized.

Nanostructures generated by the lift-off method are limited with respect to their aspect ratio. An increased amount of deposited material (corresponding to a high thickness of functional layers) will degrade the resist mask, e.g. by reducing hole diameters. Unless this behavior is exploited on purpose for conical nanostructures [157], it results in rather unfavorable non-rectangular side-walls of the pattern [158], particularly for thick samples [159]. If the thickness of the deposited materials is increased even more, they will stick down the resist pattern which cannot be lifted off any more. In that case the resist becomes insoluble. As an alternative, simply increasing the resist height diminishes the obtainable lateral resolution. It shall be noted that the restrictions on the aspect ratio of classical lift-off nanopatterns can be partly circumvented when the classical lift-off is combined with a novel membrane projection lithography [160], which proved to be suitable to fabricate micrometer-scale metamaterial unit cells with higher vertical aspect ratios [161].

2.6.4 Pattern duplication methods

Pattern duplication methods have in common that they require an already nanostructured master sample which either serves as a mask or is duplicated. Typical examples for these applications are photolithography and nanoimprint lithography (NIL), respectively. Duplication techniques are used to achieve high throughput, low-cost and high reproducibility. For the purpose of experimental prototyping, pattern duplication methods are less common since they inherently depend on the fabrication process of the master sample. Currently, the field of optical metamaterial fabrication is dominated by slow but versatile pattern generation methods like EBL and FIB, but on the long run pattern duplication methods offer an alternative application perspective. Basing on first successful reports of NIL-fabricated metamaterials [162, 163], NIL and related methods will gain importance for the field once metamaterials are transferred from an academic platform to a mass production oriented environment.

2.6.5 Self-assembling methods

The described top-down approaches for the current fabrication of optical metamaterials are adapted for rapid prototyping and the demonstration of first principal experiments. However,

they are unlikely to suit for obtaining true bulk quantities let alone standardized mass production. Instead bottom-up approaches using self-organization of suitably tailored metaatoms have attracted increasing interest because of the rich assembling behavior and the collective properties that can potentially be engineered [164]. The functionalization of bottom-up approaches is a very innovative field, and it is very likely to grow with regard to optical metamaterials in the near future [165]. For instance, self-assembling methods, though not directly applicable to optical metamaterial fabrication at the moment, can be expanded by exploiting complementary nanopattern transfer steps including noble metal deposition [166]-[168]. Other highly promising methods were inspired by origami, the Japanese art of paper folding, and have convincingly demonstrated the self-assembly [169] and three-dimensional self-folding of prestructured nanopatterns [170, 171].

2.7 Experimental characterization of optical metamaterials

2.7.1 Normal-incidence far-field spectroscopy

Standard transmission and reflection intensity measurements were done with a commercially available Lambda 950 photo spectrometer from *Perkin Elmer*. Equipped with a deuterium and a halogen lamp, this instrument covers a working wavelength range from the ultraviolet to the near-infrared. The internal beam path of the spectrometer contains only reflective components and two Littrow mounted grating monochromators for the short and long wavelength range. The nearly monochromatic beam is split into signal and reference and chopped at 46 Hz. By this means, the ratio between the two beams is recorded for each single wavelength. Via an adjustable Glan Taylor prism the signal beam can be linearly polarized in the plane normal to the principal light direction. To measure transmittance, the signal beam propagated normally through a sample fixed in an home-built sample holder. For reflectance measurements the signal beam was incident on the sample with an 8° inclination to the sample normal. Both signal and reference beam entered an integrating sphere with a combination of a photomultiplier tube and a detector based on strained InGaAs, allowing for a broadband spectral sensitivity from $0.2\ \mu\text{m}$ to $2.5\ \mu\text{m}$ ¹⁶. Through these measurements we obtain the transmittance $t_{x,y}$ and the reflectance $r_{x,y}$ which are the squared moduli of the complex transmission and reflection coefficients corresponding to the x - or y -polarization axis, i.e.

¹⁶For details, see <http://las.perkinelmer.com/Catalog/ProductInfoPage.htm?ProductID=L6020322>, 22 Dec 2010. Historically, we worked with a lead sulfide (PbS) photodiode until February 2009. This period of time comprises the measurements reported in chapters 3 and 6.

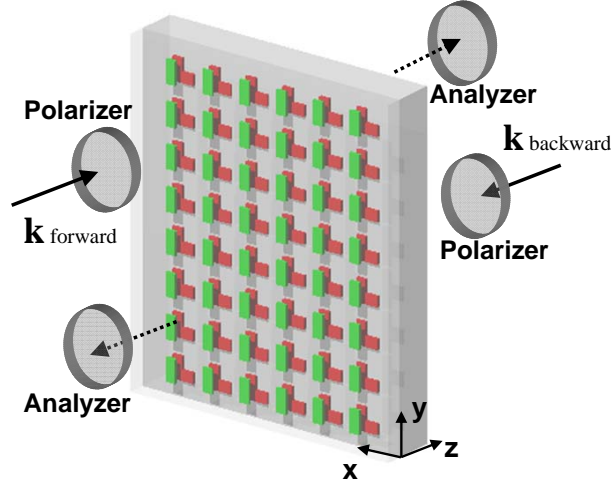


Fig. 2.4: Schematic of the experimental setup to measure the amplitudes of the transmission matrix. Normally incident light was linearly polarized before propagating through the sample and subsequently analyzed by means of a second linear polarizer.

$$t_{x,y} = |T_{x,y}|^2, \quad (2.43)$$

$$r_{x,y} = |R_{x,y}|^2. \quad (2.44)$$

The acquired data was directly recorded and processed via the integrated software *UV Winlab 5.1*. Prior to any sample measurement, a so-called autozero spectrum accounting for the spectral dependence of sources, detectors and all optical components in the beam path was carried out for each state of linear polarization. The accuracy of this calibration was regularly cross-checked by recording a 0% (blocked beam) and a 100% plain baseline. Deviations from those baselines indicated if the spectral distribution of the halogen lamp changed during data acquisition. Furthermore, the recorded spectrum of each metamaterial sample was normalized to the respective unstructured substrate both for transmission and reflection.

In order to record the squared moduli of the full Jones matrices of the metamaterials described in chapters 4 and 5 ($t_{ij} = |T_{ij}|^2$), transmittance measurements were taken for all four possible combinations of horizontally and vertically polarized source and detector and for wave propagation in both directions. As shown in Fig. 2.4, an analyzer (a second linear polarizer) was placed behind the sample. Propagation in backward direction was mimicked by flipping the sample normal to its plane.

For the special case of the validation measurement with circularly polarized light (see Sec. 4.4.2), a super-achromatic quarter wave plate (RSU 2.4.10, 600...2700 nm wavelength) from *Bernhard Halle GmbH* was introduced in the optical beam path between the first polarizer and the sample under investigation. By proper adjustment of the first polarizer,

linear polarization was converted into either left-handed circular polarization (LCP) or right-handed circular polarization (RCP).

2.7.2 Angular resolved transmittance spectroscopy

The measured transmittance data presented in Sec. 3.3.3 was recorded with a spectroscopic setup at the Institute of Physics at the Martin-Luther-Universität Halle-Wittenberg. It consisted of a 250 W halogen light source from *LOT Oriel*, beam shaping optics and a motorized goniometer holding the sample. Detection was done with an indium gallium arsenide (InGaAs) photodiode. The diode signal and a reference from a chopper driver were fed into a lock-in amplifier. Again, each recorded spectrum had to be normalized to the respective unstructured substrate. This setup allowed for polarization and angular resolved transmission and reflection spectroscopy for wavelengths from 0.8 μm to 1.6 μm . The accessible angular range was basically limited to 55° by the finite area size of the metamaterial sample with respect to the beam size of the measurement setup.

2.7.3 Interferometric optical phase measurements

Broadband transmission phase measurements covering a spectrum ranging from 0.6 μm to 1.7 μm were carried out for the metamaterial reported in chapter 4. In addition to the transmittances $t_{ij} = |T_{ij}|^2$ obtained from amplitude measurements (see Sec. 2.7.1), optical interferometry delivered the associated phase information and allowed for an unambiguous determination of the complex transmission coefficients T_{ij} . The setup, which was operated by Ekaterina Pshenay-Severin and Matthias Falkner, basically consisted of a white-light Fourier-transform spectral interferometer [172] equipped with a supercontinuum light source SuperK Versa from *KOHERAS*. Details of the underlying Jamin-Lebedeff interferometric scheme can be found in [173, 174]. In contrast to previous works, the physical quantities characterizing optical activity of chiral optical metamaterials (see Sec. 2.4.4) could be extracted exclusively based on measurements without the need for additional numerical input.

Chapter summary

This chapter provided the conceptual framework needed for the description and investigation of optical metamaterials. It was postulated that symmetry breaking of metaatoms and their respective arrangement is a key parameter either to outperform natural optical media or even to obtain new optical functionalities that have no equivalent counterparts in nature. Depending on the optical target function that should be addressed, one of the numerous

physical quantities must be carefully chosen to describe the characteristic features of a particular metamaterial. Besides effective optical properties in the sense of wave parameters, alternative optical target functions are the dispersion relation, the optical response itself and other quantities that can be directly derived from the latter. In this thesis, polarization conversion dichroism, asymmetric transmission, circular dichroism and circular birefringence will be of relevance. Furthermore the current state of nanofabrication technology dedicated to the fabrication of optical metamaterials was reviewed. For the samples described in this thesis, EBL in combination with thin film evaporation and the lift-off method turned out to be a successful strategy. The chapter is closed with a description of the utilized experimental characterization techniques. Having explored the theoretical, technological and experimental basics relevant to the treatment of optical metamaterials, we will now come to the core of this thesis.

3 High-symmetry metaatoms for polarization insensitivity

In this chapter, the detailed fabrication and optical characterization of a planar negative-index metamaterial with a fourfold rotational symmetry is described. Compared with the established double fishnet structure, our novel design termed “Swiss cross” structure eliminated the drawback of polarization-dependent effective optical properties for normally incident light. A Swiss cross metamaterial sample was fabricated and experimentally analyzed for both normally and obliquely incident light. The comparison with numerical simulations associated an effective refractive index of $n_{\text{eff}}=-1.9$ for normal incidence at an operational wavelength of $1.4\ \mu\text{m}$. Accounting for the high $C_{4,z}$ symmetry of the unit cell, this statement holds independently of the incident polarization state, which was achieved for the first time in field of optical metamaterials. Nevertheless, we extended our studies to oblique incidence and revealed a generally strong angular dependence due to the mesoscopic structure of the sample and its associated spatial dispersion. All experiments are backed up by numerical simulations. It is shown that the spectral and angular domains of negative refraction as well as its strength depend strongly on the light’s propagation direction and polarization state. Our results clearly indicate that a description of the Swiss cross metamaterial in terms of effective material properties is not adequate. The significance of their limited applicability is highlighted.

3.1 Metamaterial designs for a negative refractive index

Among various desirable and exotic properties of general metamaterials, the pursuit for a negative effective index of refraction attracted possibly the greatest interest in the past [5]. We will use the term “negative refractive index” throughout this chapter, while recalling its meaning as a wave parameter according to the conclusions drawn in Sec. 2.3.2. The general statement given there will be elucidated in detail at the very example of the metamaterial presented here. The angular dependence of the effective refractive index in the resonant domain of a real optical metamaterial due to its inherent spatial dispersion will be explicitly demonstrated.

3.1.1 The double fishnet design

Because of technological challenges in obtaining bulk materials, negative-index metamaterials were usually fabricated as a single functional layer only. Nevertheless, first successful stacking technologies have been reported [6, 129, 134]. Due to the immense number and variations of design proposals for negative-index metamaterials operating at various spectral domains, the following considerations are restricted to metamaterials that I) consist of one functional layer only, II) show a negative-index behavior for near-infrared or visible wavelengths and III) have actually been subject to experimental demonstration.

Common design proposals for planar negative-index metamaterials are based on appropriately tailored nanostructures supporting plasmonic eigenmodes. In the optical domain, split ring resonators [57] and cut-wire pairs [58, 59] constituted promising approaches, but were restricted to longer wavelengths due to the design-dependent saturation of the magnetic response at optical frequencies [175]. First and foremost, the so-called (double) fishnet structure, firstly reported by Zhang et al. in 2005 [60], was shown to have the best optical performance of all realized designs to date in terms of its figure of merit (FOM). The FOM is considered to be a simple and straightforward quality criterion for negative-index metamaterials [176] and is defined as the ratio of the moduli of the real and imaginary parts of $n_{\text{eff}}(\omega)$ in the negative-index spectral range.

The physical working principle of the general fishnet structure is briefly recalled following [177]. Vertically, the structure comprises a three-layer stack (metal-dielectric-metal). The design can be intuitively understood as a composition of “magnetic atoms” and “electric atoms” in the lateral direction as shown in Fig. 1a in [178]. The electric atoms are the long metal wires parallel to the incident electric-field vector. Their passive behavior corresponds to a diluted metal [179]. The plasma frequency of a diluted metal will be lower when compared to a true bulk metal, yet it must be kept slightly above the targeted operation frequency. This implies that the real part of $\epsilon_{\text{eff}}(\omega)$ is negative while its magnitude is not too large. The resonance wavelength of the magnetic atoms is determined by the width of the cut-wire pairs, which are as well aligned parallel to the polarization vector of the electric field. An electric quadrupole and a magnetic dipole moment stem from the antisymmetric plasmon polariton eigenmode of the two coupled metal layers and evoke a resonance in $\mu_{\text{eff}}(\omega)$ [180], which can also take negative values for a limited spectral range¹.

Different implementations of the fishnet design can be classified according to their polarization-sensitivity and to their number of free geometrical parameters. The latter is important for adjusting the optical response, e.g. in terms of the effective plasma frequency of $\epsilon_{\text{eff}}(\omega)$ and the resonance frequency of $\mu_{\text{eff}}(\omega)$:

¹The physics of cut-wire pairs is further detailed in Sec. 6.2.

1. The first class comprises fishnet structures with holes of square or circular shape on a square lattice [60, 111]. These fishnets exhibit a $C_{4,z}$ symmetry which translates directly into polarization independence for normal incidence (parallel to the z -axis). The number of free lateral design parameters² is only two: the lateral hole size and the lattice constant. In fact, it was shown that the optical performance of $C_{4,z}$ symmetric fishnets is inferior due to a deterioration of the magnetic resonance and thus leads to a low FOM [177].
2. Featuring only a $C_{2,z}$ symmetry, the second class consists of fishnet structures with rectangular or elliptical holes. The symmetry breaking allows for an additional free parameter since the lateral hole sizes now differ in x - and y -direction. This degree of freedom enabled the demonstration of negative-index metamaterials with the highest FOMs in the optical domain compared to competing designs [177, 181, 182, 183]. However, they suffered from a strong polarization dependent response [72], as one usually aims at optimizing the geometry for a predefined orientation of the structure relative to the illuminating polarization. Clearly, for many future applications of metamaterials a polarization-insensitive response is highly desirable.

In essence, in practical applications of the fishnet design one had to relinquish either polarization independence or one geometrical degree of freedom. A novel negative-index metamaterial design which is presented in the next section, rendered this choice unnecessary³.

3.1.2 The Swiss cross design

The Swiss cross design was invented simultaneously and independently by different researchers. It was first mentioned as a (geometrically) “isotropic-fishnet” along with other variations by Kafesaki et al. [185], and adapted for the terahertz [186] and gigahertz domain [187] later on. Conceptually, the structure comprises a metal-dielectric-metal layer stack in the vertical direction. Laterally, the unit cell consists of a cruciform aperture. Because of its striking resemblance to the flag of Switzerland, we will refer to it as the Swiss cross. From its $C_{4,z}$ symmetry it is evident that the unit cell will show a polarization-independent response for normal incidence. The structure can essentially be understood as an isotropic cut-wire pair combined with orthogonally oriented wires. The number of free lateral geometry parameters is three, since one can adjust independently the width and the length of the cross arms as well as the lattice constant. Thus, when compared to a

²Vertical parameters are spared since their number is equal in all cases under consideration.

³We note that only after our own publication [184], an optical polarization-independent fishnet structure was reported [111]. Its high losses were compensated later on by active gain [40]. Alternative approaches based on coupled waveguide geometries [95, 96] still lacked experimental realization during the compilation of this thesis.

polarization-independent fishnet with circular or square holes, the Swiss cross design offers the advantage of an additional degree of freedom. Consequently, one can tune independently the resonance frequency of $\epsilon_{\text{eff}}(\omega)$ and the effective plasma frequency of $\mu_{\text{eff}}(\omega)$, resulting in a better FOM.

3.2 Single layer nanofabrication technology

In the following we describe the tools and detailed technological recipes that were used for the fabrication of the Swiss cross metamaterial and for the other nanostructures reported in this thesis. The choice of a technology for any nanostructure fabrication depends primarily on the available resources at the given location. Our key tool was EBL combined with thin film evaporation and lift-off, which in my opinion is the standard procedure for approximately 80% of today's metamaterial prototypes. We applied this technology because of its high resolution (<50 nm), pattern flexibility and convincing sample quality regarding topographical and optical properties. Within the process resolution limit almost every pattern is feasible. The main shortage of EBL is that it is a serial writing process. Hence it is normally used to write small areas of the order of $300 \mu\text{m} \times 300 \mu\text{m}$ in the field of metamaterial fabrication.

By contrast, our electron beam writer Vistec SB350 OS (*Vistec Electron Beam GmbH, Jena*) was specifically developed to meet the needs of optical applications [188]. It allows to process areas of more than $100 \text{mm} \times 100 \text{mm}$ at reasonable fabrication times by means of a variable-shaped beam pattern generation [189]. The largest EBL-made metamaterials reported in literature so far were of the order of 1mm^2 [190], but their comparably large lattice periods of several μm rendered them suitable for the terahertz range of the spectrum, excluding the optical spectral domain.

In the following, our recipes will be described in detail. The starting point was a 4 inch diameter fused silica wafer which was 1 mm thick and polished on both sides. Prior to processing, it was cleaned by a standard cleaning process. For the EBL, we faced the choice between two types of electron beam resists: Standard polymethyl methacrylate (PMMA) and the chemically amplified resist FEP171.

- **PMMA:** Invented already in the year 1968 [191], PMMA and its variations are still widely used in EBL. Upon electron beam irradiation the long polymeric chains are fragmented into shorter ones. Shorter chains are more dissolvable for the developer, typically methyl isobutyl ketone (MIBK). PMMA was proven to be the first choice for the lift-off process in countless contributions [57, 157, 192].

For the metamaterials reported in chapters 4 and 5, the following procedure was used: A 85 nm thick layer of the PMMA-copolymer AR-P 610 from *Allresist Berlin GmbH*

was prepared by spin coating and tempered at 210 °C for 10 minutes. Subsequently, the resist AR-P 671 from the same supplier was spin coated with the same thickness and baked at 180 °C for 30 minutes. This preparation resulted in two PMMA layers with two different electron selectivities in order to provide an undercut resist profile. Next, a 10 nm thick gold layer was thermally evaporated to ensure a conducting surface during electron beam exposure. For patterns with a low filling fraction, typical electron exposure doses were of the order of 400 $\mu\text{C}/\text{cm}^2$. If the pattern filling fraction was higher, the respective doses had to be decreased. After the wet chemical removal of the gold conductance layer in an aqueous solution of potassium and potassium iodide, the samples were developed in a 1:1 MIBK:isopropanol solution for 30 seconds, rinsed with isopropanol and blown dry with nitrogen.

- **FEP171:** This chemically amplified positive-tone resist from *Fujifilm* was evaluated with respect to its suitability for the lift-off method. Even though FEP171 is a common mask making resist with high wet etching resistance, its use for lift-off purposes has not been reported in the literature to the best of my knowledge. Chemically amplified resists are based on acid generation during exposure and a thermo-catalytical amplification of this acid combined with a cross linking reaction of the resist polymer during a post exposure bake. In comparison to PMMA based resists they enable an increased sensitivity of more than one order of magnitude and are therefore readily applied by the semiconductor chip industry.

In this work the wafer was evaporated with a 10 nm film of indium tin oxide (ITO). This thin film layer served as a transparent conductive oxide with a sheet resistance of $<10^{-3} \Omega\text{m}$ [193] and prevents charging effects during the following electron beam exposure⁴. The ITO film remained on the substrate after fabrication and must not perturb the optical function of the metamaterial placed on top of it⁵. Next, a 300 nm thick layer of FEP171 resist was spun onto the surface at 1400 rpm and baked at 120 °C for 3 minutes. Depending on the desired nanopattern, the applied electron doses were adjusted between 11 and 13 $\mu\text{C}/\text{cm}^2$. These doses are slightly higher than those of the specifications from *Fujifilm* to achieve an undercut profile even in a single layer of resist. After exposure, the wafer underwent a post exposure bake at 110 °C for 1 min. The resist was developed in OPD4262 developer for 40 seconds. This process

⁴An alternative to a transparent conductive oxide at the bottom of the resist is a charge dissipating agent on top of the resist layer [194]. However, this entails the drawback of an additional fabrication step when dissolving the agent after exposure.

⁵This was ensured by measuring its optical transparency in the visible and near infrared (mean extinction coefficient smaller than 0.2 for a 10 nm thin ITO layer at $\lambda=1.4 \mu\text{m}$). Numerical simulations employing the experimentally obtained optical constants of the ITO film reveal that its influence was of minor importance to the overall optical properties of the metamaterial.

was applied for the fabrication of the structures reported in chapters 3 and 6.

After exposure and development, an adhesion promoting titanium film with a thickness of 3 nm⁶ and the desired functional layer stack were deposited onto the resist patterned wafer by physical vapor deposition. The deposition rates were <0.1 nm/s aiming at a superior sample quality compared to higher rates [195]. For our metamaterial structures either a single layer of gold or a three layer stack of gold-magnesia-gold with a maximum thickness of 100 nm were typical. Gold (Au) and magnesia (MgO) were thermally and electron beam evaporated, respectively (see Sec. 2.6.2). Subsequently the wafer was immersed in acetone for more than four hours and finally the lift-off was performed supported by sonication. The resulting nanostructures comprise the evaporated layer stack with the inversion of the exposed lateral pattern. Due to the lift-off procedure we usually obtain non-perpendicular side walls with typical angles of 10°-15° with respect to the substrate normal. All fabrication steps and the final patterns were routinely monitored by SEM inspections.

A few remarks shall be spent on the advantages and shortcomings of the two evaluated resist systems. For the fabrication of experimental prototypes of metamaterials, PMMA did work well in accordance with the experiences of many other researchers in this field. On the downside, it requires comparably high electron exposure doses (in particular, if an undercut resist profile is desired) resulting in relatively long exposure times. Furthermore, the reproducibility of a specific pattern from sample to sample turned out to be rather challenging with PMMA, due to numerous and partially uncontrollable process parameters that determine the final outcome [196].

This major shortcoming was partially lifted when working with FEP171. Its highly standardized usage according to the supplier's terms of use guarantees an accurate reproducibility of the desired pattern. In fact, performing test exposures on small scales and repeating them with identical exposure parameters on large areas resulted in a confirmation of the test results within the resolution accuracy of the overall process. Secondly, and this is an important point, we achieve at least an order of magnitude faster patterning than PMMA-based EBL. However, chemically amplified resists show an increased surface and line edge roughness due to the statistical and locally nonuniform distribution of the photochemical events [197]. As for optical metamaterial fabrication including metal lift-off, this drawback is not crucial since the sizes of the metal crystal grains are of the same order as the local resist pattern fluctuations (see Sec. 2.6.2). After the metal deposition step, the line edge roughnesses of the final nanostructures were comparable in our experiments; regardless of the used resist. Summing up, this technological achievement illustrates an important step toward the creation of large-area planar metamaterials in an high-throughput oriented environment.

⁶The thickness of the titanium film is below its percolation threshold.

3.3 Experimental investigation of the Swiss cross

The Swiss cross metamaterial was fabricated by the FEP171 lift-off technique as described in Sec. 3.2 and is shown in Fig. 3.1. All geometry parameters are detailed in the figure caption. The ends of the Swiss cross arms have a circular shape with a diameter corresponding approximately to the width of the arms. The specific design parameters were chosen to match the resonance frequencies to our available spectroscopic characterization equipment as described in Sec. 2.7, but can be tuned to other wavelengths as well. It is worth mentioning that the footprint of the Swiss cross metamaterial extends uniformly over $3\text{ mm} \times 3\text{ mm}$, which was possible thanks to the comparably short EBL exposure time of FEP171.

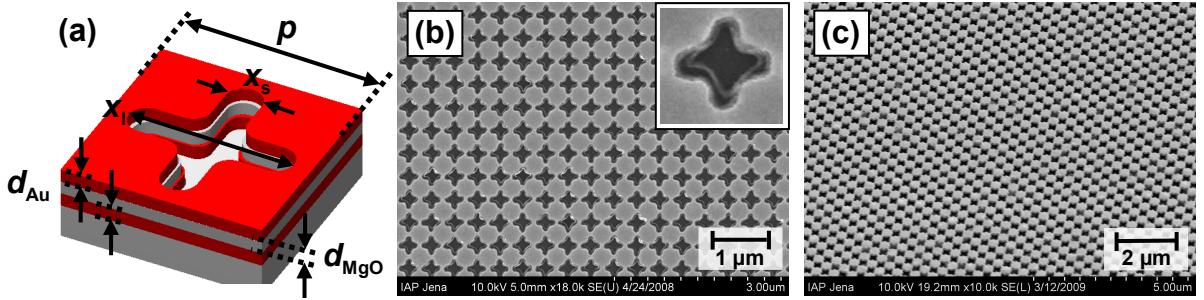


Fig. 3.1: a) Schematic sketch of the Swiss cross metamaterial unit cell with the definition of the geometrical parameters: $p=410\text{ nm}$, $x_1=310\text{ nm}$, $x_s=80\text{ nm}$, $d_{\text{Au}}=30\text{ nm}$, $d_{\text{MgO}}=37.5\text{ nm}$. b) Top view and c) 45° tilted view SEM micrograph of the fabricated metamaterial with lattice constants of 410 nm in both lateral directions. The inset of b) shows a magnified top view of the unit cell.

3.3.1 Determination of polarization sensitivity for normal incidence

The Swiss cross was optically characterized by normally incident transmission and reflection spectroscopy as explained in Sec. 2.7.1. Measurements were done as a function of the polarization angle for linearly polarized incident light. In Fig. 3.2 spectral scans of transmittance and reflectance⁷ from $\lambda = 0.4\ \mu\text{m}$ to $\lambda = 1.8\ \mu\text{m}$ with varying polarization angles from 0° to 180° in steps of 5° are plotted. Only minor deviations from the theoretically predicted complete polarization insensitivity have been observed⁸. For instance, considering the spectral position of the principal transmission resonance at $\lambda=1.05\ \mu\text{m}$, a wavelength deviation over all polarization angles up to $\pm 10\text{ nm}$ can be noticed. The amplitude maximum of the transmission resonance varies by $\pm 1.5\%$. However, these effects can be attributed to imperfections of the fabricated structure with respect to the idealized Swiss cross. From a systematic examination of SEM images we observed an unintentional, weak twist of the

⁷Because of the expected polarization insensitivity, we can set $t = t_x = t_y$ and $r = r_x = r_y$.

⁸The low signal-to-noise ratio in the wavelength range from $0.9\ \mu\text{m}$ to $1.0\ \mu\text{m}$ in the reflection spectra is due to low sensitivity of the detector and does not bear any physical meaning.

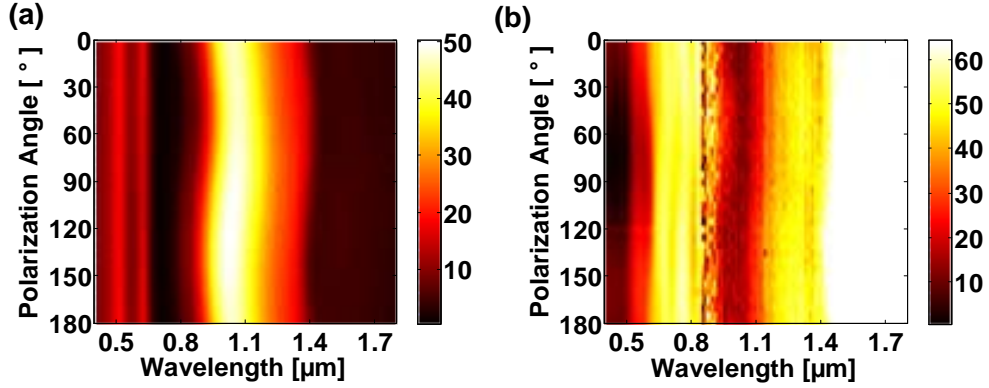


Fig. 3.2: Measured a) transmittance and b) reflectance spectra of the Swiss cross metamaterial as functions of the wavelength and the incoming linear polarization state from 0° to 180° in steps of 5° at normal incidence.

outer cross arms (toward an inverted gammadion-like structure [9]) that slightly violates the $C_{4,z}$ symmetry and induces a weak polarization dependency. Most probably the twist is due to the serial writing procedure of EBL and a time hysteresis of the resist⁹. Nevertheless, this shortcoming can be fixed through the use of an adapted exposure regime. There is no fundamental physical objection that would contradict the polarization-independent response of the ideal design.

3.3.2 Effective properties for normal incidence

To retrieve effective optical properties of the structure, the measurements were compared to simulated data obtained by the FMM method (see Sec. 2.5.1). We compare simulated reflection, transmission and absorption data for a polarization parallel to one arm of the Swiss cross. This configuration corresponds to a polarization angle of 0° in the measurements. The absorption was calculated as the difference of the sum of transmission and reflection to unity, i.e. $a = 1 - t - r$. The experimental and simulated spectra shown in Fig. 3.3 demonstrate a good correspondence over the entire wavelength range, covering all essential spectral features. Note that the width and the strength of the resonances are reproduced with remarkable agreement. Particularly, for the context of this discussion three main resonances are discernible. The first (1) and the second (2) resonance arise at a wavelength of $0.83 \mu\text{m}$ and $1.05 \mu\text{m}$, respectively. The third (3) and most relevant resonance in the context of this investigation occurs at wavelengths around $1.4 \mu\text{m}$.

The physical origin of the resonances can be elucidated best from the retrieved effective optical material properties. Though their limited validity for mesoscopic metamaterials is acknowledged (see Sec. 2.3.2), here we show exemplarily how effective properties give

⁹When the Swiss cross pattern is sequentially composed during the exposure, temperature and charge gradients are expected to add up to a twist of the cross arms after the resist development.

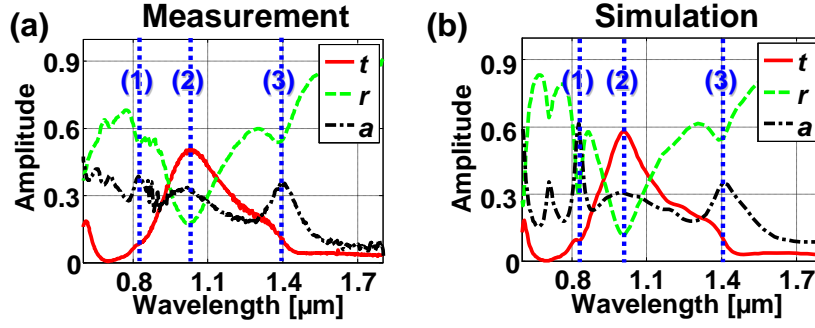


Fig. 3.3: Measured a) and simulated b) transmittance, reflectance and absorption spectra for 0° polarization. Measurements with the orthogonal polarization delivered virtually identical results. The absorption spectra were calculated from measured and calculated data, respectively. The numbers (1), (2) and (3) mark the wavelength positions of the three resonances of particular interest.

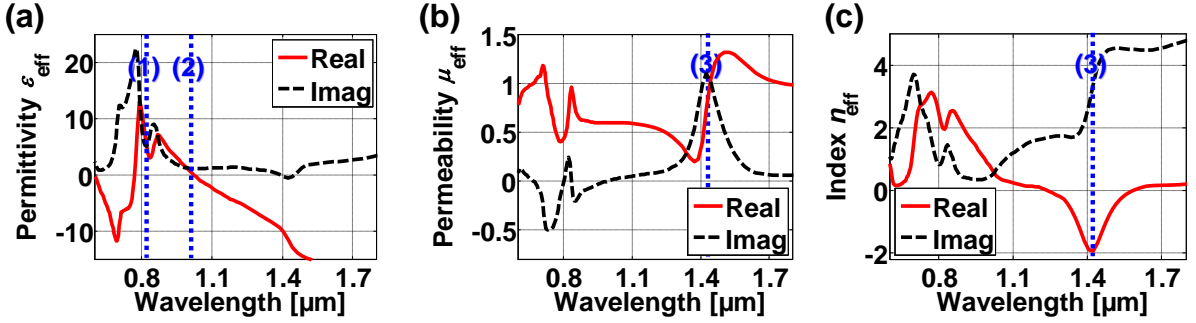


Fig. 3.4: a) Effective electric permittivity $\epsilon_{\text{eff}}(\lambda)$, b) effective magnetic permeability $\mu_{\text{eff}}(\lambda)$, and c) effective refractive index $n_{\text{eff}}(\lambda)$ as retrieved from the FMM simulations. The numbers (1), (2) and (3) mark the wavelength positions of the three resonances of particular interest.

preliminary insight into the underlying physics and can serve to simplify the description of light propagation inside a Swiss cross metamaterial. For this purpose we relied on the rigorously computed complex reflection and transmission spectra and applied the retrieval procedure described in Sec. 2.3.1. Results are presented in Fig. 3.4, where $\epsilon_{\text{eff}}(\lambda)$, $\mu_{\text{eff}}(\lambda)$ and $n_{\text{eff}}(\lambda)$ are shown. Again it is emphasized that the retrieved properties are universal for all states of polarization at normal incidence within the limits of manufacturing tolerances.

- The resonance (1) at a wavelength of $0.83 \mu\text{m}$ is associated with the symmetric localized plasmon-polariton resonance excited in the cut-wire pairs. The current in the cut-wires oscillates in-phase at this wavelength. As their dipole moments add up constructively, strong dispersion in the effective permittivity with a Lorentzian line shape can be observed (Fig. 3.4a). For our specific implementation of the Swiss cross design the resonance (1) is superimposed by the onset of the first diffraction order of the structure, which deteriorates its typical lineshape.
- Regarding resonance (2), we notice that the effective electric permittivity $\epsilon_{\text{eff}}(\lambda)$ is char-

acterized by a Drude-type dispersion relation with a plasma frequency corresponding to $\lambda = 1.05 \mu\text{m}$ (Fig. 3.4a). This wavelength exhibits the cutoff wavelength for the fundamental guided eigenmode in an infinitely extended metal waveguide having the shape of a Swiss cross [198]. At larger wavelengths the fundamental mode is evanescent, causing $\epsilon_{\text{eff}}(\lambda)$ to be negative [199].

- Finally, the effective magnetic permeability $\mu_{\text{eff}}(\lambda)$ shows a Lorentzian resonance (3) centered around $\lambda=1.4 \mu\text{m}$ (Fig. 3.4b). The origin of this spectral feature can be understood by an investigation of the electric displacement currents in both metallic layers. At a wavelength of $1.4 \mu\text{m}$ the currents are π out-of-phase and give rise to an electric quadrupole and a magnetic dipole moment [101, 200]. This is the signature of an antisymmetric plasmon polariton mode induced in the cut-wire pairs, backing up our original statement. Choosing the physically correct branch of $\Re[n_{\text{eff}}(\lambda)]$ in Eq. 2.16, we formally obtain the real part of the effective index of refraction $\Re[n_{\text{eff}}(\lambda)]=-1.9$ around $\lambda=1.4 \mu\text{m}$ (Fig. 3.4c) with a FOM of 0.7. An increase of this quality criterion is expected upon optimizing the structure for a better matching of the resonance wavelength of the effective permeability to the plasma frequency of the effective permittivity, which is feasible by the lateral and vertical geometry freedoms of design. It is admitted that $\mu_{\text{eff}}(\lambda)$ remains positive at $\lambda=1.4 \mu\text{m}$, which classifies the fabricated Swiss cross as a single-negative metamaterial [201].

3.3.3 Angular dependent transmission measurements

One of the most challenging issues of metamaterial research is the design of structures that provide the desired optical properties for all angles of incidence. This includes optically isotropic metamaterials and metamaterials with a specifically tailored anisotropic optical response. Generally, the angular spectral response is highly relevant for imaging systems on the basis of optical metamaterials. To evaluate the performance of a particular metamaterial design it is therefore necessary to investigate its response for all propagation directions, i.e., all angles of incidence. We performed exactly this measurement for the Swiss cross metamaterial. In the case under consideration, the azimuth angle Φ and the polarization of the incoming light were fixed while the angle of incidence Θ and the wavelength were varied as free parameters. The measurement technique is described in Sec. 2.7.2 and the results are compared to FMM simulations. In Fig. 3.2 the zeroth diffraction order of the measured and simulated transmission spectra are shown for $\Phi=0^\circ$ and $\Phi=45^\circ$ and for both TE and TM polarizations. By definition, TE denotes the situation when the polarization vector is parallel to the substrate plane. Note that the spectra for $\Theta=0^\circ$ (corresponding to the very top line of each subfigure in Fig. 3.5) are equal to the results shown in Fig. 3.3, regardless of

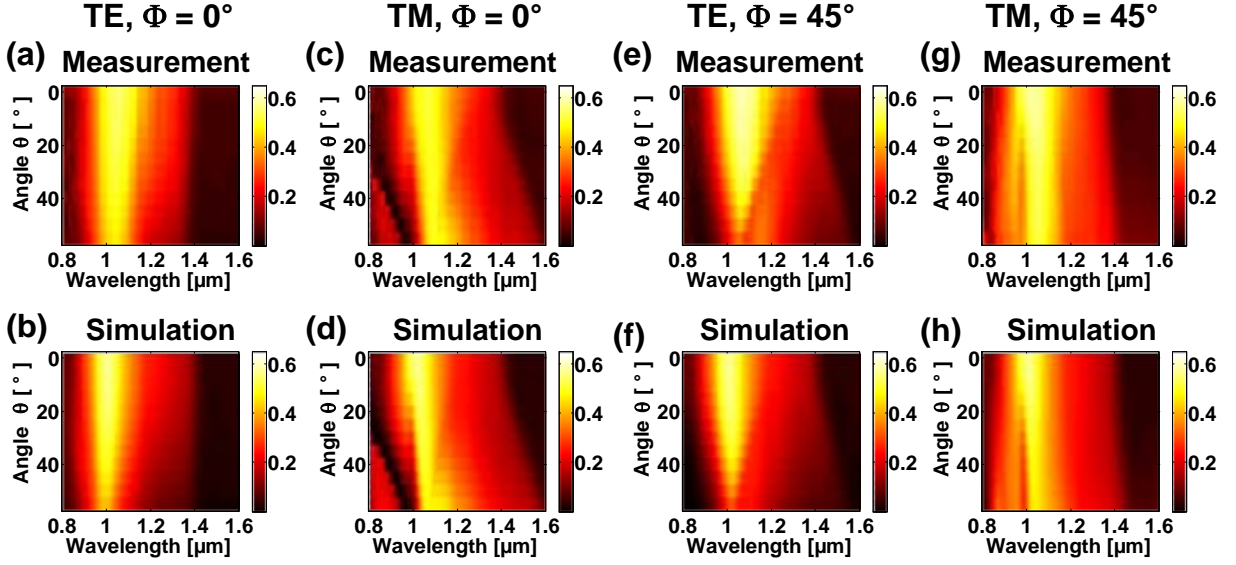


Fig. 3.5: Transmittance spectra of the Swiss cross metamaterial for four combinations of polarization states and planes of incidence in dependence of the wavelength and the angle of incidence Θ in steps of 5° . Upper row: measured data. Lower row: simulated data. a) and b) TE polarization at $\Phi=0^\circ$. c) and d) TM polarization at $\Phi=0^\circ$. e) and f) TE polarization at $\Phi=45^\circ$. g) and h) TM polarization at $\Phi=45^\circ$.

Φ and the polarization state. As outlined in the previous section, for normal incidence the transmission is identical in all scenarios.

In essence, the comparison of experiment and simulation provides a remarkable, almost perfect agreement for all planes of incidence and polarization states. In particular, all experimental features of the spectra are fully revealed in the simulations. The four investigated configurations were chosen, since for these high symmetry directions no polarization rotation occurs. For both planes of incidence the structure is mirror symmetric with respect to this plane. The polarization states of the field in the effective metamaterial can then be decomposed into TE- and TM-polarized eigenstates. No coupling occurs between them, hence the polarization state of the incoming waves is preserved. Only for these particular cases ($\Theta=0^\circ$ and $\Phi \in [0^\circ, 45^\circ]$) the Swiss cross can be described as an effective anisotropic medium. For all other angles Φ the transmitted and reflected light exhibits different polarization states and the effective medium cannot be described as anisotropic. The same holds for $\Theta > 0$ where the transmission evolves differently for $\Phi=0^\circ$ and $\Phi=45^\circ$ with increasing Θ . For a truly homogeneous medium with $C_{4,z}$ symmetry the linear optical response must not depend on Φ [74].

Relying on the above observations, we can further detail the limits of the effective medium regime of the Swiss cross metamaterial. In Figs. 3.5c and d, one can discern abrupt variations appearing for smaller wavelengths (and larger angles of incidence). They indicate the onset of a higher propagating diffraction order in the substrate. This higher diffraction

order is significantly excited for TM polarization only. For $\Phi=45^\circ$ the first diffraction order appears for much smaller wavelengths or larger angles of incidence, respectively, since the effective period is increased by a factor of $\sqrt{2}$. Of course the effective medium description of metamaterials is restricted to wavelength domains where only the zeroth diffraction order is propagating. It is noteworthy that for one particular excitation condition, the spectral response of the Swiss cross turns out to be robust against the angle of incidence Θ . For TE polarization and $\Phi=0^\circ$ (Figs. 3.5a and b) the first diffraction order is two orders of magnitude weaker. To recall, the associated negative-index domain is centered at a wavelength of about $1.4\ \mu\text{m}$. As a result, for one certain polarization state and one plane of incidence, $n_{\text{eff}}(\lambda)$ is observed to be almost independent of the angle of incidence, which is another step toward optical isotropy. For this special case, the practical realization of a one-dimensionally (cylindrical) focusing lens based on a Swiss cross metamaterial seems feasible if illuminated with TE-polarized light.

Finally we will relate those results to the current state of literature. Again, to compare the necessary effort regarding measurement techniques and the different metamaterial regimes, the considerations will be constrained to the optical spectral range. Remarkably, there were only few attempts where optical metamaterials were experimentally probed by obliquely incident fields and for different polarizations. Initial reports regarded split ring resonator metamaterials, since for such metaatoms oblique incidence is necessarily required to couple to “magnetic resonances”. This was shown in the first place for a discrete set of incidence angles [57]. The presumably first transmittance spectra for a tilted negative-index optical fishnet were raised by Dolling et al. [45]. However, systematic and finely resolved data of the angular response of optical metamaterials was lacking until the publication of our manuscript [78]. After that similar investigations were reported [79]-[84]. Generally speaking, they consistently confirm changes in the optical spectra at varying angles of incidence and different input polarizations. In particular, Lin and Roberts reported on transmission measurements of cross-shaped apertures in a single metallic layer [84] which coincide very nicely with the results shown in Fig. 3.5. Taking all together, it is imperative to point out that spatial dispersion governs the optical properties of the majority of current planar optical metamaterials [75, 76]. Alternative concepts claiming for an approximate isotropic negative-index [85, 95, 96] still lacked experimental realization during the compilation of this thesis.

3.3.4 Angular resolved effective properties and application limits

Basing on the remarkable agreement between experiments and numerics, and for the first time to the best of my knowledge, it was possible to draw conclusions concerning the angular

dependency of the effective properties that are commonly ascribed to optical metamaterials. An extension of the retrieval procedure was proposed as a valuable tool to determine effective optical properties at oblique incidence [72]. Relying on this approach, the dependence of a negative index on the angle of incidence of the incoming light could be examined both experimentally and theoretically at the example of the Swiss cross metamaterial. This procedure was performed by Christoph Menzel and shall only be mentioned because of the close context to this thesis. The main results are shown in Fig. 3 of [78]. Note that n_{eff} is understood as an alternative representation of the effective propagation constant k_z according to $n_{\text{eff}} = c/\omega\sqrt{k_x^2 + k_y^2 + k_z^2}$, inferring no supplementary information. In essence, the derived effective optical properties depend both on the polarization state and the angle of incidence reflecting the effect of spatial dispersion on the optical response [76]. Therefore, $\epsilon_{\text{eff}}(\omega)$ and $\mu_{\text{eff}}(\omega)$ lose their meaning since they have to be determined for every angle of incidence and polarization state separately. Such angular resolved effective properties cannot be considered as material parameters in the classical sense. They may only serve as a simplified description of light propagation inside the metamaterial and have to be understood as wave parameters [76, 77]. Any attempt to use the Swiss cross as an imaging device will be limited by this variation [202]. However, for the special case of TE polarization and $\Phi=0^\circ$ as discussed above, negative refraction is observed to be almost independent on the angle of incidence Θ .

Chapter summary

In order to experimentally investigate optical metamaterials, an effective and reproducible nanostructure technology had to be established in the first place. We demonstrated the fabrication of mixed metal and dielectric patterns with feature sizes down to 80 nm. The usage of a variable-shaped electron beam pattern generator and a chemically amplified electron beam resist, which is a novelty for the field, has been shown to effectively speed up the fabrication of planar metamaterials. With this technique, one major constraint of current planar negative-index metamaterials in the optical spectral range, namely their strong dependence on the state of polarization of the interacting radiation, could be addressed. A polarization-insensitive spectral response had not been achieved for this special class of metamaterials, though it would be desirable for potential applications. The insensitivity of polarization was explored basing solely on symmetry considerations of a unit cell called the Swiss cross metamaterial. The universality of this property for all states of polarization at normal incidence constituted a novelty in the optical spectral domain. Furthermore, the dependence of an effective refractive index on the angle of incidence of the incoming light was examined both experimentally and theoretically. Our findings strongly suggest that the effective refractive index of current planar metamaterials should rather be considered as a

wave parameter comprising the orientation of both the medium and the wave illumination scheme.

4 Three-dimensional chiral metaatoms for huge optical activity

The increase of the complexity of the geometrical shape of metaatoms turned out to be a key feature to access exceedingly high optical activity. As defined in Sec. 2.4.4, optical activity is observed in systems containing chiral objects and is quantitatively expressed in terms of circular dichroism δ and circular birefringence Σ . In this chapter, a three-dimensional, chiral, metallic metaatom called loop-wire is demonstrated to operate for visible and near-infrared wavelengths. The constituting metamaterial was fabricated by the stacking of multiple single layers of complexly shaped nanostructures which together form the metaatoms. Combining spectroscopic and interferometric characterization techniques, the full complex transmission response of the loop-wire metamaterial was accessed. This complete set of experimental data allowed to quantify circular dichroism, circular birefringence and polarization eigenstates without any additional numerical input. Particularly, the polarization output state after propagation through the loop-wire metamaterial could directly be calculated for any excitation configuration. Driven into resonance, one single layer of the fabricated metamaterial yielded, among others, pure polarization azimuth rotation exceeding 50° at $\lambda = 1.08 \mu\text{m}$ in the absence of linear dichroism and linear birefringence. This experimentally obtained value is larger than that of any linear, passive and reciprocal medium reported to date.

4.1 Optical activity from chiral metaatoms

4.1.1 Quasi-planar and three-dimensional chiral metamaterials

As it was outlined in Sec. 2.4.4, chiral objects are supposed to be three-dimensional objects by definition. Nevertheless, due to the inherently planar patterned surfaces as they are obtained from most state-of-the-art nanofabrication technologies (see Sec. 2.6), the majority of optical metamaterials consists of nanostructured single thin films. Though these two aspects seem to be incompatible in the context of the creation of chiral metamaterials, there have been some successful efforts to constrain chirality to two dimensions. Following a seminal paper by Papakostas et al. [9], so-called quasi-planar chiral metamaterials were introduced. They consist of planar metaatoms on a flat substrate that cannot be superimposed with

their in-plane mirror images without being lifted off the plane. These metaatoms are, e.g. gammadions or rosettes sculptured in a thin metal film [203]-[207]. Though this class of metamaterials has proven to produce higher optical activity than naturally occurring media¹, it is noteworthy that the specific spatial arrangement of their metaatoms is essential for their usability. In fact, only the presence of the substrate breaks the mirror symmetry in light propagation direction and manifests the chiral nature of the overall system comprising metaatoms and substrate [70, 203, 204]. If, for instance, such essentially two-dimensional metaatoms were lifted from the substrate and put in a random or amorphous spatial arrangement, any evidence of optical activity would be lost.

In order to investigate truly three-dimensional chiral metaatoms for the optical domain, other fabrication techniques are called for. Multi-photon photopolymerization (see Sec. 2.6.1) appears to be a promising candidate, if its spatial resolution can be further increased [127]. The same perspective holds for the very recently introduced method of membrane projection lithography [160], which combines pre-patterned three-dimensional unit cells with the benefits of well-established thin-film deposition techniques. The most straightforward way to create three-dimensional metaatoms is the multiple stacking of two nanostructured layers containing two either quasi-planar chiral or even achiral metaatoms. This ansatz has led to bi-layered chiral structures [209]-[216]. Compared to quasi-planar chiral metamaterials, their optical activity is significantly higher due to the excitation of antisymmetric plasmonic modes² in the two metallic layers [211]-[213]. Before the compilation of this thesis, the largest rotation angle per unit propagation length was observed for a suitable lateral and vertical arrangement of two layers of coupled split-ring resonators, amounting to 30.43° at an operational wavelength of $3\ \mu\text{m}$ [215].

4.1.2 Single-block three-dimensional chiral metaatoms

As opposed to quasi-planar and bi-layered chiral metamaterials, there is a third class built of inherently three-dimensional metaatoms consisting of a single structural element per unit cell only. Such single-block metaatoms retain their strength to modify the polarization state of light even if they were put in a random arrangement, just like natural glucose molecules in solution. To date, very few single-block chiral metaatoms operating in the terahertz [10] and mid-infrared wavelength domains [35] have been experimentally realized, and particularly their operation at shorter wavelengths has been elusive so far. This state of the art is mainly due to technological challenges associated with the purposeful creation of three-dimensional

¹A complementary approach has shown that the effect can be explained in terms of elliptical dichroism without requiring chirality [208].

²The underlying resonance mechanism is equivalent to the magnetic resonance in double-fishnet structures (see Sec. 3.1.1).

objects on the nanoscale [127, 161], despite of some recent advances in the bottom-up synthesis [217] and modeling [218] of noble metal nanoparticles in chiral molecules. It follows that there is a lack of experimental evidence concerning single-block chiral metaatoms in a simple analogy to glucose molecules. One may presume that the true potential of optical activity in artificial plasmonic media was not fully revealed yet. Additionally, single-block chiral metaatoms will retain this feature when arranged in spatially disordered configurations, as they can be obtained from self-assembling or chemically randomized fabrication schemes [164]-[168].

4.1.3 The loop-wire metaatom

One particular metamaterial design proposal addressing this issue is the so-called loop-wire metaatom [219]. This structure consists of a cut-wire split-ring resonator combination. It was also called modified Omega-particle [220] in the context of artificial electromagnetic media, though earlier investigations specified it as wire braid [221]. The loop-wire metaatom, its excitation configuration and the respective definition of the coordinate system are schematically depicted in Fig. 4.1.

The loop-wire metaatom exhibits only a $C_{2,y}$ rotational symmetry, while mirror symmetries are completely absent. Thus optical activity can be anticipated to occur for arbitrary oblique light incidence and hence also for a random arrangement of the metaatoms in a passive host, in analogy to solubilized glucose molecules. The design is based on a joint excitability of an electric and a magnetic dipole resonance (4.1a). Basically, a linearly x -polarized incoming wave will resonantly excite an oscillating current in the metaatom by driving the wires. The current flow is directed into a coupled split-ring resonator (the loop) and excites a magnetic dipole response [222]. The field scattered from the overall loop-wire metaatom is accompanied by a strong electric field component that is polarized normal to the incident polarization state. This low-frequency resonance may also be called antisymmetric mode since the electron current flows in the two arms of the split-ring resonators are π out of phase. Equivalently, a symmetric mode is sustained by the particle under the same excitation conditions at higher frequencies (4.1b). Here the currents in the two arms of the split ring co-oscillate, which renders the emitted radiation to be accompanied by an effective electric dipole perpendicularly oriented to the incoming x -polarized electric field. Accordingly, both eigenmodes have a partial conversion of the electric field component into the perpendicular polarization state in common. In essence, this loop-wire particle is expected to show optical activity in terms of a combination of circular birefringence and circular dichroism in a broad spectral domain. As a result, elliptically polarized light will be perceived in the optical far-field.

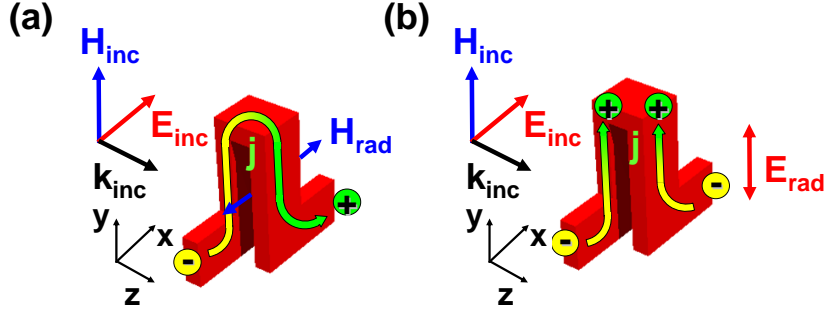


Fig. 4.1: Definition of the coordinate system and schematic view of the loop-wire metaatom with its two dominating plasmonic eigenmodes. The red-green arrows indicate the induced electron current flow directions. a) Low-frequency mode associated with the excitation of a dominant magnetic dipole response oscillating parallel to the incoming electric field vector. b) High-frequency mode associated with the excitation of a dominant electric dipole response oscillating perpendicular to the incoming electric field vector. Higher order modes are equally supported, e.g. when the induced electron currents in the structure suffer from an increasing number of nodes.

It is stressed that the chiral nature of the loop-wire metamaterial is purely structural, i.e. only dependent on the very shape of its constituting plasmonic metaatoms. In order to eliminate optical activity stemming either from substrate induced symmetry breaking or from unintentional twists between adjacent layers during fabrication, it is imperative to embed the metaatoms in a homogeneous environment with a dielectric constant matched to the substrate. This task was accomplished in a $2\text{ mm} \times 2\text{ mm}$ array of loop-wire metaatoms, fabricated according to the procedure described in the next section.

4.2 Multilayer nanofabrication technology

To fabricate an optical loop-wire metamaterial as well as the sample described in chapter 5, the stacking of a distinct number of lithographically generated nanostructures [129, 134] was applied. To do so, the first layer was equipped with additional alignment marks to allow for a precise lateral alignment of subsequent process lithography steps. For multilayer fabrication we preferred the usage of PMMA instead of FEP171 as EBL resist. The reason for this choice was that the necessary gold conductance layer could be conveniently deposited before and removed after each single EBL exposure step³. After the finishing of the first single layer as described in Sec. 3.2, this layer was planarized by means of hydrogen silsesquioxane (HSQ; xR-1541:MIBK 1:1 from *Dow Corning*, sometimes also called spin-on glass). We adapted a process optimized for obtaining superpolished substrates for use in the EUV region of light [132]. The HSQ solution was spin coated such that a 120 nm thick film would have

³Alternatively, the FEP171 resist could have been used for multilayer fabrication as well, provided that the necessary ITO conductance layer underneath was reliably grounded during each of the EBL steps.

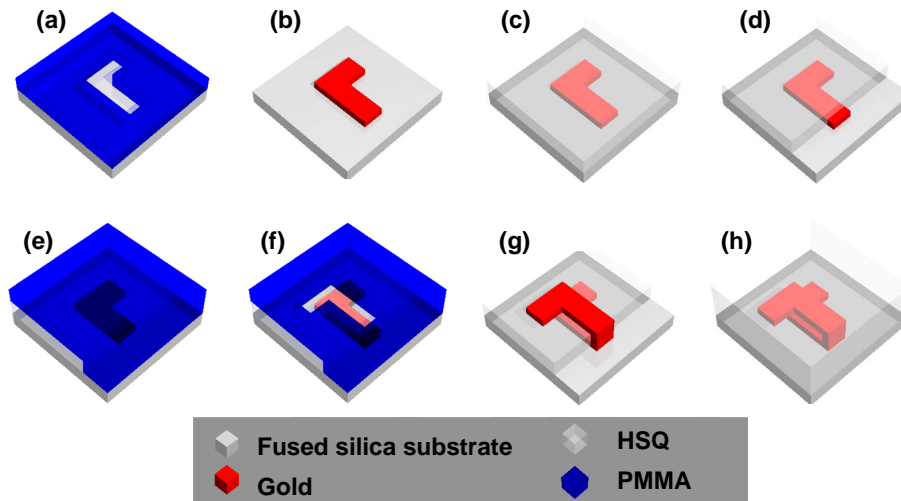


Fig. 4.2: Simplified schematic of the fabrication of a single loop-wire metaatom. a) L-shaped hole defined in PMMA via EBL on a fused silica substrate. b) Thermal evaporation and lift-off of the bottom L-shaped gold metaatom. c) Planarization with HSQ, tempering, UV-curing and RIBE to an overall thickness of 110 nm with respect to the substrate plane. d) Groove defined by EBL, and etched via ICP and RIBE to lay open a part of the long arm of the L-shaped gold particle. e) Spin coating with PMMA, planarizing the whole structure. f) Conjugated L-shaped hole defined in PMMA by EBL. g) Thermal evaporation and lift-off of the upper L-shaped gold metaatom. The groove prepared in the second EBL-step enables a metal connection with the lower L-shaped particle. h) Planarization with HSQ followed by tempering and UV-curing to surround the loop-wire metaatom with a homogeneous dielectric environment.

been obtained on a planar substrate. Then the samples were baked for 2 min at 120 °C and for 5 min at 170 °C on a hot plate to remove residual solvents. A curing step was performed with ultraviolet light for 1 hour. The benefit of HSQ is that the finished coating is mechanically stable and optically nearly equivalent to the silica substrate underneath. The effect of planarization was checked with atomic force microscopy (AFM). Before planarization, the peak-to-valley height of the gold nanostructures was approximately 50 nm. After planarization we observed residual modulations with a peak-to-valley height of less than 8 nm. In some cases, the modulation was in the range of the detectable surface roughness which corresponded to optimal planarization. After this step, the fabrication of another layer on top could be done as described above. The samples reported in the current and in the following chapter consist of three and two individually structured layers, respectively.

Since the fabrication process of the loop-wire metaatoms was rather demanding (it comprised three times EBL, two times metal lift-off and numerous dry etching steps), a concise description shall be devoted to this technology in particular. The whole process chain is schematically displayed in Fig. 4.2. Basically, two metallic nanoparticles (called L-structures in the following) with two orthogonally oriented arms of different lengths are placed on top of each other and separated by a dielectric spacer. They are arranged such that the two

long arms are parallel aligned and the two short arms are directed in opposite directions. The two long arms are connected at their extremities, thus forming a loop-wire metaatom altogether. The process flow for a periodic array of loop-wire structures begins with the definition of an L-shaped hole in PMMA by EBL (Fig. 4.2a) followed by a lift-off step to obtain the first (bottom) layer with an L-shaped, 50 nm high nanoparticle made of gold (Fig. 4.2b). The layer was planarized with HSQ and back-etched with CF_4 -based RIBE until a distance of 110 nm from the plane of the substrate was reached. At this stage, a quasi-planar surface covering the L-structures was obtained (Fig. 4.2c). After depositions of 20 nm chromium and 200 nm FEP171 resist, a second EBL-step was performed to define a groove perpendicular to the long arm of the L-shaped nanoparticles. This groove was transferred through the chromium via ICP etching and into the cured HSQ protection layer via RIBE. The advancement of this etching was controlled by an SEM inspections. The latter two steps were repeated until the HSQ layer was removed from the extremity of the longer arm of the gold L-structure (Fig.4.2d). Spin-coating with a another bilayer of PMMA covered the whole structure including the groove in the HSQ (Fig.4.2e). The third and last EBL step defined an L-shaped hole in the PMMA with the shorter arm of the structure pointing in the opposite direction (Fig.4.2f). Subsequent thermal evaporation and lift-off of another 50 nm gold layer led to the formation of the top L-structure connected to the lower L-nanoparticle at the extremity of its longer arm (Fig.4.2g). The alignment accuracy between top and bottom layer was better than 20 nm. Finally, the whole structure was embedded and planarized with HSQ to ensure a homogeneous dielectric surrounding of the metaatoms (Fig.4.2h). Taking altogether, this process flow allowed for the fabrication of an array of single-block, three-dimensional metaatoms called loop-wire particles with smallest feature sizes of less than 100 nm. Note that the obtained structures are about one order of magnitude smaller than contemporary three-dimensional and single-block metaatoms fabricated by top-down approaches [10]. With appropriate modifications, this technology can be applied to other optical metamaterial designs as well.

4.3 Experimental characterization of the loop-wire metamaterial

The geometry of the fabricated metaatoms together with their geometrical parameters as deduced from topographical measurements are given in Fig. 4.3a. The metaatoms were periodically arranged on a square lattice with periods of 500 nm in both lateral directions. Taking into account the refractive index of the substrate ($n=1.44$), this assured that the structures were smaller than the wavelength of light for $\lambda > 500 \text{ nm} \cdot 1.44 = 720 \text{ nm}$. Their height, i.e. the spatial extension along the principal light propagation direction amounts to

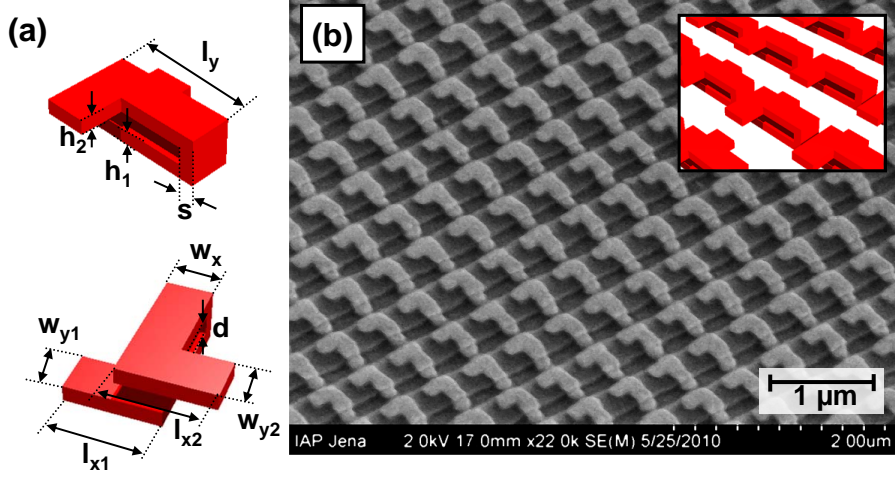


Fig. 4.3: a) Two sketches of the loop-wire metaatom from two different perspectives with the definition of all geometrical parameters as used in the simulations: $l_{x1} = 280$ nm, $l_{x2} = 290$ nm, $l_y = 420$ nm, $w_x = w_{y1} = w_{y2} = 155$ nm, $h_1 = h_2 = 50$ nm, $d = 60$ nm, $s = 50$ nm. b) A tilted view scanning electron microscopy (SEM) image of a manufactured loop-wire array with a periodic lattice of 500 nm in both lateral directions. The inset shows a corresponding schematic of the same arrangement of the metaatoms if they were freely pending in air.

160 nm. The absolute values of the other geometrical parameters of the metaatoms are of minor relevance here, since the fabricated loop-wire particle was not geometrically optimized to meet, e.g., a specific target value of optical activity. An oblique incidence SEM micrograph showing the loop-wire metaatoms prior to planarization (corresponding to the fabrication status of Fig. 4.2g) is shown in Fig. 4.3b and proves the high quality of the sample, though small structural deviations from the idealized design are observable. Their influence on the optical properties will be discussed in Sec. 4.5.

The loop-wire metamaterial was experimentally characterized for wavelengths ranging from $0.65 \mu\text{m}$ to $1.7 \mu\text{m}$ both by conventional optical far-field transmission spectroscopy at normal incidence (see Sec. 2.7.1) and an interferometric measurement of the absolute phase delays⁴ (see Sec. 2.7.3). Utilizing the notation of the four coefficients of the Jones matrix T_{ij} as defined in Eq. 2.28 and their squared moduli $t_{ij} = |T_{ij}|^2$, the measurement results are shown in Figs. 4.4a and b. They suggest a vivid spectral dispersion of the loop-wire metamaterial over the entire spectral range of interest. In particular, we note a pronounced resonant dip in the transmittance spectrum at a wavelength of about $1.08 \mu\text{m}$ for both transverse polarization directions, which can be most likely associated to the strong coupling of a plasmonic eigenmode to the external illumination. It will be shown later on that this

⁴The interferometric setup was only ready to be operated during the final working period of this thesis. Accordingly and in a chronological order, among all metamaterials reported here, only the loop-wire structure was interferometrically characterized.

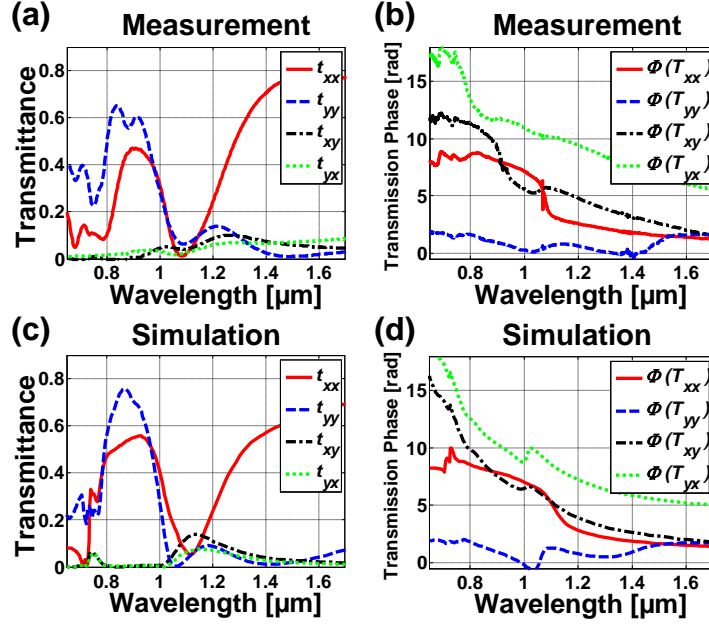


Fig. 4.4: Comparison of measured and simulated transmittance and transmission phase delay spectra of the fabricated loop-wire metamaterial. a) Measured transmittances and b) measured phase delays of the four Jones matrix coefficients. c) Simulated transmittances and d) simulated phase delays of the four Jones matrix coefficients.

resonance is also linked to record-breaking optical activity evoked by the metamaterial⁵.

To comply with the standard of optical metamaterial characterization, the complex coefficients T_{ij} were additionally computed by means of the FMM (see Sec. 2.5.1) and are shown in comparison to the experimental data in Figs. 4.4c and d. In the simulation, the loop-wire structure was described according to the geometry given in Fig. 4.3a with the inclusion of an appropriate rounding of sharp edges. The comparison of the measured to the simulated data reveals a qualitatively convincing agreement, in particular the width and the strength of the most prominent resonance features are quite well reproduced. This agreement makes us confident in stating that our fabricated loop-wire array meets the basic topographical and spectral characteristics of the design. Minor deviations are attributed to an approximate parametrization of the complex geometry of the loop-wire metaatoms in the simulation when compared to their fabricated counterparts. The suspected structural imperfections are due to inherent limitations of the applied nanofabrication technology, and cannot be fully accounted for by the FMM simulation. Though the agreement between measurement and simulation could probably be further improved, such an improvement will not yield addi-

⁵It is not intended here to establish an unambiguous correlation between the plasmonic eigenmodes of the metaatoms and the distinct resonant features observed in the spectra. The loop-wire metaatom is rather understood as a single-block complex structure that sustains numerous hybridized plasmonic modes whose respective excitation strengths depend critically on the specific orientation of the polarization state and the wavelength of incoming electromagnetic radiation.

tional physical insight since we aim to proceed our investigation by exclusively relying on the experimental data⁶.

As a particular aspect, we wish to mention that the off-diagonal elements T_{xy} and T_{yx} corresponding to the black dashed-dotted and green dotted lines in Figs.4.4a and b are generally not equal over the entire spectral domain under investigation. Recalling the arguments of Sec. 2.4.3, we notice here the signature of broadband polarization conversion dichroism and asymmetric transmission of linearly polarized light originating from spatial symmetry breaking in propagation direction (see Sec. 5.1.2 for further details). Symmetry breaking is unintentionally present due to structural non-idealities of our fabricated loop-wire metamaterial, although it can be partly reproduced by the FMM (Figs. 4.4c and d).

4.4 Optical activity of the loop-wire metamaterial

4.4.1 Assessment of the complex Jones matrix

The curves shown in Figs. 4.4a and b represent the complete set of data to characterize the transmission properties of the loop-wire metamaterial. If we assume the metamaterial to be linear, reciprocal and non-depolarizing, the data shown in Figs. 4.4a and b allows for an unambiguous determination of the complex Jones matrix in the linear polarization base by purely experimental means. Relying on the definitions given in Sec. 2.4.2, the real and imaginary parts of T_{ij} are plotted in Fig. 4.5. Most notably, by means of our combined spectroscopic/interferometric approach, we access also its off-diagonal elements T_{xy} and T_{yx} . To the best of my knowledge, this complete set of data has never been experimentally raised before for an optical metamaterial.

4.4.2 Experimental validation of the Jones matrix

In order to check the validity of the measured Jones matrix, a broadband spectroscopic measurement with circularly polarized light was additionally performed. Its results could be analytically cross-checked on the basis of the Jones calculus to probe for the accuracy of the coefficients T_{ij} as shown in Fig. 4.5. The setup described in Sec. 2.7.1 was supplemented with a quarter wave plate to transmit either LCP or RCP light through the loop-wire metamaterial, in analogy to similar measurements of circular dichroism [35, 215]. The emerging polarization state of light was further analyzed by a linear polarizer behind the sample, dis-

⁶To be precise, structural imperfections in the z -directions of the metaatoms as anticipated from Fig. 4.3b, potential lateral misalignment of subsequent layers, potential imperfect planarization of the HSQ and its potential dispersion are not taken into account.

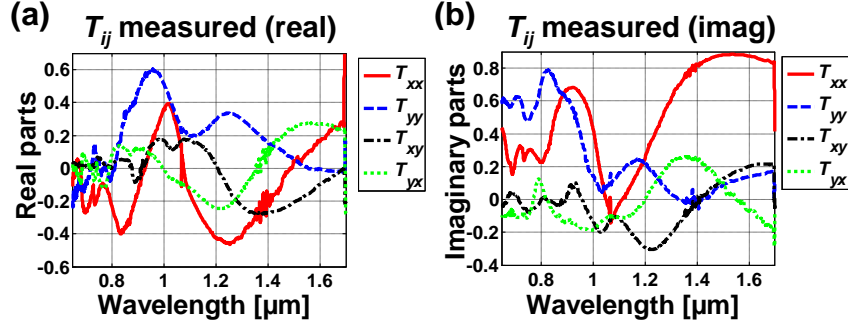


Fig. 4.5: a) Real and b) imaginary parts of the coefficients T_{ij} of the linear Jones matrix \hat{T}_{lin} of the loop-wire metamaterial as determined from measurements. The four elements T_{ij} are represented by differently colored curves.

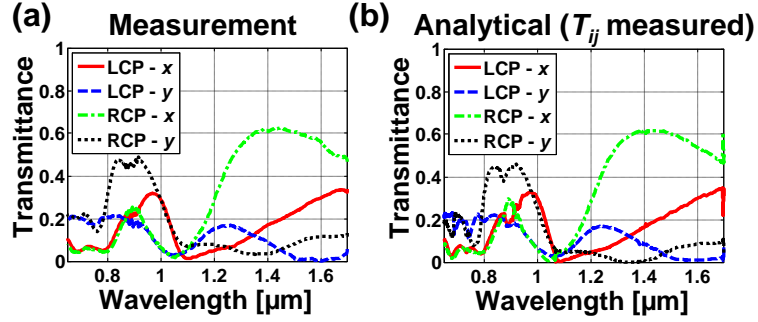


Fig. 4.6: a) Directly measured transmittances of the loop-wire metamaterial for circularly polarized light and b) corresponding transmittances as analytically calculated from the experimentally determined Jones matrix \hat{T}_{lin} . The different colors indicate four polarization combinations of the incoming polarization state and the linear polarizer behind the metamaterial: red solid (blue dashed) line - LCP incident light and analyzer aligned in $x(y)$ -direction; green dashed-dotted (black dotted) line - RCP incident light and analyzer aligned in $x(y)$ -direction.

criminating the x - and y -polarization components. The measured transmittances for the four possible combinations of polarization configurations are shown in Fig. 4.6a. For comparison, this setup is modeled by straightforward multiplication of the experimentally determined Jones matrix of the loop-wire metamaterial with the respective well-known Jones matrices of all polarization elements involved (Fig. 4.6b). It is striking that the overall agreement of both approaches is almost perfect. This agreement allows to rule out three potential sources of error:

- First, the alignment of all polarization-manipulating elements in the optical beam path is always non-ideal within the limits of experimental accuracy, but was shown to be of minor relevance here.
- Second, potential differences between the measured and calculated data would have been a clear indication for a degrade of the coherence in polarization from the nanostructures, requiring the Jones calculus to be replaced in favor of the Müller matrix formalism [223]. Accordingly, depolarizing effects are negligible in the loop-wire meta-

material. This finding constitutes a retrospective justification of the assumption of non-depolarizability.

- Third, using the measured coefficients T_{ij} in the context of the classical Jones calculus was validated to be an equivalent alternative to the experiment itself. This validation was the original aim of the experiment with circularly polarized light.

We interpret these results as a solid basis to conclude that the measured Jones matrix \hat{T}_{lin} accurately represents the optical response of the fabricated loop-wire metamaterial. Taking all together, in the following we exclusively rely on \hat{T}_{lin} to quantify its optical activity.

4.4.3 Circular dichroism and circular birefringence from the loop-wire metamaterial

Optically active media are most effectively characterized in terms of circular dichroism δ and circular birefringence Σ (see Sec. 2.4.4). In order to do so, it is convenient to transform \hat{T}_{lin} into the circular polarization base \hat{T}_{circ} according to Eq. 2.33. Depending only on the two diagonal elements T_{++} and T_{--} of \hat{T}_{circ} , δ and Σ are obtained from Eqs. 2.41 and 2.42. Note again that both quantities as derived for the loop-wire metaatoms are solely based on measurements without additional numerical input.

The plots of δ and Σ are shown in Fig. 4.7. As expected, the strongly modulated optical response of the metamaterial manifests itself in a remarkable impact on the polarization state of incoming light, yielding strongly fluctuating values of both circular dichroism and birefringence over the entire spectral range under consideration. In Fig. 4.7a two distinct extrema of $\delta=-0.3$ (around $\lambda=0.9\ \mu\text{m}$) and $\delta=-0.45$ (around $\lambda=1.5\ \mu\text{m}$) can be identified. At these wavelengths the difference between the magnitudes of the two diagonal elements of the Jones matrix in the circular base is maximized. The wavelengths corresponding to the three roots of δ , i.e. $\delta=0$, are found at $\lambda=0.79\ \mu\text{m}$, $\lambda=0.98\ \mu\text{m}$ and $\lambda=1.25\ \mu\text{m}$. Their significance will be detailed below. Even more eye-catching from Fig. 4.7b, Σ features a strong dispersion at wavelengths between $1.0\ \mu\text{m}$ and $1.5\ \mu\text{m}$, allowing to access the full angular range of the polarization azimuth.

We will now discuss the influence of the structural anisotropy of the loop-wire metaatoms. As they exhibit no $C_{4,z}$ symmetry, they are not polarization-independent for normal incidence. This design-related anisotropy causes linear birefringence in addition to the originally desired optical activity. It is emphasized that δ and Σ are deduced from the circular polarization base according to the above definitions. Therefore these values imply an averaging over all possible linear polarization states of incoming light. In our case the criterion $\delta=0$ does not a priori yield a pure rotation of the polarization state for linearly polarized incoming light, as it is the case for $C_{4,z}$ symmetric chiral metaatoms with circular polarization

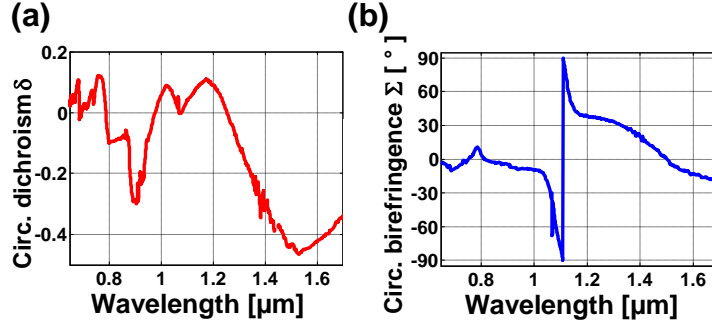


Fig. 4.7: a) Circular dichroism δ and b) circular birefringence Σ of the loop-wire metamaterial as calculated from the experimentally determined Jones matrix.

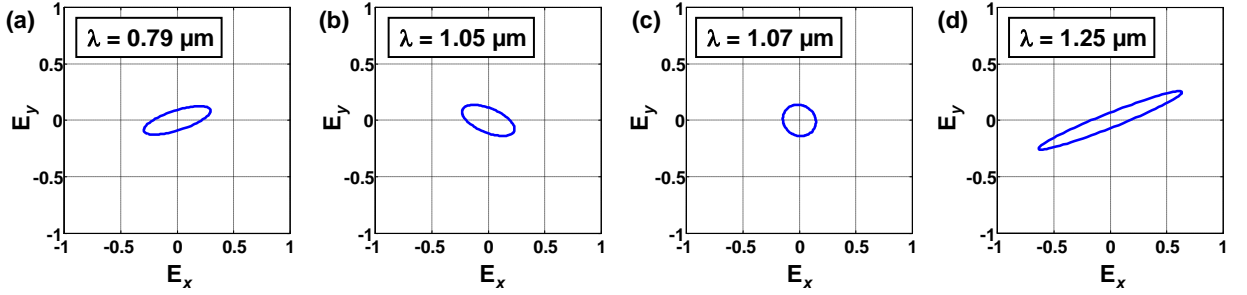


Fig. 4.8: Output polarization states of x -polarized incoming waves after propagation through the periodic array of the loop-wire metamaterial for selected discrete wavelengths as calculated from the measured data. Note that a) and d) correspond to $\delta[\lambda=0.79 \mu\text{m}]=0$ and $\delta[\lambda=1.25 \mu\text{m}]=0$.

eigenstates [209]–[214]. In fact, the output polarization state generally becomes elliptical due to non-zero values of T_{+-} and T_{-+} . This is demonstrated by directly calculating the polarization state upon transmission through the metamaterial by inserting the measured \hat{T}_{lin} into Eq. 2.28. The incoming wave was chosen to be linearly polarized in x -direction to predominantly excite the x -aligned loops, matching the resonance excitation conditions of the loop-wire metaatoms as illustrated in Fig. 4.1. The output polarization states are shown exemplarily for selected wavelengths of $0.79 \mu\text{m}$, $1.05 \mu\text{m}$, $1.07 \mu\text{m}$ and $1.25 \mu\text{m}$ in Fig. 4.8. Apparently, there is no obvious correlation between the output polarization state and the roots of δ , which exist, e.g. at $\lambda=0.79 \mu\text{m}$ (corresponding to Fig. 4.8a) and $\lambda=1.25 \mu\text{m}$ (corresponding to Fig. 4.8d). Such rather arbitrary ellipticity is usually undesired if it comes to potential applications of three-dimensional chiral metaatoms.

In a gedankenexperiment, the anisotropy of the metamaterial could be compensated easily by constructing a $C_{4,z}$ symmetric, polarization-independent supercell consisting of four metaatoms with an appropriate in-plane rotation [10, 215]. The off-diagonal elements T_{+-} and T_{-+} of the associated Jones matrix would then be identically zero [224], while (under the assumption of negligible interaction between adjacent loop-wire particles) the diagonal elements T_{++} and T_{--} would not be affected upon this rearrangement, i.e. $T_{++} = \langle T_{++} \rangle$

and $T_{--} = \langle T_{--} \rangle^7$. It follows that $C_{4,z}$ symmetrically oriented loop-wire metaatoms would yield pure circular birefringence, i.e. polarization azimuth rotation without linear birefringence and linear dichroism, at all wavelengths where $\delta=0$. Particularly, this pure circular birefringence would amount to $\Sigma=36.15^\circ$ at a wavelength around $1.25 \mu\text{m}$. This value would be the largest rotation angle of an optically active metamaterial reported to date, exceeding the previous record [215]. The normalization to the thickness of one metaatom layer (160 nm) would deliver a specific rotation of $2.25 \cdot 10^5 \text{ }^\circ/\text{mm}$. Compared to, e.g. crystalline quartz [225] ($20 \text{ }^\circ/\text{mm}$), fluorite thin films [226] ($150 \text{ }^\circ/\text{mm}$), cholesteric liquid crystals [227] ($10^3 \text{ }^\circ/\text{mm}$) or artificially sculptured dielectric thin films [228] ($6 \cdot 10^3 \text{ }^\circ/\text{mm}$), the rotation per unit propagation length of the loop-wire metamaterial would be many orders of magnitude larger. In this respect, the loop-wire metaatoms would even outperform the so far highest value of $1.4 \cdot 10^5 \text{ }^\circ/\text{mm}$ reported for a bi-layered chiral metamaterial at longer wavelengths [215].

Furthermore, by scanning for roots of δ at shorter wavelengths but still in the sub-wavelength regime, we find $\Sigma=-10.45^\circ$ and $\Sigma=-8.75^\circ$ at wavelengths of $0.79 \mu\text{m}$ and $0.98 \mu\text{m}$, respectively (Fig. 4.7). Following the above argumentation, pure polarization azimuth rotation would be obtained at these wavelengths in a $C_{4,z}$ symmetric supercell arrangement of loop-wire metaatoms. These results are a strong indication for the potential of polarization control in nanoscale chiral structures even at the edge of the visible spectral domain⁸.

4.4.4 Pure polarization azimuth rotation from the loop-wire metamaterial

Nevertheless, pure azimuth rotation can also be obtained from the experimentally realized periodic loop-wire array without requiring a rearrangement of the metaatoms. To prove this statement, we again use Eq. 2.28 to directly calculate the transmitted polarization state

⁷Alternatively, each of the loop-wire particles could be randomly rotated around the z -axis, thus forming a statistical ensemble of metaatoms with random orientation in the xy -plane. In the Jones calculus, such a rotation can be easily mimicked by a multiplication of the Jones matrix with the standard rotation matrix and its inverse. Assuming weak electromagnetic interaction between adjacent loop-wire metaatoms, the whole ensemble of randomly rotated loop-wire metaatoms would then be represented by the integral over all possible values of in-plane rotations of \hat{T}_{circ} from 0 to 2π [220]. The mathematical result would be equivalent to the $C_{4,z}$ symmetric arrangement.

⁸We note that the investigation of a three-dimensional bulk chiral metamaterial composed of metaatoms whose orientations are completely randomized in space, would require their Jones matrices to be known for all angles of incidence. Since the loop-wire particle holds great promise to exhibit huge optical activity regardless of its orientation, this investigation may be subject to future work.

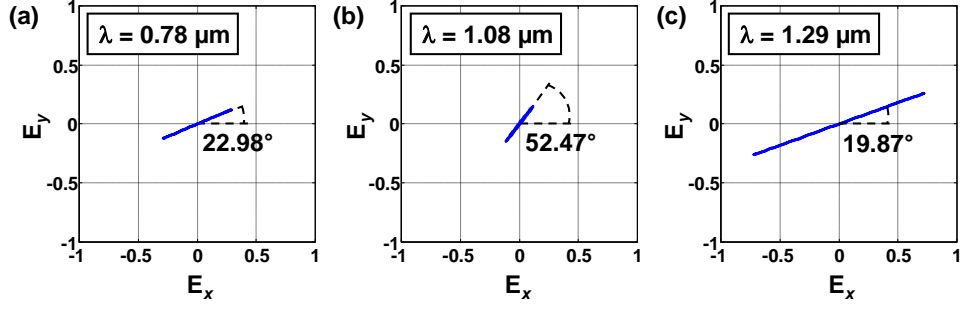


Fig. 4.9: Linear output polarization states of x -polarized incoming waves after propagation through the periodic array of the loop-wire metamaterial for selected discrete wavelengths as calculated from the measured data. The numbers indicate the angle of polarization rotation with respect to the x -axis.

under the same excitation conditions as in the previous section⁹. According to Fig. 4.9, linear polarization is obtained at wavelengths of $0.78 \mu\text{m}$, $1.08 \mu\text{m}$ and $1.29 \mu\text{m}$. The corresponding rotation values of the polarization azimuth read as 22.98° , 52.47° and 19.87° , respectively. In particular, the polarization rotation of 52.47° at $\lambda=1.08 \mu\text{m}$ is higher than the one extracted for the case of a $C_{4,z}$ symmetric arrangement (see Sec. 4.4.3). Hence it is also higher than any other documented value for linear, passive and reciprocal optical media. The according specific rotation, when normalized to the thickness of 160 nm of the metaatoms, amounts to $3.28 \cdot 10^5 / \text{mm}$.

The price one has to pay for such a giant polarization rotation are high optical losses due to the excitation of a plasmonic resonance in the metaatoms. From Fig. 4.4a it can be deduced that the transmitted intensity (the sum of the red solid and the green dotted line) for incoming x -polarization is below 4% at this particular wavelength. We note that there is still room for improvement to decrease the absorption while the main effect may be retained. This could be achieved, as the short history of metamaterials suggests, by the fine-tuning of the free geometrical parameters of the geometry of the loop-wire metaatom.

4.5 Visualization of polarization eigenstates

We proceed in analyzing the polarization eigenstates, i.e. the two polarization states that are not altered upon propagation through the fabricated loop-wire metaatoms. Recently, it was shown that the specific polarization eigenstates of any metamaterial are bijectively related to its spatial symmetry [44]. As mentioned before, ideal loop-wire metaatoms that

⁹Apart from the original design guideline of the loop-wire metaatom (Fig. 4.1) there is no actual need to restrict this investigation to x -polarized incoming light. In fact, pure polarization azimuth rotation in the sense above is found also for other wavelengths, if the incoming polarization azimuth is rotated along the optical axis with respect to the metamaterial (or vice versa).

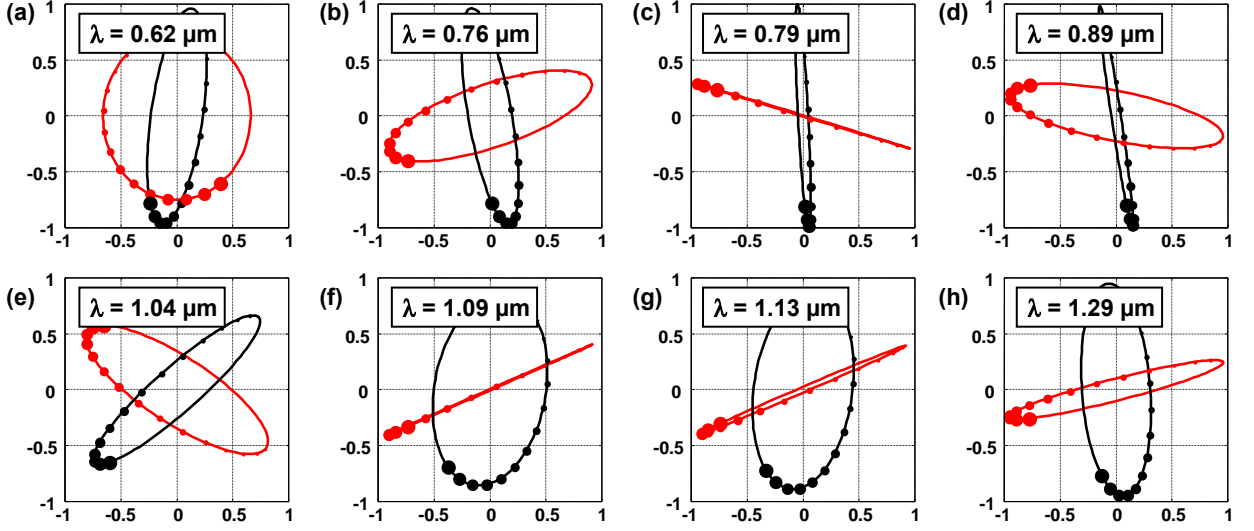


Fig. 4.10: Eigenstates of polarization as calculated from the measured data for selected discrete wavelengths. The sense of rotation is indicated by increasing spot sizes. The eigenstates are found to be a), b), e), h) elliptical and counterrotating; d), g) elliptical and corotating or c), f) combined elliptical and almost linear.

are periodically arranged on a lattice have a $C_{2,y}$ symmetry in the absence of fabrication imperfections. Following the classification scheme from [44], the eigenstates of polarization of such an ideal loop-wire metamaterial are nonorthogonal, elliptical and counterrotating, i.e., they come in pairs of eigenwaves with a clockwise and a counter-clockwise rotation, respectively. However, supposing the $C_{2,y}$ symmetry was broken in the fabricated sample as anticipated already from SEM inspections (Fig. 4.3b), the polarization eigenstates may no more obey predefined mutual relations. In this context, rather exotic eigenstates have been predicted theoretically for low-symmetry metaatoms [14]. In other words, the visualization of the eigenstates of polarization constitutes a valuable and non-invasive tool to judge on the spatial symmetry of a metamaterial.

Since we acquired the full Jones matrix \hat{T}_{lin} , its eigenvectors (i.e. the polarization eigenstates of the metamaterial) can be directly calculated for any wavelength measured. Exemplarily, we present the eigenvectors of \hat{T}_{lin} at selected wavelengths in Fig. 4.10. For the longest part of the spectral range under consideration (for wavelengths ranging from $0.65 \mu\text{m}$ to $1.7 \mu\text{m}$), the eigenvectors are elliptical and counterrotating in agreement with the expectation of a $C_{2,y}$ symmetric metamaterial. Four representative cases are shown in Figs. 4.10a, b, e and h. Nevertheless, at singular wavelengths like $\lambda=0.79 \mu\text{m}$ or $\lambda=1.09 \mu\text{m}$ (Figs. 4.10c and f), one of the polarization ellipses degenerates to a linear state. Furthermore we found also clockwise corotating ellipses, for instance, at $\lambda=0.89 \mu\text{m}$ or $\lambda=1.13 \mu\text{m}$ (Figs. 4.10d and g). In fact, such an observation can only be made in arbitrary complex metamaterials with a $C_{2,z}$ symmetry at most [44], which indicates that the designed $C_{2,y}$ symmetry is broken in the fabricated loop-wire metaatoms. Methodologically, the change of the rotation

sense of the polarization eigenstates can be regarded an optical footprint of spatial symmetry breaking. As it was demonstrated here, the rotation sense enables to indicate differences between the idealized design of a metamaterial and its fabricated counterpart by a purely optical investigation.

Chapter summary

During the last years, artificially nanostructured chiral thin films were shown to exhibit optical activity superior to that of natural media. In this chapter, a novel optical metamaterial built of sub-wavelength, chiral, single-block, three-dimensional metaatoms called loop-wires was enqueued in this line. We have presented its design, top-down fabrication and experimental characterization. By measuring both the amplitudes and the phase delays transmitted through the metamaterial for visible and near-infrared wavelengths, the complex Jones matrix could be unambiguously reconstructed over a broadband spectral range and allowed to access all quantities related to transmissive optical activity phenomena. We deduce from this Jones matrix that one single layer of the loop-wire metaatoms yields huge and broadband optical activity for the accessed spectral range. In particular, if the metaatoms had been assembled in a polarization-independent arrangement, the loop-wire metamaterial would exhibit pure polarization azimuth rotation of 36.15° at a wavelength around $1.25\ \mu\text{m}$. However, for the actually fabricated loop-wire array an even higher value of 52.47° is found at a wavelength around $1.08\ \mu\text{m}$. It is claimed that the loop-wire metamaterial, taking into account its thickness, shows the largest values of pure polarization azimuth rotation among all linear, passive and reciprocal optical media that are known at the time of the writing of this thesis. Furthermore, its polarization eigenstates were directly derived from experimental data and are shown to yield an optical footprint of unintentional spatial symmetry breaking of the metaatoms.

5 Low-symmetry metaatoms for asymmetric transmission

In this chapter we consider metaatoms with an almost minimum symmetry and show how this geometric degree of freedom of design translates into a new physical phenomenon that is genuine to three-dimensional low-symmetry metaatoms at normal light incidence. Relying on a very recent theoretical prediction [44], linear conversion dichroism and, as a direct result, asymmetric transmission for forward and backward propagating linearly polarized light was observed experimentally for the first time in a reciprocal medium.

5.1 Design of low-symmetry metaatoms

Only during the past five years, metamaterial research was extended toward investigations of low-symmetry structures that permit curious phenomena of light propagation. As outlined in Sec. 2.2.2, all common metamaterials can be classified in five categories only, each of them uniquely determined by the symmetries of their metaatoms and their respective periodic lattices, the Jones matrices associated with their transmissive response and their polarization eigenstates [44]. Following this classification, the lowest-symmetry class of metamaterials with almost no inherent symmetry planes is called “arbitrary complex media”. Such media are allowed to have at most a rotational $C_{2,z}$ symmetry in the plane perpendicular to the principal direction (z -axis). Explicitly, the M_{xy} symmetry must be broken. Meeting these requirements, the effect of asymmetric transmission of linearly polarized light at normal incidence gets observable. As described in Sec. 2.4.3, asymmetric transmission is defined as the effect that the power transmitted through a device differs for illumination with a fixed polarization from opposite sides.

It should be mentioned that an alternative means of symmetry breaking is an appropriate tilt of a periodic and lossy sample with respect to the incoming light, i.e., oblique incidence [229]. In this case, a low degree of symmetry is not necessarily inherent to the metamaterial itself; but to the overall setup comprising the metamaterial sample and the illumination scheme altogether. According to [229], asymmetric transmission can occur for any lossy array of particles, when its projection onto the plane normal to the direction of incidence is planar chiral and anisotropic. However, in my opinion such arbitrarily oblique

incidence on a rather unspecific medium does not provide an intuitive physical picture regarding the classification and purposeful design of metaatoms, as it is attempted here.

5.1.1 Asymmetric transmission of circularly polarized light

Studies of other groups concerning the characteristics of light propagation in low-symmetry metamaterials revealed an asymmetric transmission, but solely for circularly polarized light [13, 208, 223, 230, 231]. The idea behind those metamaterials was to evoke a circular conversion dichroism. This quantity corresponds to left-to-right and right-to-left circular polarization conversion efficiencies that are different from each other and reversed for opposite propagation directions of the incident wave. Once obtained, circular conversion dichroism results in directionally asymmetric total transmission of circularly polarized waves. This was demonstrated at quasi-planar chiral metamaterials [9, 70, 232] which are composed of metaatoms without structural variation in the principal propagation direction (see Sec. 4.1.1). The preserved M_{xy} symmetry makes them only chiral in two dimensions [97]. Thus, strictly speaking, the metaatoms reported in [13, 208, 223, 230, 231] are intrinsically achiral in three dimensions since their mirror images are congruent with the structures themselves if operated from the backside (if the influence of the substrate was neglected). This remaining symmetry was exactly the reason why asymmetric transmission had not been observed so far for linearly polarized light.

5.1.2 Asymmetric transmission of linearly polarized light

To observe asymmetric transmission of linearly polarized light, a truly three-dimensional and lowest-symmetry metamaterial is required¹. As mentioned above, the key for obtaining asymmetric transmission in any polarization base is the nearly complete symmetry breaking of the metaatoms - in particular in propagation direction. It is noteworthy that in real metamaterial devices chirality occurs intrinsically because a substrate is practically always present [72, 97]. However this effect acts only as a very weak perturbation and is hardly observable, ruling out its possible exploitation in an application. Hence asymmetric transmission of linearly polarized light could not have been observed, because its magnitude was too weak to be safely attributed to a true physical mechanism rather than to an insufficient measurement accuracy. A substantial enhancement of the symmetry breaking may only be achieved by a pronounced structural modification of the metaatoms in the third dimension.

To meet the aforementioned requirements we designed a simple metaatom that is essentially three-dimensional, anisotropic, chiral, and consists of strongly coupled plasmonic

¹The metaatoms must have no higher symmetry than $C_{2,z}$.

elements. Note that resonant, plasmonic metaatoms considerably enhance the effect of asymmetric transmission but are not required to observe the very effect. To rule out asymmetric effects due to the presence of a substrate, the metaatoms should be completely embedded in an index-matched dielectric host. The geometry of the structure is shown in Figs. 5.1a and b. It consists of two closely spaced layers. The bottom layer comprises an L-shaped metallic particle and the top layer a single nanowire. This combination breaks the symmetry in the principal propagation direction and leads to a genuine three-dimensional chiral metaatom. Furthermore, the whole structure causes an anisotropic response, additionally giving rise to asymmetric transmission of circularly polarized light.

5.2 Experimental observation of asymmetric transmission

The metamaterial was fabricated by stacking two EBL-structured layers as detailed in Sec. 4.2. Each of the two layers was subsequently planarized with HSQ matching the refractive index of the fused silica substrate. Hence it was ensured that the metaatoms were surrounded by a homogeneous dielectric environment compensating for potential bianisotropy stemming from the substrate [233]. For the exposure of the top layer, multiple alignment marks were used to ensure an alignment accuracy of better than 20 nm to the bottom layer (Fig. 5.1c). The metaatoms were periodically arranged on a square lattice with periods smaller than the wavelength such that only the zeroth diffraction order propagates in the spectral region of interest. The detailed geometrical values of the metaatoms are given in the caption of Fig. 5.1, however, their absolute proportions are of minor relevance here. This is due to the fact that as long as the metamaterial sustains the required low degree of symmetry, it will serve for a principle demonstration of asymmetric transmission. The spectral position where the very effect occurs can easily be tuned to other wavelengths as well.

5.2.1 Observation of linear conversion dichroism

The measurement of a sample in forward and backward direction between collinear and crossed polarizers was described in Sec. 2.7.1. Here we recall the definition of the Jones matrix according to Eq. 2.28. The squared moduli $t_{ij} = |T_{ij}|^2$ of the entries of this matrix were determined experimentally for the metamaterial under consideration (Figs. 5.2a and b). Clearly t_{xy} and t_{yx} interchange for opposite propagation directions proving that all elements in the linear base are different in general. Additional deviations between the forward and backward propagation are negligible and can be most likely attributed to a non-ideal alignment of the polarizers. For comparison, the complex transmission coefficients T_{ij} were computed by FFM (see Sec. 2.5.1) and the transmittances are shown in Figs. 5.2c

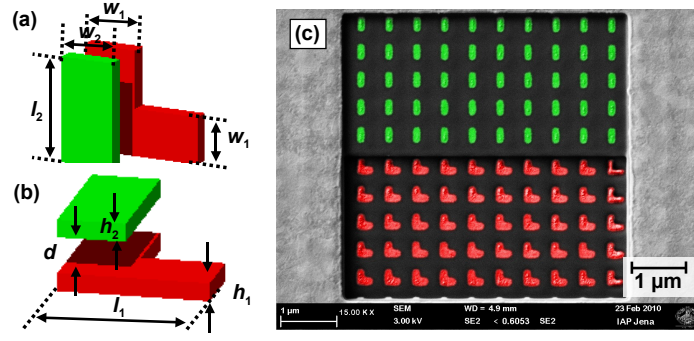


Fig. 5.1: a), b) Two schematic sketches of the metamaterial unit cell from two different perspectives with the definition of the geometrical parameters: $l_1=l_2=290$ nm, $w_1=w_2=130$ nm, $h_1=h_2=40$ nm, $d=80$ nm. c) Top view SEM micrograph with false colors of the fabricated metamaterial. The metaatoms were completely embedded in an index-matched dielectric. FIB slicing at two different depths revealed the two layers composing the metamaterial. Green and red colors represent the nanowires and the L-structures in the top and bottom layer, respectively. The periods in both the x - and y -direction are 500 nm.

and d. All parameters for the simulation were taken from the measured geometry and the experimental setup configuration. The experimental and numerically computed intensities are in almost perfect agreement. Minor deviations are attributed to an only approximative modeling of the geometrical parameters of the structure as deduced from supplementary SEM images. As expected from the design of the metaatoms the spectra reveal a complex multi-resonant behavior. We do not intend to detail all features of the optical response of this metamaterial². The specific hybrid plasmonic eigenmodes can be accessed, e.g., within the framework of an analytical multipole approach [101]. Here, focus will be put on three immediate observations.

First, note that t_{xy} and t_{yx} interchange when k_z is reversed³. This interchange strongly supports our assumption of the validity of reciprocity of the metamaterial (see Eq. 2.29), since only reciprocal, non-magnetic constituents are involved.

Second, it is apparent from the spectra that the off-diagonal elements differ in a broad spectral range. Namely, $t_{xy} \neq t_{yx}$ from $1.0 \mu\text{m}$ to $1.5 \mu\text{m}$, which constitutes the first experimental manifestation of a linear conversion dichroism ($\Psi_{\text{lin}} \neq 0$). Linear conversion dichroism (applicable to linearly polarized light) can be considered as the analogon to circular conversion dichroism (applicable to circularly polarized light), as reported in [13]. Recalling the discussion in Sec. 2.4.3, $\Psi_{\text{lin}} \neq 0$ constitutes a necessary and sufficient condition for the occurrence of asymmetric transmission of linearly polarized light.

²Generally speaking, the two components comprising the metaatoms sustain three lowest order plasmonic resonances; one may be associated with the nanowire and the two others with the L-shaped particle. The coupling of these particles results in a complex response featuring various resonances.

³Of course the interchange of the t_{xy} and t_{yx} for the numerical data is ideal, therefore Fig. 5.2d contains some redundant information.

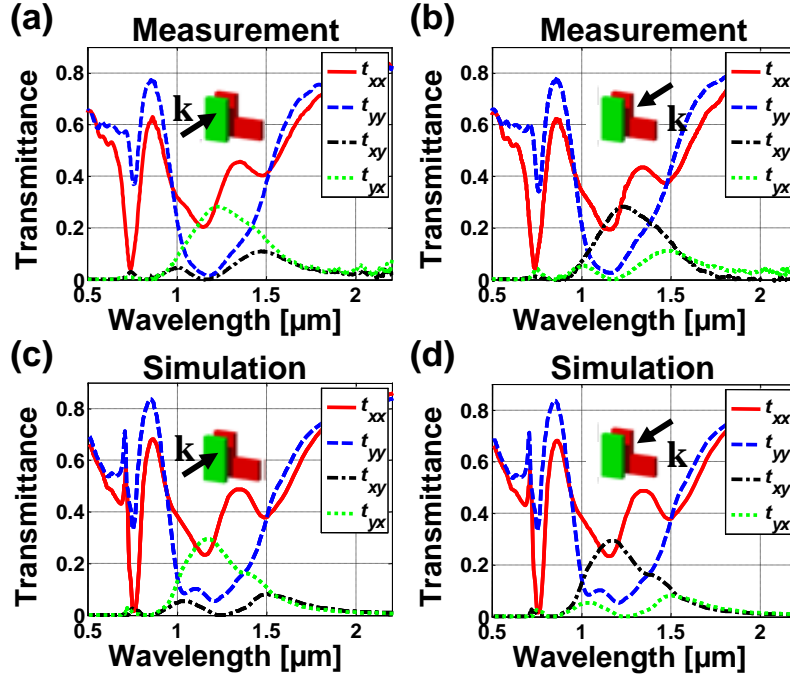


Fig. 5.2: Transmittance of the four Jones Matrix coefficients of the metamaterial. a), b) Measurements and c), d) FMM simulations. The wave vector \mathbf{k} of the plane waves illuminating the metamaterial was directed in a), c) forward and b), d) backward direction.

Third, at an approximate wavelength of $1.2\ \mu\text{m}$ the polarization conversion efficiency for forward (backward) propagating x -polarized (y -polarized) light into the orthogonal polarization state is larger than 25% ($t_{yx} > t_{xx}$ for forward propagation, respective $t_{xy} > t_{yy}$ for backward propagation). This is the footprint of the strong chiral nature of the metaatoms.

5.2.2 Observation of asymmetric transmission

The values for the asymmetric transmission Δ were calculated according to Eqs. 2.32 and 2.40 in the linear as well as in the circular base and are displayed in Fig. 5.3. Clearly, they are different for different bases and achieve values up to 25% in the linear base. The asymmetry for a certain state is of course identical to the asymmetry for the complementary state with negative sign since the total transmission for unpolarized light from both sides has to be the same in a reciprocal medium. The absolute values of $\Delta^{(x)} = -\Delta^{(x)} \neq 0$ in Fig. 5.3a correspond to what is acquired when calculating the differences in the total transmissions (i.e. transmission measured with a polarization insensitive detector) for linearly polarized waves incident on the front and back side of the metamaterial. They represent the key result of this chapter, which is the first experimental proof of asymmetric transmission of linearly polarized light enabled by truly three-dimensional chiral metaatoms. Along with this, the metamaterial additionally shows asymmetric transmission in the circular polarization base

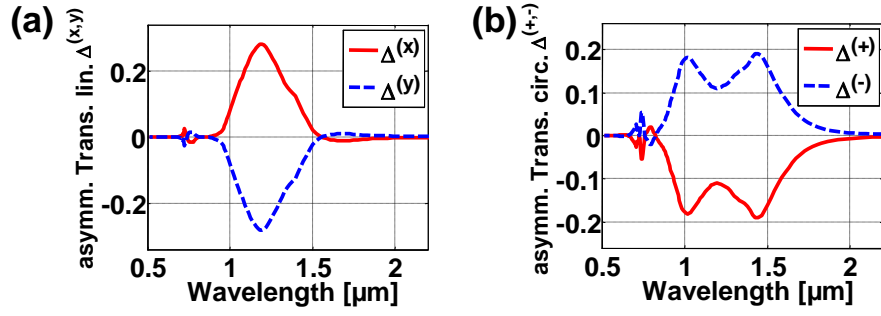


Fig. 5.3: a) Asymmetric transmission $\Delta^{(x,y)}$ for the linear polarization base and b) asymmetric transmission $\Delta^{(+,-)}$ for the circular polarization base as determined from the numerical data. The color of the lines indicates the particular polarization input state.

(Fig. 5.3b), since the nondiagonal elements in the circular base are different as well. This observation is in accordance with previous interpretations of asymmetric transmission of circularly polarized light as a result of circular conversion dichroism [13, 208, 223, 230, 231].

Chapter summary

In this chapter, the first experimental observation of linear conversion dichroism and asymmetric transmission of linearly polarized light in a three-dimensional low-symmetry metamaterial was reported. Contrary to previous works focusing exclusively on circularly polarized light, the key for asymmetric transmission in any polarization base is the complete symmetry breaking of the metaatom. The composition of three-dimensional chiral metaatoms considerably enriches the variety of transmission functionalities and offers yet a new degree of freedom of design for metamaterials. This novel physical effect is not available by simply relying on natural resources of optical media, which evidences the supernatural of metamaterials.

6 Disorder and amorphization of high-symmetry metaatoms

In the last three chapters we considered a stepwise decrease of the degree of symmetry of metaatoms and the correspondence to their associated optical properties. In fact, there is an alternative way to affect the overall symmetry in a metamaterial. Our model system of choice was a planar metamaterial assembled of cut-wire pair metaatoms. Leaving the $C_{4,z}$ symmetry of the metaatom itself untouched, we introduce a precisely controllable degree of positional disorder in the metamaterial, therefore perturbing the periodic lattice arrangement of the metaatoms in a deterministic fashion. Our approach can be regarded as a continuous symmetry breaking with respect to the periodicity of a metamaterial. This study inhibits a fundamental difference to the vast majority of investigations of optical metamaterials, whose metaatoms were usually assembled in strictly periodic arrangements. This state of the art is mainly due to the limited resources of contemporary computational facilities. As a result, the direct comparison between an experimentally available disordered system containing a large number of constituents and its rigorous numerical treatment is rather challenging. In the study presented here, we have realized the first deterministic experimental and numerical demonstration of an amorphous metamaterial and have shown how the scattering response of an individual metaatom affects the averaged far-field response of the ensemble. Additionally we assigned for the first time effective optical properties to truly amorphous metamaterials. The major relevance of our results to the field of synthesis of self-assembling metamaterials (see Sec. 2.6.5) is discussed.

6.1 Transition from periodic to amorphous arrangements

6.1.1 Introduction of deterministic disorder

Positional disorder in a planar metamaterial can be introduced by adding a random displacement to the position of each metaatom in each lateral direction independently. Here we choose the displacements Δx and Δy such that they are uniformly distributed within the intervals

$$\Delta x, \Delta y \in \left[-\frac{Dp}{2}, +\frac{Dp}{2}\right], \quad (6.1)$$

where p is the lattice constant of the referential periodic system. D is a dimensionless disorder parameter to control and quantize the degree of disorder. With other words, $D=0$ corresponds to a periodic lattice arrangement while for $D = 1$ the center position of each metaatom can randomly extend between the boundaries of the former unit cell. If D is larger than one, each metaatom can even be placed beyond those boundaries. For practical reasons, a minimum interparticle separation d_{\min} between adjacent metaatoms had to be enforced. Otherwise, the resonance properties of the individual metaatoms would have been predominantly affected by evanescent coupling. Moreover, d_{\min} fairly reflects the physical situation of hard spheres in standard routines to fabricate self-organized metamaterials using, e.g., charged colloidal beads. After implementing the algorithm in a *Matlab* code¹, two-dimensional coordinate sets of disordered metaatoms could be generated, each one governed by D and d_{\min} . Figure 6.1 shows six SEM micrographs of fabricated metamaterials where each bright dot represents a single metaatom. While D varies, d_{\min} was kept constant to 66 nm^2 . Similar approaches using other parametrization sets have been utilized in other optical systems [234]-[237].

6.1.2 Statistical assessment of the system

Now we will classify the “randomness” in our metamaterial and verify that really amorphous structures are created with this algorithm. By definition, “amorphous” refers to a conglomerate whose constituents inhibit a limited degree of short-range order, while long-range order is completely absent. Among various mathematical means, the most appropriate one to classify positional disorder is the radial distribution function, also called pair correlation function $g(r)$ [238]. This dimensionless quantity can be calculated for any system containing a large number of particles at fixed positions, just like our metaatoms. The parameter

¹The algorithm works in the following way: Starting from a periodic lattice, the order of all positions (x,y) of all metaatoms was randomized. This randomization of the order of placement itself ensured that the positions of all metaatoms were not correlated [234]. Then, Δx and Δy were added to the first (x, y) pair and the corresponding metaatom position was fixed. After that, the next position was randomized and so on. If the placement of a metaatom violated the restriction enforced on d_{\min} with respect to any other metaatom already fixed, Δx and Δy were rejected and a new pair within $[-D/2p, D/2p]$ was generated. The algorithm converged quickly as long as d_{\min} was not chosen too large.

²The choice of this specific value turned out to be a good compromise between two counteracting aspects: Smaller values of d_{\min} were tested and resulted in the unintentional merging of a rather big number of adjacent metaatoms during fabrication. On the other hand, if d_{\min} was too large the disorder algorithm failed to converge. Equivalently, the higher d_{\min} the stronger is the enforcement of the periodicity which we actually aim to perturb here.

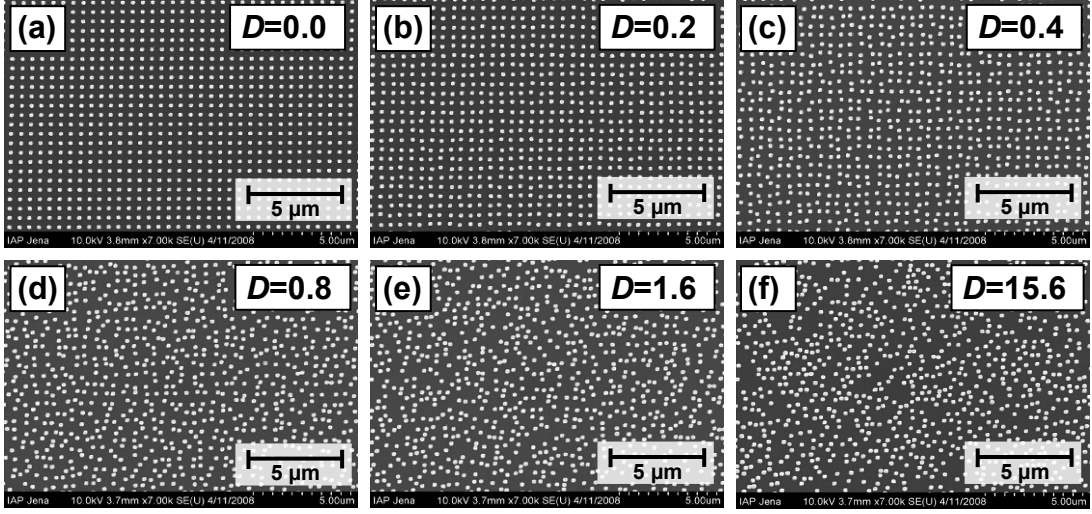


Fig. 6.1: Equally magnified, top view SEM micrographs of metaatoms in arrangements with implementations of different values of disorder D .

r denotes the interparticle separation between adjacent metaatoms which is normalized to the underlying periodic lattice. The pair correlation function $g(r)$ then describes how the particle density varies as a function of the distance from a particular metaatom. Hence $g(r)$ offers a two-dimensional statistical mapping of the distances between the centers of pairs of particles [239]. Applied to the situation of two dimensions, it is evaluated by counting the numbers of particles that lie within a circular shell, dr , of radius r from an arbitrary origin in the plane. This is repeated for a range of radii and many arbitrary points selected as the origin. The statistical average of these numbers, normalized with respect to the average particle number density $\langle \rho \rangle$ and the sampling area $da = 2\pi r dr$ for a particular radial distance r , gives the pair correlation function

$$g(r) = \frac{1}{\langle \rho \rangle} \frac{dn(r, r + dr)}{da(r, r + dr)}. \quad (6.2)$$

In periodic structures $g(r)$ shows not only one peak (corresponding to short-range order) but also higher order peaks (long-range order). On the other hand, long-range order should be completely absent in a truly amorphous structure. Therefore, if our metamaterial is really amorphous, we expect only one discernible peak around $r=1$. For completeness it is noteworthy that $g(r)$ of a fully randomized structure will not show any features at all indicating the lack of both short- and long-range order [238]. Such a structure could be implemented in our case by setting d_{\min} equal to zero while D is sufficiently large. However, this consideration is practically not relevant due to the finite extension of any physical metaatom.

The pair correlation function $g(r)$ was calculated for a sufficiently large section of the arrangements depicted in Fig. 6.1. The results are shown in Fig. 6.2. As expected, $g(r)$

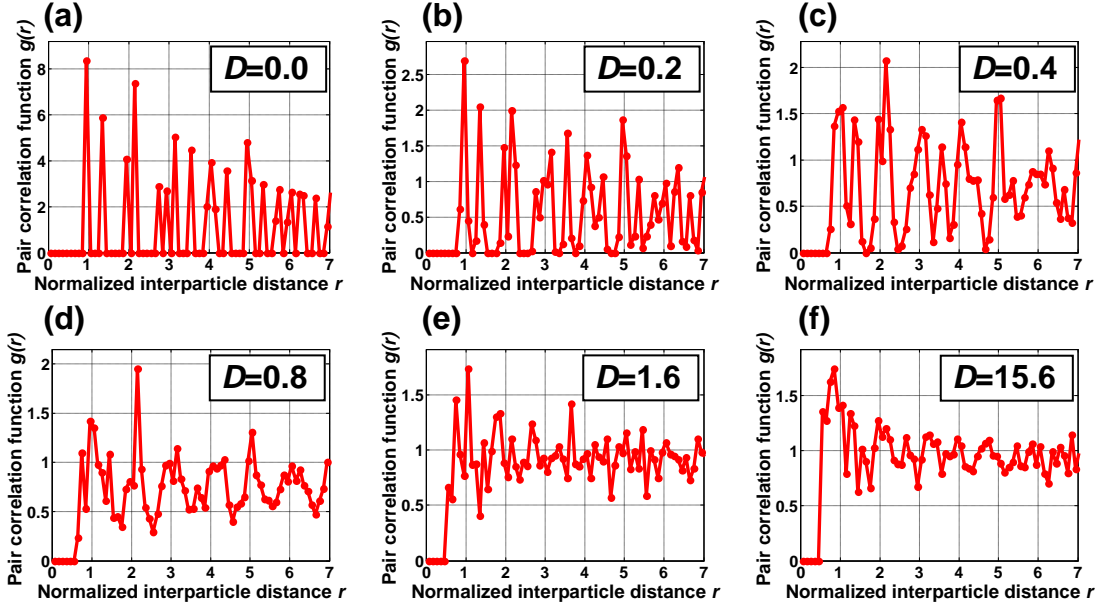


Fig. 6.2: Pair correlation function $g(r)$ for a two-dimensional assembly of particles with different degrees of disorder D as outlined in the text. a) Periodic, b)-d) partially disordered and e)-f) amorphous system.

displays discrete peaks for the periodic arrangement (Fig. 6.2a). With increasing D , those peaks are gradually reduced and smeared out (note that the y -axes scale differently in the subfigures of Fig. 6.2). Though there is no distinct threshold between a partially disordered and an amorphous system, it can be clearly seen in Fig. 6.2e and f that for large values of D only the first peak around $r=1$ survives while $g(r>1)$ gives a noisy signal with a mean value around one³. Short-range correlation is present because the particles were not allowed to take positions in the ultimate vicinity of other particles. Consequently, $g(r)$ is identical zero for small values⁴ of r . Correlation functions of that type are a clear indication of an amorphous structure. It is therefore proven that Eq. 6.1 together with the side condition $d_{\min}>0$ can mimic the transition of a metamaterial from a periodic (or crystalline) to an amorphous state.

6.2 Plasmonic modes in cut-wire pair metaatoms

Recent studies to understand the effect of positional disorder on the optical functionality considered single and double split-ring resonators in various spectral domains [235]-[237]. However, the emphasis was exclusively on metaatoms where only electric dipoles could be excited under normally incident illumination. It is imperative to extend those studies toward

³Note that the actual values of $g(r)$ depend on the individual implementation of disorder which can vary for a given D , but its principal behavior will always support our statement.

⁴To be precise, $g(r)=0$ for all r smaller than the sum of d_{\min} and the lateral size of a metaatom.

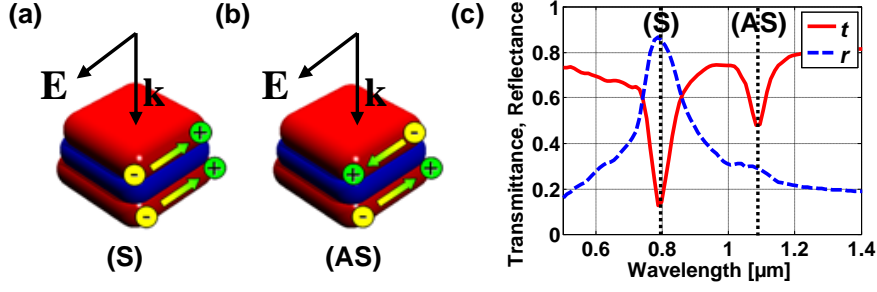


Fig. 6.3: Schematic of a cut-wire pair metaatom excited at a) the symmetric (S) and b) the antisymmetric (AS) plasmonic eigenmode. The wave vector \mathbf{k} denotes the light propagation direction and \mathbf{E} the polarization of the electric field. The colored arrows represent the a) in-phase and b) out-of-phase oscillations of the current densities in the metal wires. c) Simulated prototypical spectrum showing the two resonances corresponding to the symmetric (S) and antisymmetric (AS) mode in transmittance t and reflectance r .

more complex metaatoms that support higher order multipoles to develop a comprehensive understanding of disordered metamaterials. The simplest structure that fulfills this goal is the cut-wire pair [180]. This metaatom received an enormous attention from the community since both an electric quadrupole and a magnetic dipole can be excited at normal incidence. The cut-wire pair is therefore regarded as one of the key building blocks to obtain a magnetic response at optical frequencies [58, 59].

Each metallic cut-wire supports a localized plasmon polariton. In a dimer system (two cut-wires in close proximity), the strong coupling of plasmonic modes causes a hybrid splitting of the resonance into a symmetric and an antisymmetric mode [101, 240]. Since for the high-frequency symmetric mode the current densities in both arms are in phase, it effectively acts as an electric dipole. By contrast, the current densities in both arms oscillate π out-of-phase for the low-frequency antisymmetric mode evoking an electric quadrupole and a magnetic dipole moment [101, 200]. In an ensemble of metaatoms, the two modes translate into the far-field response by dips in the transmittance and peaks in the reflectance, although the latter is rather weak for the antisymmetric eigenmode (Fig. 6.3).

6.3 Sensitivity of plasmonic modes to positional disorder

The cut-wire pairs were fabricated on a silica substrate with the technique outlined in Sec. 3.2. For this study we required the metaatoms to be $C_{4,z}$ symmetric to suppress a polarization-dependent response for normal incidence illumination. Despite of their quadratic footprint, we will consistently use the expression “cut-wire pairs” in the following. Each cut-wire pair consisted of two 30 nm gold layers separated by 45 nm of magnesia with side lengths $s_{x,y} = 180$ nm in both lateral directions. For reference, a perfectly periodic sample ($D=0$) with lattice constants $p_{x,y} = 512$ nm was fabricated. The corresponding area filling fraction

of $f = s_{x,y}^2/p_{x,y}^2 \approx 12.4\%$ remained unaltered on average for all samples by keeping the number of metaatoms and hence their average density constant. Eleven different samples with different values of D ranging from 0 to 1000 were fabricated on the same wafer. Each sample had a footprint of $3\text{ mm} \times 3\text{ mm}$ and a selection of SEM pictures is shown in Fig. 6.1. As shown above, this set represents a gradual transition from a periodic to an amorphous planar metamaterial.

6.3.1 Experimental observations

The optical properties of all samples were characterized by transmission and reflection spectroscopy by means explained in Sec. 2.7.1. At normal incidence virtually identical spectra have been obtained for both linear polarization states parallel to either lattice vector, which is in agreement with the $C_{4,z}$ symmetry of the cut-wire pair metaatom. The investigated spectral domain ranged from wavelengths of $0.5\ \mu\text{m}$ to $1.2\ \mu\text{m}$, comprising the two principal resonances of the metamaterial⁵. The spectral results are shown in Fig. 6.4. For the periodic arrangement ($D=0$) two dips appear in the transmission spectrum (Fig. 6.4a) situated at wavelengths of $0.8\ \mu\text{m}$ and $1.05\ \mu\text{m}$ which are related to the symmetric and antisymmetric plasmon polariton eigenmodes of the metaatom, respectively. The former is also confirmed by a noticeable peak in reflection (Fig. 6.4b) at $0.8\ \mu\text{m}$. A considerably different sensitivity of the two resonances was observed for an increasing degree of disorder. While the antisymmetric resonance at $\lambda=1.05\ \mu\text{m}$ almost perfectly sustains in width and magnitude even for $D=1000$, the symmetric resonance blue shifts by about $30\ \text{nm}$, broadens and its magnitude decays already at a low level of disorder $D=1$.

These astoundingly different characteristics can be explained on the basis of the cut-wire pair eigenmodes and their resulting in-plane interactions. In this context, the plane of interest lies in the center of each metaatom and is parallel to the substrate surface. For the high frequency symmetric eigenmode (Fig. 6.3a) the two cut-wires act as an electric dipole. In the lateral plane of the metamaterial the scattered fields from all metaatoms always interfere constructively. Most notably, it causes a strong field that is polarized along the incidence polarization. Therefore, the local electric field driving each metaatom consists of the illuminating external field superimposed by the field scattered from all metaatoms. In the periodical arrangement this is not detrimental since the illumination conditions are identical for all metaatoms in the lattice. However, upon the transition to the amorphous state, the scattered fields from all metaatoms lose their fixed phase relation and their individual driving forces are modified. The results are a strong homogeneous line broadening and a resonance

⁵The low signal-to-noise ratio in the wavelength range from $0.9\ \mu\text{m}$ to $1.0\ \mu\text{m}$ in the reflection spectra is due to low sensitivity of the detector (a PbS photodiode at that time) and does not bear any physical meaning.

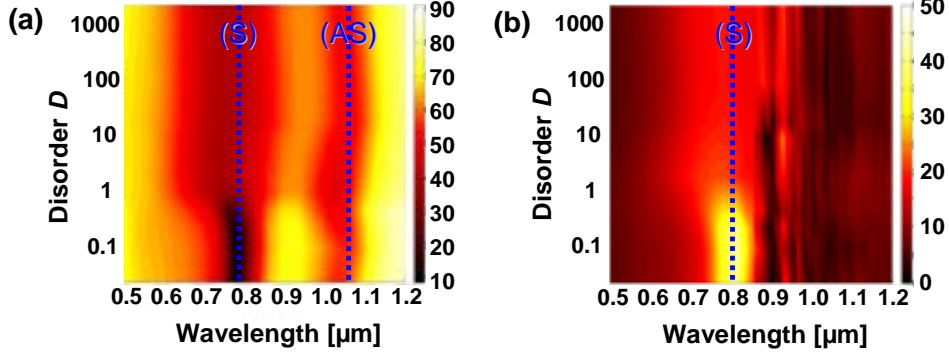


Fig. 6.4: Measured a) transmittance and b) reflectance as functions of the wavelength and the disorder parameter D (logarithmic scale). Both spectra are recorded for discrete values of D and interpolated to guide the eye. The blue dotted lines indicate the positions of the symmetric (S) and antisymmetric (AS) resonance.

damping. This observation had been firstly predicted by Haynes et al. and was ascribed to radiative dipolar coupling (which has a $1/r$ dependence on the interparticle distance r) and dipole scattering retardation (which multiplies the dipole scattered field by e^{ikr}) [241].

Complementary results are obtained when these arguments are applied to the antisymmetric low frequency mode (Fig. 6.3b). As already discussed in Sec. 6.2, the out-of-phase dipole oscillations generate a scattered field which is dominated by an electric quadrupole and a magnetic dipole contribution. However, in the lateral plane of the metamaterial both multipoles lack an in-plane polarized field component due to destructive interference of the scattered fields from the upper and the lower cut-wires. The only nonzero field component in the lateral plane is that normal to the substrate. Since the cut-wire pair sustains only a resonant response for in-plane field components for the spectral range under investigation, this scattered field has no influence here. Therefore, the driving force of each metaatom is solely the external illumination and the spectral response is independent of the arrangement, namely periodic or amorphous. This effect was not observed so far, since positional disorder had only been investigated in electric dipole-dominated metamaterials [235]-[237].

6.3.2 Numerical simulations and effective properties

To compare these spectra with theoretical predictions, we performed FDTD simulations (see Sec. 2.5.2) of the system for no ($D=0$), moderate ($D=0.3$), and high ($D=3$) positional disorder. The simulations were constrained to a sufficiently large supercell with a size of $7\ \mu\text{m} \times 7\ \mu\text{m}$ containing 196 metaatoms. This size was checked to be large enough for the peculiarities of the individual implementations of disorder to have a negligible impact on the results (Fig. 6.5). The supercell was truncated by periodic boundaries in the lateral

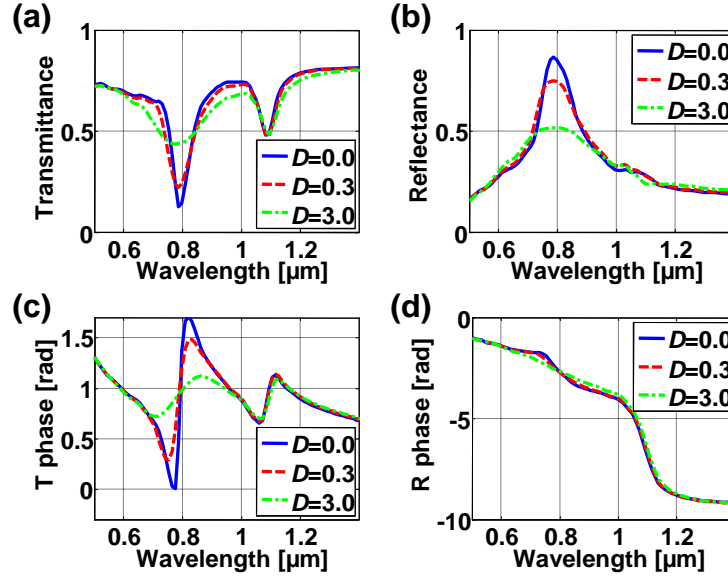


Fig. 6.5: Simulated a) transmittance, b) reflectance, c) transmission phase delay and d) reflection phase delay of the cut-wire pair metamaterial as functions of the wavelength and D .

dimensions whereas perfectly matched layers were used along the propagation direction.

The two plasmonic resonances are confirmed to appear at the wavelengths $0.8\ \mu\text{m}$ and $1.1\ \mu\text{m}$ for $D=0$. Their identification as the symmetric and antisymmetric eigenmodes of the cut-wire pair structure is supported by supplementary investigation of the near-field at the resonant wavelengths⁶. Moreover, all experimental observations in transmission and reflection that occur for an increasing degree of disorder are fully reproduced. With D increasing, the symmetric resonance at $0.8\ \mu\text{m}$ broadens, blue shifts, decays, and nearly vanishes already for $D=3$. This evolution does not apply for the antisymmetric eigenmode at $1.1\ \mu\text{m}$. While D increases, the dip in the transmitted amplitude and its corresponding phase evolution retain their strength and width almost unaffected. It is confirmed that the antisymmetric eigenmode is nearly invulnerable to positional disorder.

Thanks to the fact that the FDTD delivers not only amplitude (Figs. 6.5a and b) but also phase information (Fig. 6.5c and d) and based on the remarkable agreement between measured and simulated spectra, the computed complex spectra allowed us to determine effective material properties for the periodic, the weakly disordered, and the amorphous metamaterial. Even though it is clear that due to the mesoscopic size of the metaatoms, the response of the metamaterials cannot be described adequately by spatially non-dispersive material properties (see Sec. 2.3.2), we proceed using the retrieval algorithm from Sec. 2.3.1

⁶The antisymmetric resonance appears at slightly longer wavelengths in comparison to the experiment. This is most likely due to small deviations from the topography of the metaatoms. Note that geometry parameter scans on such large domains were not possible due to the huge computational effort required by the FDTD method.

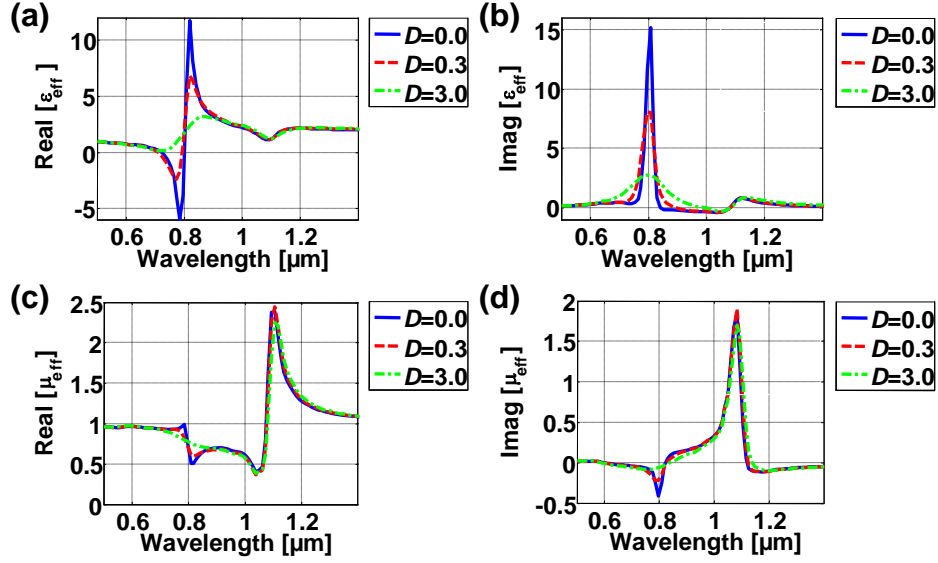


Fig. 6.6: Wavelength-dependent effective properties of the periodic ($D=0.0$), the weakly disordered ($D=0.3$), and the amorphous cut-wire pair metamaterial ($D=3.0$). a) Real and b) imaginary parts of the effective electric permittivity $\epsilon_{\text{eff}}(\lambda)$. c) Real and d) imaginary parts of the effective magnetic permeability $\mu_{\text{eff}}(\lambda)$.

to illustrate the principal effects.

In Fig. 6.6 we attribute effective properties to the metamaterial along its transition from a periodic to an amorphous state. From those properties similar conclusions can be drawn as for the transmission and reflection spectra. Firstly, the high frequency resonance at $\lambda = 0.8 \mu\text{m}$ that induces a Lorentzian dispersion in the effective permittivity $\epsilon_{\text{eff}}(\lambda)$ strongly decreases with increasing disorder D (Figs. 6.6a and b). Since the electric dipoles excited in the metaatoms cease to oscillate in phase, the resonance is homogeneously broadened, causing a degradation of the induced dispersion. Our second important finding concerns the persistence of the antisymmetric resonance of $\mu_{\text{eff}}(\lambda)$ at $\lambda = 1.1 \mu\text{m}$, whose strength, line shape, and width are preserved practically independently of D . Since this resonance is usually employed as a “magnetic resonance” in metamaterial designs [58, 59], one may conclude that the effective magneto-optical properties of many current negative-index metamaterials are only marginally affected by the very arrangement of the metaatoms. It should be emphasized however, that our results strictly apply to planar metamaterials only [242].

6.4 Top-down and bottom-up amorphous metamaterials

In the preceding section it was shown that the so-called magnetic resonance in common planar metamaterials is invulnerable to positional disorder and deterministic amorphization. This finding establishes a previously missing link to metamaterials fabricated by chemical synthesis or self-assembling methods (“bottom-up”, see Sec. 2.6.5), where regularly ordered

lattices cannot be simply realized without additional efforts [164]-[168]. Nowadays the vast majority of optical metamaterials is fabricated by costly and time consuming serial writing processes such as EBL (“top-down”). Moreover, it seems elusive to fabricate true bulk metamaterials by a sequential stacking of single functional layers [6, 129, 134]. This situation hinders the transfer of fundamental concepts from an academic into an industrial environment where true applications shall be implemented.

Accordingly, quick and reliable fabrication schemes based on self-assembling or chemically randomized processes will ease the applicability of large-scale metamaterials. From our findings we can conclude that a magnetic resonance will most likely be retained if the top-down fabrication of metamaterials was substituted by bottom-up approaches. Moreover, in order to incorporate a potentially negative-index metamaterial into an imaging application, it ought to show a weak spatial dispersion [202]. However, the mesoscopic arrangement of metaatoms in most of the present metamaterials causes inevitably a high degree of anisotropy and strong spatial dispersion [75, 243, 244]. These constraints can be possibly lifted by employing amorphous metamaterials, provided that the metaatoms obey to the quasi-static limit (see Sec. 2.1.3). Accordingly, true optical isotropy in the sense of Sec. 2.4.1 is anticipated for sufficiently small metaatoms that are randomly arranged in space [245, 246]. Thus our experimental and numerical results are especially valuable for the so far elusive prediction of optical properties of bottom-up fabricated metamaterials.

6.5 Symmetry reduction by anisotropic positional disorder

After the robustness of the antisymmetric resonance against positional disorder was shown, the degradation of the symmetric resonance can be further studied. To probe for another aspect of the lack of periodicity, we analyzed how disorder in one transverse direction influences the optical properties of the samples. In the following, this one-dimensional type of disorder is called “anisotropic” while the two-dimensional case will be referred to as “isotropic”. The motivation for the approach was twofold. Firstly, the nearest-neighbor interactions of adjacent metaatoms can be discriminated with respect to their electromagnetic eigenmodes and to the polarization vector of the incident field. Secondly, anisotropic disorder constitutes an elegant way to break the symmetry in an arrangement of otherwise geometrically isotropic unit cells like the cut-wire pairs. Thus it provides a new degree of freedom for the design of biaxial anisotropic metamaterials as demanded for certain imaging applications [202].

The sample fabrication and measurement was done in full analogy to the procedure described in Sec. 6.1.1 and Sec. 6.3 with the only modification of Eq. 6.1, where Δy was set to zero for the case of anisotropic disorder. The considered cut-wire pairs had identical geometrical and material parameters as those described in Sec. 6.3. This approach resulted in a

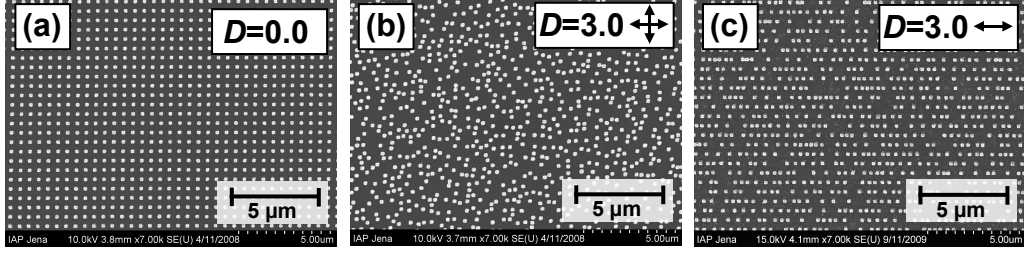


Fig. 6.7: Equally magnified, top view SEM micrographs of the fabricated metamaterials associated with different types of positional disorder. a) Periodic cut-wire pair metamaterial with $D=0.0$. b) Two-dimensional (isotropic) disorder with $D=3.0$. c) One-dimensional (anisotropic) disorder with $D=3.0$.

distinction between two-dimensional (isotropic) and one-dimensional (anisotropic) positional disorder (Fig. 6.7). In the latter case, the disorder is regarded to be a vector pointing in the x -direction. We restricted our considerations to the relevant values of $D=3.0$, as it contains sufficient information. In particular, the conclusions to be drawn for $D>3.0$ are not affected, since the statistical displacement of a metaatom from its regular grid position outnumbers the average size of the metaatom⁷.

In the following, we restrict our investigations to the spectral region containing the symmetric resonance. The persistence of the antisymmetric mode against positional disorder was shown in Sec. 6.3 and depends neither on the degree of the disorder nor on its isotropic or anisotropic character. The decay mechanism of the symmetric resonance for isotropic disorder was explained in Sec. 6.3. Two-dimensional disorder combined with a $C_{4,z}$ symmetry of the metaatoms renders the optical response polarization-independent. By contrast, it is expected to depend on the polarization vector for the case of anisotropic disorder. A perceptible difference is anticipated, since the angular distribution of the scattered field of an electric dipole is also strongly anisotropic.

We distinguish the two cases when the electric field is polarized either parallel or perpendicular to the disorder vector. If the electric field is polarized parallel to the disorder vector, the oscillator strength in the excited cut-wire pairs is in general lower. Particularly, if two metaatoms are brought in close proximity along the chains, the arrangement resembles a coupled-antenna configuration where the feed gap between the two antennas sustains an extraordinarily strong field enhancement at resonance [247]. However, performing a spatial averaging these extrema are negligible and a rather constant field emerges. If the electric field is perpendicularly polarized to the disorder vector, the picture appears differently. Since the scattered field of an electric dipole is strongest perpendicular to its orientation, the scattered

⁷The ensembles are then indistinguishable, which was confirmed both statistically in Sec. 6.1.2 and experimentally in Sec. 6.3. Again, the only restriction we enforced was to set the minimum separation d_{\min} between adjacent metaatoms to 66 nm.

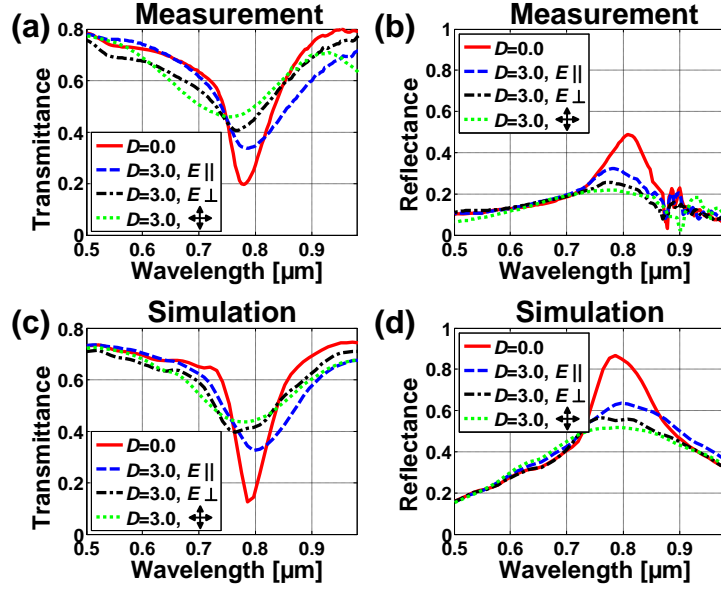


Fig. 6.8: Measured a) transmittances and b) reflectances of periodic, anisotropic disordered and isotropic disordered metamaterials showing a polarization-sensitive degradation of the symmetric resonance; and corresponding simulated c) transmittances and d) reflectances. Red solid lines - $D=0.0$, periodic sample, independent of polarization ; Blue dashed lines - $D=3.0$, anisotropic disorder with parallel oriented electric field \mathbf{E} ; Black dashed-dotted lines - $D=3.0$, anisotropic disorder with normal oriented electric field \mathbf{E} ; Green dotted lines - $D=3.0$, isotropic disorder, independent of polarization.

field that adds to the external illumination depends more sensitively on disorder. Thus the interaction between the cut-wire pairs is stronger since the amplitude of the field above each metaatom is strongly fluctuating.

Based on these considerations we expect the strongest effect on the optical properties of the sample, when compared to the periodic case, to occur for the sample that exhibits an isotropic disorder. The influence of an anisotropic disorder perpendicular to the incident polarization will be slightly weaker. An even further decrease of this influence will be observed for the anisotropic disorder being parallel to the incident polarization. These distinct impacts of isotropic and anisotropic disorder translate directly into the far-field response of the metamaterial. Figure 6.8 displays the degradation of the symmetric resonance in transmission and reflection. The overall agreement regarding the discrimination between measurements and FDTD is very good, though we observe some absolute discrepancies between measured (Fig. 6.8c) and simulated (Fig. 6.8d) reflection, which are attributed to fabrication imperfections. The resonance at $\lambda=0.8\ \mu\text{m}$ is strongest for a periodic arrangement of metaatoms in the metamaterial, when all excited dipoles oscillate coherently in phase (red solid lines in Fig. 6.8). Compared to isotropic disorder which is insensitive to the polarization (green dotted lines in Fig. 6.8), a smaller resonance degradation is found for the case of anisotropic disorder. The degradation is diminished slightly when the polarization of the electric field

is orthogonal to the anisotropic disorder vector (black dashed-dotted lines in Fig. 6.8). The weakest degradation in comparison to the perfect periodic case is found for a polarization vector that is parallel to the disorder vector (blue dashed lines in Fig. 6.8). These findings are consistent with the interpretation of electric dipole-dipole interactions between neighboring metaatoms in the near-field.

Anisotropic disorder provides an alternative means of symmetry breaking in an arrangement of geometrically isotropic metaatoms. Furthermore it details how the analysis of scattering properties of neighboring metaatoms is the key to the physical understanding of the optical response of any metamaterial [242]. Accordingly, our results constitute a solid benchmark for analytical multipole theories for metamaterials [101], whose exploration is subject to ongoing work.

Chapter summary

In this chapter we investigated the deterministic breaking of the translational symmetry in a periodic metamaterial. By introducing a precisely controllable degree of positional disorder into a planar assembly of cut-wire pairs, its impact on the plasmonic resonances sustained by these metaatoms could be observed. This deterministic disorder was implemented by means of an algorithm that assigned to each single metaatom its individual spatial position. The algorithm was governed by a disorder parameter D which was chosen to be proportional to the maximum bounds of the individual random displacement of each metaatom with respect to its original position on a periodic lattice. Increasing D allowed to mimic the transition from a periodic to an amorphous planar structure, which was statistically validated by means of a pair correlation function. The accordingly fabricated samples were optically characterized and revealed different sensitivities of the two main resonances for increasing disorder. In consistency with the literature, the symmetric resonance sustained by the metamaterial suffers strongly from disorder and decays rapidly when the periodic arrangement of the metaatoms degrades. On the other hand and for the first time, the antisymmetric resonance was shown to be largely unaffected by an arbitrary degree of positional disorder. These experimental results were fully confirmed by FDTD simulations and explained by considering the eigenmodes of the metaatoms and their resulting in-plane interactions. In addition, we retrieved for the first time the effective optical properties of a periodic, a weakly disordered and an amorphous metamaterial. Finally, anisotropic disorder was shown to constitute yet another means of symmetry breaking in an ensemble of otherwise geometrically isotropic metaatoms to obtain a polarization-sensitive optical response. Our findings have important implications for bottom-up fabricated metamaterials, since the strong limitation of the necessity of a periodic lattice in the respective design concepts is relaxed. The statement saying that

the magnetic properties of planar metamaterials in periodic or amorphous arrangements are equivalent may bridge the conceptual gap between top-down and bottom-up fabricated metamaterials.

7 Summary and outlook

This thesis intends to provide technological and experimental contributions to the field of resonant metamaterials built of deliberately tailored metallo-dielectric inclusions, called metaatoms. While the majority of contemporary metamaterials is constructed to be operated at gigahertz or terahertz frequencies, the structures considered here aim at the less investigated and technologically more challenging part of the optical range of the spectrum. The selection of the studied metaatoms was related to a reduction of their degree of spatial symmetry, thus following a transition from high-symmetry to low-symmetry metamaterials. It was shown that symmetry breaking can lead to an extraordinary enhancement of known effects or even completely new physical phenomena. Great care was taken with respect to the choice of the proper optical target functions that express these properties in a physically sound way.

Before working on design-related and experimental aspects of optical metamaterials, a reproducible and high-quality nanofabrication technology for metallo-dielectric metaatoms with feature sizes smaller than 100 nm had to be established. Two approaches based on electron beam lithography and the metal lift-off technique, differing in the choice of the respective electron beam resist, were presented in detail. Both methods were shown to enable the fabrication of planar nanostructured metamaterials covering macroscopic areas of several square millimeters and could be repeated to facilitate subsequent stacking of several layers. Specifically, the previously unreported usage of a chemically amplified electron beam resist for a lift-off technique decreases the typical exposure time by approximately one order of magnitude in comparison to classical PMMA-based resists. It is stressed that this newly established nanostructure technology offers the potential to fabricate optical metamaterials in a reproducible way and on large scale, as it will be required for their implementation in real-world applications.

On this technological basis, we were able to optically characterize an alternative design for planar negative-index metamaterials operating at telecommunication wavelengths. This novel, four-fold rotational Swiss cross structure combined the benefits of a polarization independent response and an additional geometrical degree of freedom in comparison to the established double fishnet design. The insensitivity of the incident polarization state of normally incident light was experimentally demonstrated at optical frequencies for the first time. Furthermore, by showing that the optical response and consequentially the effective optical

properties of the Swiss cross inherently depend on the angle of incidence, we revealed this metamaterial to exhibit strong spatial dispersion. The therefrom formulated consequences affect a large group of contemporary negative-index media and may contribute to a more differentiated interpretation of their effective optical properties like $\epsilon_{\text{eff}}(\omega)$ and $\mu_{\text{eff}}(\omega)$.

Furthermore, we lifted a severe restriction of chiral optical metamaterials that were mainly composed of single layered thin films or vertical sequences thereof. An original loop-wire metamaterial consisting of single-block, truly three-dimensional and chiral metaatoms was spectroscopically and interferometrically investigated at visible and near-infrared wavelengths. By purely experimental means and without the input of additional numerical data, it was shown to exhibit optical activity in terms of pure polarization azimuth rotation that outperforms any linear, passive and reciprocal medium known to date, from both natural and artificial origins. The polarization output upon exciting this loop-wire metamaterial with an arbitrary input and the associated polarization eigenstates could be directly visualized from the reconstruction of the full Jones matrix over a broad spectral range, which was achieved for the first time for an optical metamaterial. The eigenstates of polarization were proven to serve as an optical footprint of the breaking of spatial symmetries in the metaatoms.

For the first time, the only recently predicted directional asymmetry in the transmission of linearly polarized and near-infrared light could be demonstrated experimentally. This was achieved by the creation of metaatoms with the lowest possible symmetry, in particular by including a structural symmetry breaking in the principal direction of light propagation. Asymmetric transmission is allowed in non-magnetic metamaterials if the propagation of linearly polarized light is accompanied by a pronounced polarization conversion dichroism. This novel and physically counterintuitive effect may be lined up with optical activity and the famous Faraday effect in magnetized matter. It is a pivotal example of a new phenomenon that could not be observed in natural media, but gets amenable by systematic symmetry breaking in optical metamaterials.

Moreover, we have investigated the impact of positional disorder in a planar cut-wire pair metamaterial, evaluating the transition from periodic to amorphous metamaterials. This transition can be regarded as a deterministic symmetry breaking of the periodic lattice of the metaatoms, while their geometrical shape itself remained untouched. It was revealed that the electric and magnetic resonances of the system possess a different sensitivity to planar disorder. This finding was correlated to the excited plasmonic eigenmodes and their respective in-plane scattered fields. For the first time, effective optical properties were assigned to an amorphous metamaterial. Our conclusions have major relevance concerning the evaluation of such effective properties of future metamaterials fabricated by bottom-up approaches. In addition, anisotropic disorder, being defined as positional disorder in one transverse direction only, was shown to be an alternative means of symmetry breaking in an

arrangement of otherwise geometrically isotropic unit cells, thus revealing a new degree of freedom for metamaterial design.

The key results of this thesis are based on experimental observations of symmetry-related effects in optical metamaterials which were fabricated by a demanding nanostructure technology. Although a close correspondence between experiments and theory was always desired and obtained by means of complementing numerical simulations, it is emphasized that the experiments themselves exhibit a major scientific contribution on their own. Two examples shall be mentioned here: First, the asymmetric transmission of linearly polarized light would have remained an indistinct and even counterintuitive prediction unless verified by a direct and clear experimental observation. Second, complex nanooptical systems like, e.g., the one consisting of disordered cut-wire pair metaatoms, may be too large to be fully investigated by analytical or numerical means. In that case it did happen that the initiating experiment gives new physical stimuli by the observation of unexpected effects that advanced the respective theoretical work to explain them.

The results of this work allow to draw several conclusions with respect to the future research on optical metamaterials and their spatial symmetries. First of all, the ways of symmetry breaking that were shown here do not constitute a claim of completeness. The herein considered metamaterials may rather be regarded as some hand-picked examples that demonstrate the general validity of the conceptual approach. It is difficult to foresee whether other novel electromagnetic effects may be revealed if this research direction is further explored, simply because the alleged effects are still unknown. However, while the degrees of freedom of natural media are usually bound to a thermodynamic equilibrium, artificially structured matter must not obey this fundamental limitation. Therefore the breaking of spatial symmetries in a metamaterial is maybe the most distinguishing feature of such artificial over natural media.

In the past, the primary optimization criteria of many metamaterial designs were the index of refraction at preferably high frequencies, its “negativeness” and its associated figure of merit. Despite of the simplified assumptions implied, the concept of effective optical properties in general and the effective index of refraction in particular have proven to constitute a valuable means to describe the light interaction with complexly nanostructured matter in a convenient way. Recently, the dispersion relation of a metamaterial has gained relevance as an alternative and partly more meaningful optical target function on which constraints should be imposed. Thus a novel class of advanced metamaterials aiming at tailoring the dispersion relation or other optical target functions is currently emerging. The constituting metaatoms may be based on established metamaterial unit cells like the double fishnet or the Swiss cross as presented in this thesis. However, these approaches are likely to raise rather

strict requirements on the respective metamaterial designs in that, e.g., a large number of free geometrical parameters must be optimized. Moreover, in my opinion it is extremely demanding to precisely meet these almost non-tolerant design requirements in fabrication and to provide satisfactory experimental results from this novel class of advanced metamaterials.

Another route that should be followed is the transition of metamaterial fabrication from essentially planar, lithographic technologies to alternatives that are capable of fabricating bulk media containing large amounts of truly three-dimensional metaatoms. Achieving this step could turn out to be a necessary prerequisite to lift optical metamaterials from a platform of academic interest and proof-of-principle demonstrators into real-world applications. In this work we established electron beam lithography, lift-off methods and stacking technologies of multiple layers as a reliable means to fabricate prototypes of truly three-dimensional, chiral and low-symmetry metaatoms. To date, large scale electron beam lithography and the related nanopattern transfer technologies are of primary importance for the field of research. Presumably, they will preserve this relevance in the medium term. This is mainly due to the reason that enormous scientific and engineering expertise has been invested into these technologies over decades, mostly motivated by the requirements of the semiconductor industry. Nevertheless, they remain costly and time-consuming serial processes, and in the long term potential alternatives are asked for. Various approaches including multi-photon photopolymerization, membrane projection lithography, origami-inspired three-dimensional self-folding of planar templates and bottom-up fabrication techniques, i.e. the functionalization of self-assembling or chemically synthesized nanostructures, offer promising paths to complement or even partially substitute standardized nanolithography methods.

In a broader sense, there are still huge challenges, even on a fundamental level, that metamaterial research has yet to overcome. The most crucial issue that is inherently linked to strongly dispersive and/or plasmonically resonant media are their optical losses. In this thesis, this aspect was particularly highlighted at the example of the loop-wire metamaterial. Its highest optical activity in terms of a giant polarization azimuth rotation was observed at a wavelength where the structure exhibits a plasmonic resonance and thus strong optical absorption. It will be imperative to optimize the loop-wire metamaterial in order to decrease its losses to an acceptable minimum, while at the same time the magnitude of its optical activity should possibly be retained. Passive loss reduction can be achieved, e.g., by a parametric fine-tuning of all geometrical degrees of freedom of a metamaterial structure. However, since the underlying loss mechanism cannot be circumvented in principle, an active compensation by the incorporation of a gain medium exhibits the most logical solution. This argument holds for a wide class of contemporary plasmonic metamaterials, whose functionalities suffer from optical losses. Even though some successful results in active loss compensation were recently reported, their broadband applicability to metamaterials of arbitrary design and

under differentiated experimental conditions is still unclaimed territory.

An important part of prospective metamaterial research shall be devoted to the transition from homogeneous toward heterogeneous ensembles of metaatoms. All metamaterials presented in this thesis, namely the Swiss cross, the loop-wire, the cut-wire-pair and the metamaterial showing asymmetric transmission consist of periodic or amorphous arrays of identical metaatoms, which together give a common, spatially invariant optical response. However, a largely unexplored subcategory of artificially nanostructured optical media are heterogeneous arrangements of metaatoms. This field includes identical metaatoms arranged with a locally varying spatial density and, likewise, with differently scaled or shaped metaatoms that are arranged in a predefined fashion. Both approaches allow for spatial gradients of the respective optical target function of the metamaterial. In my opinion, this topical direction is still in its infancy and holds the potential to give the highest impact to material and optical sciences that metamaterials can offer. Ultimately, an universal optical transformation of space by artificial materials is envisioned.

As a concluding remark, the evidenced potential of optical metamaterials to enhance natural properties, like optical activity, or to evoke novel physical effects, such as asymmetric transmission, should be communicated to a broad research community to foster the advancement of optical metamaterials both in established and in completely new research topics of modern optics.

8 Zusammenfassung

Die vorliegende Dissertation beschäftigt sich mit künstlich hergestellten Materialien und deren elektromagnetischer Wechselwirkung mit sichtbarem und nah-infrarotem Licht. Diese sogenannten optischen Metamaterialien werden aus Einheitszellen mit Subwellenlängen-Abmessungen zusammengesetzt, welche in Analogie zu Atomen in natürlichen Materialien als Metaatome bezeichnet werden. Im Rahmen dieser Arbeit wurden metallisch-dielektrische Metaatome gezielt durch Nanostrukturierungstechnologie auf der Basis von Elektronenstrahlolithographie hergestellt, ihre optischen Eigenschaften experimentell untersucht und mit den Ergebnissen rigoroser Simulationen verglichen.

Hauptziel der Arbeit war es zu zeigen, dass durch eine Verringerung der räumlichen Symmetrie der Metaatome und des betreffenden Metamaterials optische Eigenschaften hervorgebracht werden können, die entweder natürlich vorkommende Materialien übertreffen oder sogar als optisch neuartige Effekte angesehen werden müssen. Um diese Aussagen zu untermauern, wurde für jedes hier untersuchte Metamaterial eine individuelle optische Zielfunktion definiert, die dessen besondere Funktionalität in eindeutiger Weise hervorhebt.

Im Speziellen wurde ein polarisations-unabhängiges Metamaterial namens Schweizer Kreuz analysiert, welchem für senkrechten Einfall ein negativer effektiver Brechungsindex für nah-infrarote Wellenlängen zugewiesen werden kann. Dessen Abhängigkeit vom Einfallswinkel und Polarisationszustand des einfallenden Lichtes legen es nahe, den Index als einen Wellenparameter und nicht als eine explizit dem Schweizer Kreuz zugeordnete Materialeigenschaft zu verstehen. Zudem wurden zusammenhängende, echt drei-dimensionale und chirale Metaatome hergestellt, deren hohe optische Aktivität durch eine vollständige experimentelle Bestimmung der komplexwertigen Jones-Matrizen nachgewiesen wurde. Die Rotation des Polarisationswinkels für transmittiertes Licht übertrifft für diskrete Wellenlängen die aller bisher bekannten linearen, passiven und reziproken optischen Medien. Darüber hinaus konnte durch ein Metamaterial mit minimaler Symmetrie zum ersten Mal zweifelsfrei asymmetrische Transmission von linear polarisiertem Licht experimentell nachgewiesen werden. Im letzten Teil der Arbeit wurde der Übergang von periodisch zu amorph angeordneten Metaatomen als ein alternativer Ansatz deterministischer Symmetriebrechung untersucht. Es wurde experimentell gezeigt, dass die opto-magnetischen Eigenschaften eines planaren Metamaterials unabhängig davon sind, ob seine Metaatome periodisch oder amorph angeordnet sind.

A Bibliography

- [1] V.G. Veselago: *The electrodynamics of substances with simultaneously negative values of ϵ and μ* . Sov. Phys. Usp. **10** (4), 509 (1968)
- [2] V.P. Makarov, A.A. Rukhadze, and A.A. Samokhin: *On electromagnetic waves with a negative group velocity*. Plasma Phys. Rep. **36** (13), 1129 (2010)
- [3] J.B. Pendry, A.J. Holden, D.J. Robbins, and W.J. Stewart: *Magnetism from conductors and enhanced nonlinear phenomena*. IEEE Trans. Microw. Theory Tech. **47** (11), 2075 (1999)
- [4] D.R. Smith, J.B. Pendry, and M.C.K. Wiltshire: *Metamaterials and Negative Refractive Index*. Science **305**, 788 (2004)
- [5] C.M. Soukoulis, S. Linden, and M. Wegener: *Negative Refractive Index at Optical Wavelengths*. Science **315**, 47 (2007)
- [6] J. Valentine, S. Zhang, T. Zentgraf, E. Ulin-Avila, D.A. Genov, G. Bartal, and X. Zhang: *Three-dimensional optical metamaterial with a negative refractive index*. Nature **455**, 376 (2008)
- [7] S. Linden, C. Enkrich, M. Wegener, J. Zhou, T. Koschny, and C.M. Soukoulis: *Magnetic Response of Metamaterials at 100 Terahertz*. Science **306**, 1351 (2004)
- [8] M. Buresi, D. van Oosten, T. Kampfrath, H. Schoenmaker, R. Heideman, A. Leinse, and L. Kuipers: *Probing the Magnetic Field of Light at Optical Frequencies*. Science **326**, 550 (2009)
- [9] A. Papakostas, A. Potts, D.M. Bagnall, S.L. Prosvirnin, H.J. Coles, and N.I. Zheludev: *Optical manifestations of planar chirality*. Phys. Rev. Lett. **90** (10), 107404 (2003)
- [10] S. Zhang, Y.S. Park, J. Li, X. Lu, W. Zhang, and X. Zhang: *Negative Refractive Index in Chiral Metamaterials*. Phys. Rev. Lett. **102** (4), 023901 (2009)
- [11] N. Verellen, Y. Sonnefraud, H. Sobhani, F. Hao, V.V. Moshchalkov, P. Van Dorpe, P. Nordlander, and S.A. Maier: *Fano resonances in individual coherent plasmonic nanocavities*. Nano Lett. **9** (4), 1663 (2009)

-
- [12] B. Luk'yanchuk, N.I. Zheludev, S.A. Maier, N.J. Halas, P. Nordlander, H. Giessen, and C.T. Chong: *The Fano resonance in plasmonic nanostructures and metamaterials*. Nature Mater. **9**, 707 (2010)
- [13] V.A. Fedotov, P.L. Mladyonov, S.L. Prosvirnin, A.V. Rogacheva, Y. Chen, and N.I. Zheludev: *Asymmetric propagation of electromagnetic waves through a planar chiral structure*. Phys. Rev. Lett. **97** (16), 167401 (2006)
- [14] C. Menzel, C. Helgert, C. Rockstuhl, E.-B. Kley, A. Tünnermann, T. Pertsch, and F. Lederer: *Asymmetric transmission of linearly polarized light at optical metamaterials*. Phys. Rev. Lett. **104** (25), 253902 (2010)
- [15] T. Kaelberer, V.A. Fedotov, N. Papasimakis, D.P. Tsai, and N.I. Zheludev: *Toroidal Dipolar Response in a Metamaterial*. Science **330**, 1510 (2010)
- [16] J.B. Pendry: *Negative Refraction Makes a Perfect Lens*. Phys. Rev. Lett. **85** (18), 3966 (2000)
- [17] N. Fang, H. Lee, C. Sun, and X. Zhang: *Sub-Diffraction-Limited Optical Imaging with a Silver Superlens*. Science **308**, 534 (2005)
- [18] Z. Liu, H. Lee, Y. Xiong, C. Sun, and X. Zhang: *Far-Field Optical Hyperlens Magnifying Sub-Diffraction-Limited Objects*. Science **315**, 1686 (2007)
- [19] S.W. Hell: *Far-Field Optical Nanoscopy*. Science **316**, 1153 (2007)
- [20] S.W. Hell, R. Schmidt, and A. Egner: *Diffraction-unlimited three-dimensional optical nanoscopy with opposing lenses*. Nature Photon. **3**, 381 (2009)
- [21] S. Gazit, A. Szameit, Y.C. Eldar, and M. Segev: *Super-Resolution and Reconstruction of Sparse Sub-Wavelength Images*. Opt. Express **17**, 23920 (2009)
- [22] Y. Shechtman, S. Gazit, A. Szameit, Y.C. Eldar, and M. Segev: *Super-resolution and reconstruction of sparse images carried by incoherent light*. Opt. Lett. **35** (8), 1148 (2010)
- [23] J. Valentine, J. Li, T. Zentgraf, G. Bartal, and X. Zhang: *An optical cloak made of dielectrics*. Nature Mat. **8**, 568 (2009)
- [24] L.H. Gabrielli, J. Cardenas, C.B. Poitras, and M. Lipson: *Cloaking at Optical Frequencies*. Nature Photon. **3**, 461 (2009)
- [25] R. Liu, C. Ji, J.J. Mock, J.Y. Chin, T.J. Cui, and D.R. Smith: *Broadband Ground-Plane Cloak*. Science **323**, 366 (2009)
- [26] T. Ergin, N. Stenger, P. Brenner, J. Pendry, and M. Wegener: *Three-Dimensional Invisibility Cloak at Optical Wavelengths*. Science **328**, 337 (2010)

-
- [27] B. Zhang, Y. Luo, X. Liu, and G. Barbastathis: *Macroscopic Invisible Cloak for Visible Light*. Phys. Rev. Lett. **106**, 033901 (2011)
- [28] X. Chen, Y. Luo, J. Zhang, K. Jiang, J.B. Pendry, and S. Zhang: *Macroscopic Invisibility Cloaking of Visible Light*. Nature Commun. **2**, 176 (2010)
- [29] H.T. Chen, W.J. Padilla, J.M.O. Zide, A.C. Gossard, A.J. Taylor, and R.D. Averitt: *Active terahertz metamaterial devices*. Nature **444** (7119), 597 (2006)
- [30] N. Engheta: *Circuits with Light at Nanoscales: Optical Nanocircuits Inspired by Metamaterials*. Science **317**, 1698 (2007)
- [31] A. Alu and N. Engheta: *Tuning the scattering response of optical nanoantennas with nanocircuit loads*. Nature Photon. **2**, 307 (2008)
- [32] N.I. Landy, S. Sajuyigbe, J.J. Mock, D.R. Smith, and W.J. Padilla: *Perfect metamaterial absorber*. Phys. Rev. Lett. **100** (20), 207402 (2008)
- [33] N. Liu, M. Mesch, T. Weiss, M. Hentschel, and H. Giessen: *Infrared Perfect Absorber and Its Application As Plasmonic Sensor*. Nano Lett. **10**, 2342 (2010)
- [34] T. Driscoll, H.-T. Kim, B.-G. Chae, B.-J. Kim, Y.-W. Lee, N.M. Jokerst, S. Palit, D.R. Smith, M. Di Ventra, and D.N. Basov: *Memory Metamaterials*. Science **325**, 1518 (2009)
- [35] J.K. Gansel, M. Thiel, M.S. Rill, M. Decker, K. Bade, V. Saile, G. von Freymann, S. Linden, and M. Wegener: *Gold Helix Photonic Metamaterial as Broadband Circular Polarizer*. Science **325**, 1513 (2009)
- [36] U. Leonhardt: *Optical Conformal Mapping*. Science **312**, 1777 (2006)
- [37] J.B. Pendry, D. Schurig, and D.R. Smith: *Controlling Electromagnetic Fields*. Science **312**, 1780 (2006)
- [38] V.M. Shalaev: *Transforming light*. Science **322**, 384 (2008)
- [39] S. Wuestner, A. Pusch, K.L. Tsakmakidis, J.M. Hamm, and O. Hess: *Overcoming Losses with Gain in a Negative Refractive Index Metamaterial*. Phys. Rev. Lett. **105** (12), 127401 (2010)
- [40] S. Xiao, V.P. Drachev, A.V. Kildishev, X. Ni, U.K. Chettiar, H.-K. Yuan, and V.M. Shalaev: *Loss-free and active optical negative-index metamaterials*. Nature **466**, 735 (2010)
- [41] W.J. Padilla: *Group theoretical description of artificial electromagnetic metamaterials*. Opt. Express **15** (4), 1639 (2007)

-
- [42] C. Menzel, A. Andryieuski, C. Rockstuhl, R. Iliew, R. Malureanu, F. Lederer, and A. Lavrinenko: *High symmetry versus optical isotropy of a negative index metamaterial*. Phys. Rev. B **85** (19), 195123 (2010)
- [43] W. Zhang, B. Gallinet, and O.J.F. Martin: *Symmetry and selection rules for localized surface plasmon resonances in nanostructures*. Phys. Rev. B **81** (23), 233407 (2010)
- [44] C. Menzel, C. Rockstuhl, and F. Lederer: *Advanced Jones calculus for the classification of periodic metamaterials*. Phys. Rev. A **82** (5), 053811 (2010)
- [45] G. Dolling, M. Wegener, A. Schädle, S. Burger, and S. Linden: *Observation of magnetization waves in negative-index photonic metamaterials*. Appl. Phys. Lett. **89** (23), 231118 (2006)
- [46] U. Kreibig and M. Vollmer: *Optical properties of metal clusters*. Springer Berlin (1995)
- [47] P.B. Johnson and R.W. Christy: *Optical Constants of the Noble Metals*. Phys. Rev. B **6** (12), 4370 (1972)
- [48] S. Kawata: *Near-field optics and surface plasmon polaritons*. Springer Heidelberg (2001)
- [49] G. Mie: *Beiträge zur Optik trüber Medien, speziell kolloidaler Metallösungen*. Annalen der Physik **330** (3), 377 (1908)
- [50] C.F. Bohren and D.R. Huffman: *Absorption and scattering of light by small particles*. Wiley New York (1983)
- [51] R.M. Walser: *Electromagnetic metamaterials*. Proc. SPIE **4467**, 1 (2001)
- [52] D. Schurig, J.J. Mock, B.J. Justice, S.A. Cummer, J.B. Pendry, A.F. Starr, and D.R. Smith: *Metamaterial Electromagnetic Cloak at Microwave Frequencies*. Science **314**, 977 (2006)
- [53] A.V. Kildishev and V. Shalaev: *Engineering space for light via transformation optics*. Opt. Lett. **33** (1), 43 (2008)
- [54] M.S. Wheeler, J.S. Aitchison, and M. Mojahedi: *Three-dimensional array of dielectric spheres with an isotropic negative permeability at infrared frequencies*. Phys. Rev. B **72** (19), 193103 (2005)
- [55] V. Yannopoulos: *Artificial magnetism and negative refractive index in three-dimensional metamaterials of spherical particles at near-infrared and visible frequencies*. Appl. Phys. A **87** (2), 259 (2007)
- [56] K. Vynck, D. Felbacq, E. Centeno, A.I. Cabuz, D. Cassagne, and B. Guizal: *All-Dielectric Rod-Type Metamaterials at Optical Frequencies*. Phys. Rev. Lett. **102** (4), 133901 (2009)

- [57] C. Enkrich, M. Wegener, S. Linden, S. Burger, L. Zschiedrich, F. Schmidt, J.F. Zhou, T. Koschny, and C.M. Soukoulis: *Magnetic Metamaterials at Telecommunication and Visible Frequencies*. Phys. Rev. Lett. **95** (20), 203901 (2005)
- [58] V.M. Shalaev, W. Cai, U.K. Chettiar, H.K. Yuan, A.K. Sarychev, V.P. Drachev, and A.V. Kildishev: *Negative index of refraction in optical metamaterials*. Opt. Lett. **30** (24), 3356 (2005)
- [59] G. Dolling, C. Enkrich, M. Wegener, J.F. Zhou, C.M. Soukoulis, and S. Linden: *Cut-wire pairs and plate pairs as magnetic atoms for optical metamaterials*. Opt. Lett. **30** (23), 3198 (2005)
- [60] S. Zhang, W. Fan, N.C. Panoiu, K.J. Malloy, R.M. Osgood, and S.R.J. Brueck: *Experimental Demonstration of Near-Infrared Negative-Index Metamaterials*. Phys. Rev. Lett. **95** (13), 137404 (2005)
- [61] D. Schattschneider: *The plane symmetry groups: their recognition and notation*. American Mathematical Monthly **85** (6), 439 (1978)
- [62] V.A. Fedotov, M. Rose, S.L. Prosvirnin, N. Papasimakis, and N.I. Zheludev: *Sharp Trapped-Mode Resonances in Planar Metamaterials with a Broken Structural Symmetry*. Phys. Rev. Lett. **99** (14), 147401 (2007)
- [63] A. Christ, O.J. Martin, Y. Ekinici, N.A. Gippius, and S.G. Tikhodeev: *Symmetry Breaking in a Plasmonic Metamaterial at Optical Wavelength*. Nano Lett. **8** (8), 2171 (2008)
- [64] T. Pakizeh, A. Dmitriev, M.S. Abrishamian, N. Granpayeh, and M. Käll: *Structural asymmetry and induced optical magnetism in plasmonic nanosandwiches*. J. Opt. Soc. Am. B **25** (4), 659 (2008)
- [65] A.E. Miroshnichenko, S. Flach, and Y.S. Kivshar: *Fano resonances in nanoscale structures*. Rev. Mod. Phys. **82** (3), 2257 (2010)
- [66] D.R. Smith, S. Schultz, P. Markoš, and C.M. Soukoulis: *Determination of effective permittivity and permeability of metamaterials from reflection and transmission coefficients*. Phys. Rev. B **65** (19), 195104 (2002)
- [67] D.R. Smith, D.C. Vier, T. Koschny, and C.M. Soukoulis: *Electromagnetic parameter retrieval from inhomogeneous metamaterials*. Phys. Rev. E **71** (3), 36617 (2005)
- [68] X. Chen, T.M. Grzegorzcyk, B.-I. Wu, J. Pacheco, and J.A. Kong: *Robust method to retrieve the constitutive effective parameters of metamaterials*. Phys. Rev. E **70**, 016608 (2004)
- [69] X. Chen, B.I. Wu, J.A. Kong, and T.M. Grzegorzcyk: *Retrieval of the effective constitutive parameters of bianisotropic metamaterials*. Phys. Rev. E **71** (4), 046610 (2005)

- [70] C. Menzel, C. Rockstuhl, T. Paul, and F. Lederer: *Retrieving effective parameters for quasiplanar chiral metamaterials*. Appl. Phys. Lett. **93** (23), 233106 (2008)
- [71] D.H. Kwon, D.H. Werner, A.V. Kildishev, and V.M. Shalaev: *Material parameter retrieval procedure for general bi-isotropic metamaterials and its application to optical chiral negative-index metamaterial design*. Opt. Express **16** (16), 11822 (2008)
- [72] C. Menzel, C. Rockstuhl, T. Paul, F. Lederer, and T. Pertsch: *Retrieving effective parameters for metamaterials at oblique incidence*. Phys. Rev. B **77** (19), 195328 (2008)
- [73] J.J. Hopfield and D.G. Thomas: *Theoretical and experimental effects of spatial dispersion on the optical properties of crystals*. Phys. Rev. **132** (2), 563 (1963)
- [74] A. Serdyukov, I. Semchenko, S. Tretyakov, and A. Sihvola: *Electromagnetics of bi-anisotropic materials: Theory and applications*. Gordon and Breach Science Publishers (2001)
- [75] C. Menzel, T. Paul, C. Rockstuhl, T. Pertsch, S. Tretyakov, and F. Lederer: *Validity of effective material parameters for optical fishnet metamaterials*. Phys. Rev. B **81** (3), 035320 (2010)
- [76] A.I. Cabuz, D. Felbacq, and D. Cassagne: *Spatial dispersion in negative-index composite metamaterials*. Phys. Rev. A **77** (1), 13807 (2008)
- [77] C. Rockstuhl, C. Menzel, T. Paul, T. Pertsch, and F. Lederer: *Light propagation in a fishnet metamaterial*. Phys. Rev. B **78** (15), 155102 (2008)
- [78] C. Menzel, C. Helgert, J. Üpping, C. Rockstuhl, E.-B. Kley, R.B. Wehrspohn, T. Pertsch, and F. Lederer: *Angular resolved effective optical properties of a Swiss cross metamaterial*. Appl. Phys. Lett. **95** (13), 131104 (2009)
- [79] M. Decker, S. Burger, S. Linden, and M. Wegener: *Magnetization waves in split-ring-resonator arrays: Evidence for retardation effects*. Phys. Rev. B **80** (19), 193102 (2009)
- [80] A. Minovich, D.N. Neshev, D.A. Powell, I. Shadrivov, M. Lapine, I. McKerracher, H.T. Hattori, H.H. Tan, C. Jagadish, and Y. Kivshar: *Tilted response of fishnet metamaterials at near-infrared optical wavelengths*. Phys. Rev. B **81** (11), 115109 (2010)
- [81] D. Li, L. Qin, D.X. Qi, F. Gao, R.W. Peng, J. Zou, Q.J. Wang, and M. Wang: *Tunable electric and magnetic resonances in multilayered metal/dielectric nanoplates at optical frequencies*. J. Phys. D: Appl. Phys. **43**, 345102 (2010)
- [82] P.W. Kolb, T.D. Corrigan, H.D. Drew, A.B. Sushkov, R.J. Phaneuf, A. Khanikaev, S.H. Mousavi, and G. Shvets: *Bianisotropy and spatial dispersion in highly anisotropic near-infrared resonator arrays*. Opt. Express **18** (23), 24025 (2010)

-
- [83] Z. Liu, K.-P. Chen, X. Ni, V.P. Drachev, V.M. Shalaev, and A.V. Kildishev: *Experimental verification of two-dimensional spatial harmonic analysis at oblique light incidence*. J. Opt. Soc. Am. B **27** (12), 2465 (2010)
- [84] L. Lin and A. Roberts: *Angle-robust resonances in cross-shaped aperture arrays*. Appl. Phys. Lett. **97** (6), 061109 (2010)
- [85] T. Paul, C. Menzel, C. Rockstuhl, and F. Lederer: *Advanced Optical Metamaterials*. Adv. Mater. **22**, 2354 (2010)
- [86] A. Minovich, D.N. Neshev, D.A. Powell, I.V. Shadrivov, and Y.S. Kivshar: *Tunable fishnet metamaterials infiltrated by liquid crystals*. Appl. Phys. Lett. **96** (19), 193103 (2010)
- [87] N.A. Mortensen, M. Yan, O. Sigmund, and O. Breinbjerg: *On the unambiguous determination of effective optical properties of periodic metamaterials: a one-dimensional case study*. J. Europ. Opt. Soc. Rap. Public. **5**, 10010 (2010)
- [88] S.B. Raghunathan and N.V. Budko: *Effective permittivity of finite inhomogeneous objects*. Phys. Rev. B **81** (5), 054206 (2010)
- [89] L. Jelinek, R. Marques, and J. Machac: *Fishnet Metamaterials - Rules for Refraction and Limits of Homogenization*. Opt. Express **18** (17), 17940 (2010)
- [90] C.R. Simovski and S.A. Tretyakov: *On effective electromagnetic parameters of artificial nanostructured magnetic materials*. Phot. Nano. Fund. Appl. **8**, 254 (2010)
- [91] V.A. Markel and J.C. Schotland: *Homogenization of Maxwell's equations in periodic composites*. arXiv:1010.6246v1 [physics.optics] (2010)
- [92] C.R. Simovski: *On electromagnetic characterization and homogenization of nanostructured metamaterials*. J. Opt. **13**, 013001 (2011)
- [93] E. Yablonovitch: *Inhibited spontaneous emission in solid-state physics and electronics*. Phys. Rev. Lett. **58** (20), 2059 (1987)
- [94] S. John: *Strong Localization of Photon in Certain Disordered Dielectric Structures*. Phys. Rev. Lett. **58** (23), 2486 (1987)
- [95] S. Burgos, R. de Waele, A. Polman, and H.A. Atwater: *A single-layer wide-angle negative-index metamaterial at visible frequencies*. Nature Mater. **9**, 407 (2010)
- [96] E. Verhagen, R. de Waele, L. Kuipers, and A. Polman: *Three-dimensional negative index of refraction at optical frequencies by coupling plasmonic waveguides*. Phys. Rev. Lett. **105** (4), 223901 (2010)
- [97] L.R. Arnaut: *Chirality in multi-dimensional space with application to electromagnetic*

- characterisation of multi-dimensional chiral and semi-chiral media.* J. Electromagn. Waves. Appl. **11** (11), 1459 (1997)
- [98] C.R. Jones: *A New Calculus for the Treatment of Optical Systems.* J. Opt. Soc. Am **31**, 488 (1941)
- [99] R.J. Potton: *Reciprocity in optics.* Rep. Progr. Phys. **67**, 717 (2004)
- [100] B.W.T. Kelvin: *Baltimore lectures on molecular dynamics and the wave theory of light.* C.J. Clay and Sons, Cambridge University Press Warehouse (1904)
- [101] J. Petschulat, C. Menzel, A. Chipouline, C. Rockstuhl, A. Tünnermann, F. Lederer, and T. Pertsch: *Multipole approach to metamaterials.* Phys. Rev. A **78** (4), 043811 (2008)
- [102] J. Petschulat, A. Chipouline, A. Tünnermann, T. Pertsch, C. Menzel, C. Rockstuhl, and F. Lederer: *Multipole Nonlinearity of Metamaterials.* Phys. Rev. A **80** (6), 063828 (2009)
- [103] R.-L. Chern and D. Felbacq: *Artificial magnetism and anticrossing interaction in photonic crystals and split-ring structures.* Phys. Rev. B **79** (7), 075118 (2009)
- [104] J. Petschulat, A. Chipouline, A. Tünnermann, T. Pertsch, C. Menzel, C. Rockstuhl, T. Paul, and F. Lederer: *Simple and versatile analytical approach for planar metamaterials.* Phys. Rev. B **82** (7), 075102 (2010)
- [105] T.J. Davis, D.E. Gomez, and K.C. Vernon: *Simple Model for the Hybridization of Surface Plasmon Resonances in Metallic Nanoparticles.* Nano Lett. **10**, 2618 (2010)
- [106] D.K. Morits and C.R. Simovski: *Negative effective permeability at optical frequencies produced by rings of plasmonic dimers.* Phys. Rev. B **81** (20), 205112 (2010)
- [107] M.G. Moharam and T.K. Gaylord: *Diffraction analysis of dielectric surface-relief gratings.* J. Opt. Soc. Am. **72** (10), 1385 (1982)
- [108] J. Turunen: *Diffraction theory of microrelief gratings*, chap. 2, 31–52. Micro-Optics, Elements, systems and applications. Taylor & Francis, London (1997)
- [109] L. Li: *New formulation of the Fourier modal method for crossed surface-relief gratings.* J. Opt. Soc. Am. A **14** (10), 2758 (1997)
- [110] H.K. Yuan, U.K. Chettiar, W. Cai, A.V. Kildishev, A. Boltasseva, V.P. Drachev, and V.M. Shalaev: *A negative permeability material at red light.* Opt. Express **15** (3), 1076 (2007)
- [111] S. Xiao, U.K. Chettiar, A.V. Kildishev, V.P. Drachev, and V. Shalaev: *Yellow-light Negative-index Metamaterials.* Opt. Lett. **34** (22), 3478 (2009)

-
- [112] A. Taflove and S.C. Hagness: *Computational Electrodynamics: The Finite-Difference Time-Domain Method*. Artech House, 3rd ed. (2005)
- [113] A. Farjadpour, D. Roundy, A. Rodriguez, M. Ibanescu, P. Bermel, JD Joannopoulos, S.G. Johnson, and GW Burr: *Improving accuracy by subpixel smoothing in the finite-difference time domain*. Opt. Lett. **31** (20), 2972 (2006)
- [114] R. Esteban, R. Vogelgesang, J. Dorfmueller, A. Dmitriev, C. Rockstuhl, C. Etrich, and K. Kern: *Direct Near-Field Optical Imaging of Higher Order Plasmonic Resonances*. Nano Lett. **8** (10), 3155 (2008)
- [115] I. Freestone, N. Meeks, M. Sax, and C. Higgitt: *The Lycurgus cup – a Roman nanotechnology*. Gold Bulletin **40** (4), 270 (2007)
- [116] S.A. Campbell: *The science and engineering of microelectronic fabrication*. Oxford University Press New York (1996)
- [117] B. Bhushan: *Springer handbook of nanotechnology*. Springer Heidelberg (2006)
- [118] A. Boltasseva and V.M. Shalaev: *Fabrication of optical negative-index metamaterials: Recent advances and outlook*. Metamaterials **2** (1), 1 (2008)
- [119] A.N. Broers, A.C.F. Hoole, and J.M. Ryan: *Electron beam lithography–Resolution limits*. Microelectron. Eng. **32**, 131 (1996)
- [120] C. Vieu, F. Carcenac, A. Pepin, Y. Chen, M. Mejias, A. Lebib, L. Manin-Ferlazzo, L. Couraud, and H. Launois: *Electron beam lithography: resolution limits and applications*. Appl. Surf. Sci. **164**, 111 (2000)
- [121] R. Ito and S. Okazaki: *Pushing the limits of lithography*. Nature **406** (6799), 1027 (2000)
- [122] S.R.J. Brueck: *Optical and interferometric lithography-nanotechnology enablers*. Proc. IEEE **93** (10), 1704 (2005)
- [123] N. Feth, C. Enkrich, M. Wegener, and S. Linden: *Large-area magnetic metamaterials via compact interference lithography*. Opt. Express **15** (2), 501 (2007)
- [124] S. Maruo, O. Nakamura, and S. Kawata: *Three-dimensional microfabrication with two-photon-absorbed photopolymerization*. Opt. Lett. **22** (2), 132 (1997)
- [125] G. von Freymann, A. Ledermann, M. Thiel, I. Staude, S. Essig, K. Busch, and M. Wegener: *Three-Dimensional Nanostructures for Photonics*. Adv. Funct. Mater. **20**, 1038 (2010)
- [126] S.W. Hell and J. Wichmann: *Breaking the diffraction resolution limit by stimulated emission: stimulated-emission-depletion fluorescence microscopy*. Opt. Lett. **19** (11), 780 (1994)

-
- [127] J. Fischer, G. von Freymann, and M. Wegener: *The Materials Challenge in Diffraction-Unlimited Direct-Laser-Writing Optical Lithography*. Adv. Funct. Mater. **22**, 3578 (2010)
- [128] C. Enkrich, F. Pérez-Willard, D. Gerthsen, JF Zhou, T. Koschny, C.M. Soukoulis, M. Wegener, and S. Linden: *Focused-Ion-Beam Nanofabrication of Near-Infrared Magnetic Metamaterials*. Adv. Mater. **17**, 2547 (2005)
- [129] N. Liu, L.W. Fu, S. Kaiser, H. Schweizer, and H. Giessen: *Plasmonic building blocks for magnetic molecules in three-dimensional metamaterials*. Adv. Mater. **20**, 3859 (2008)
- [130] P.R. West, S. Ishii, G. Naik, N. Emani, V.M. Shalaev, and A. Boltasseva: *Searching for Better Plasmonic Materials*. Laser Photonics Rev. **1**, 1 (2010)
- [131] A. Boltasseva and H.A. Atwater: *Low-Loss Plasmonic Metamaterials*. Science **331** (6015), 290 (2011)
- [132] F. Salmassi, P.P. Naulleau, and E.M. Gullikson: *Spin-on-glass coatings for the generation of superpolished substrates for use in the extreme-ultraviolet region*. Appl. Opt. **45** (11), 2404 (2006)
- [133] G. Subramania and S.Y. Lin: *Fabrication of three-dimensional photonic crystal with alignment based on electron beam lithography*. Appl. Phys. Lett. **85** (21), 5037 (2004)
- [134] N. Liu, H. Guo, L. Fu, S. Kaiser, H. Schweizer, and H. Giessen: *Three-dimensional photonic metamaterials at optical frequencies*. Nature Mater. **7**, 31 (2008)
- [135] Y. Chen, S. Milenkovic, and A.W. Hassel: *Arrays of iso-oriented gold nanobelts*. Nano Lett. **8** (2), 737 (2008)
- [136] H. Liu, X. Zhao, Y. Yang, Q. Li, and J. Lv: *Fabrication of Infrared Left-Handed Metamaterials via Double Template-Assisted Electrochemical Deposition*. Adv. Mater. **20** (11), 2050 (2008)
- [137] M. Ruther, L.H. Shao, S. Linden, J. Weissmüller, and M. Wegener: *Electrochemical restructuring of plasmonic metamaterials*. Appl. Phys. Lett. **98**, 013112 (2011)
- [138] P. Nagpal, S.E. Han, A. Stein, and D.J. Norris: *Efficient Low-Temperature Thermophotovoltaic Emitters from Metallic Photonic Crystals*. Nano Lett. **8** (10), 3238 (2008)
- [139] C.E. Kriegler, M.S. Rill, M. Thiel, E. Müller, S. Essig, A. Frölich, G. von Freymann, S. Linden, D. Gerthsen, H. Hahn, K. Busch, and M. Wegener: *Transition between corrugated metal films and split-ring-resonator arrays*. Appl. Phys. B **96**, 749 (2009)
- [140] J.-S. Huang, V. Callegari, P. Geisler, C. Brüning, J. Kern, J.C. Prangma, P. Weinmann, M. Kamp, A. Forchel, P. Biagioni, U. Sennhauser, and B. Hecht: *Atomically flat single-crystalline gold nanostructures*. Nature Commun. **1**, 150 (2010)

- [141] M. Leskelä and M. Ritala: *Atomic layer deposition (ALD): from precursors to thin film structures*. *Thin Solid Films* **409** (1), 138 (2002)
- [142] M.S. Rill, C. Plet, M. Thiel, I. Staude, G. von Freymann, S. Linden, and M. Wegener: *Photonic metamaterials by direct laser writing and silver chemical vapour deposition*. *Nature Mat.* **7** (7), 543 (2008)
- [143] M.S. Rill, C.E. Kriegler, M. Thiel, G. von Freymann, S. Linden, and M. Wegener: *Negative-index bi-anisotropic photonic metamaterial fabricated by direct laser writing and silver shadow evaporation*. *Opt. Lett.* **34** (1), 19 (2009)
- [144] H. Im, K.C. Bantz, N.C. Lindquist, C.L. Hayner, and S.-H. Oh: *Vertically Oriented Sub-10-nm Plasmonic Nanogap Arrays*. *Nano Lett.* **10**, 2231 (2010)
- [145] S.J. Randolph, J.D. Fowlkes, and P.D. Rack: *Focused, nanoscale electron-beam-induced deposition and etching*. *Crit. Rev. Solid State Mater. Sci.* **31** (3), 55 (2006)
- [146] I. Utke, P. Hoffmann, and J. Melngailis: *Gas-assisted focused electron beam and ion beam processing and fabrication*. *J. Vac. Sci. Technol. B* **26** (4), 1197 (2008)
- [147] S. Graells, R. Alcuilla, G. Badenes, and R. Quidant: *Growth of plasmonic gold nanostructures by electron beam induced deposition*. *Appl. Phys. Lett.* **91**, 121112 (2007)
- [148] A. Botman, JJ.L. Mulders, and C.W. Hagen: *Creating pure nanostructures from electron-beam-induced deposition using purification techniques: a technology perspective*. *Nanotechnology* **20**, 372001 (2009)
- [149] S. Graells, S. Acímović, G. Volpe, and R. Quidant: *Direct Growth of Optical Antennas Using E-Beam-Induced Gold Deposition*. *Plasmonics* **5** (2), 135 (2010)
- [150] J.E. Mahan: *Physical vapor deposition of thin films*. Wiley New York (2000)
- [151] V.M. Shalaev: *Optical properties of nanostructured random media*. Springer Heidelberg (2002)
- [152] K.P. Chen, V.P. Drachev, J.D. Borneman, A.V. Kildishev, and V.M. Shalaev: *Drude Relaxation Rate in Grained Gold Nanoantennas*. *Nano Lett.* **10**, 916 (2010)
- [153] P. Nagpal, N.C. Lindquist, S.-H. Oh, and D. Norris: *Ultrasmooth Patterned Metals for Plasmonics and Metamaterials*. *Science* **325**, 594 (2009)
- [154] Y. Chen, A.S. Schwanecke, V.A. Fedotov, V.V. Khardikov, P.L. Mladyonov, S.L. Prosvirnin, A.V. Rogacheva, N.I. Zheludev, and E. Huq: *Electron beam lithography for high density meta fish scale operational at optical frequency*. *Microelectron. Eng.* **86**, 1081 (2009)
- [155] N. Liu, H. Liu, S. Zhu, and H. Giessen: *Stereometamaterials*. *Nature Photon.* **3**, 157 (2009)

- [156] H. Aouani, J. Wenger, D. Gérard, H. Rigneault, E. Devaux, T.W. Ebbesen, F. Mahdavi, T. Xu, and S. Blair: *Crucial Role of the Adhesion Layer on the Plasmonic Fluorescence Enhancement*. ACS Nano **3** (7), 2043 (2009)
- [157] J.M. Kontio, H. Husu, J. Simonen, M.J. Huttunen, J. Tommila, M. Pessa, and M. Kauhanen: *Nanoimprint fabrication of gold nanocones with 10 nm tips for enhanced optical interactions*. Opt. Lett. **34** (13), 1979 (2009)
- [158] Z. Ku, J. Zhang, and S.R. Brueck: *Bi-anisotropy of multiple-layer fishnet negative-index metamaterials due to angled sidewalls*. Opt. Express **17** (8), 6782 (2009)
- [159] G. Dolling, M. Wegener, and S. Linden: *Realization of a three-functional-layer negative-index photonic metamaterial*. Opt. Lett. **32** (5), 551 (2007)
- [160] D.B. Burckel, J.R. Wendt, G.A. Ten Eyck, A.R. Ellis, I. Brener, and M.B. Sinclair: *Fabrication of 3D Metamaterial Resonators Using Self-Aligned Membrane Projection Lithography*. Adv. Mater. **22**, 3171 (2010)
- [161] D.B. Burckel, J.R. Wendt, G.A. Ten Eyck, J.C. Ginn, A.R. Ellis, I. Brener, and M.B. Sinclair: *Micrometer-Scale Cubic Unit Cell 3D Metamaterial Layers*. Adv. Mater. **22**, 5053 (2010)
- [162] W. Wu, Z. Yu, S.Y. Wang, R.S. Williams, Y. Liu, C. Sun, X. Zhang, E. Kim, Y.R. Shen, and N.X. Fang: *Midinfrared metamaterials fabricated by nanoimprint lithography*. Appl. Phys. Lett. **90**, 063107 (2007)
- [163] I. Bergmair, M. Mühlberger, K. Hingerl, E. Pshenay-Severin, T. Pertsch, E.B. Kley, H. Schmidt, and R. Schöftner: *3D Materials Made of Gold Using Nanoimprint Lithography*. Microelectron. Eng. **87**, 1008 (2010)
- [164] N. Shalkevich, A. Shalkevich, L. Si-Ahmed, and T. Bürgi: *Reversible formation of gold nanoparticle–surfactant composite assemblies for the preparation of concentrated colloidal solutions*. Phys. Chem. Chem. Phys. **11**, 10175 (2009)
- [165] D.A. Pawlak, S. Turczynski, M. Gajc, K. Kolodziejak, R. Diduszko, K. Rozniatowski, J. Smalc, and I. Vendik: *How Far Are We from Making Metamaterials by Self-Organization? The Microstructure of Highly Anisotropic Particles with an SRR-Like Geometry*. Adv. Funct. Mater. **20**, 1116 (2010)
- [166] R. Glass, M. Möller, and J.P. Spatz: *Block copolymer micelle nanolithography*. Nanotechnology **14**, 1153 (2003)
- [167] H. Fredriksson, Y. Alaverdyan, A. Dmitriev, C. Langhammer, D.S. Sutherland, M. Zäch, and B. Kasemo: *Hole–Mask Colloidal Lithography*. Adv. Mater. **19**, 4297 (2007)

- [168] A. Dmitriev, T. Pakizeh, M. Käll, and D.S. Sutherland: *Gold-silica-gold nanosandwiches: tunable bimodal plasmonic resonators*. *Small* **3** (2), 294 (2007)
- [169] A.M. Hung, C.M. Micheel, L.D. Bozano, L.W. Osterbur, G.M. Wallraff, and J.N. Cha: *Large-area spatially ordered arrays of gold nanoparticles directed by lithographically confined DNA origami*. *Nature Nanotech.* **5**, 121 (2010)
- [170] D.J. Cho, W. Wu, E. Ponizovskaya, P. Chaturvedi, A.M. Bratovsky, S.-Y. Wang, X. Zhang, F. Wang, and Y.R. Shen: *Ultrafast response of negative index metamaterials in the near-infrared*. *Proc. of SPIE* **7205**, 72050V (2009)
- [171] J.H. Cho, A. Azam, and D.H. Gracias: *Three Dimensional Nanofabrication Using Surface Forces*. *Langmuir* **26** (21), 16534 (2010)
- [172] L. Lepetit, G. Chériaux, and M. Joffre: *Linear techniques of phase measurement by femtosecond spectral interferometry for applications in spectroscopy*. *J. Opt. Soc. Am. B* **12** (12), 2467 (1995)
- [173] V.P. Drachev, W. Cai, U.K. Chettiar, H.K. Yuan, A.K. Sarychev, A.V. Kildishev, G. Klimeck, and V.M. Shalaev: *Experimental verification of an optical negative index material*. *Laser Phys. Lett.* **3** (1), 49 (2006)
- [174] E. Pshenay-Severin, F. Setzpfandt, C. Helgert, U. Hübner, C. Menzel, C. Rockstuhl, A. Tünnermann, F. Lederer, and T. Pertsch: *Spectral characterization of metamaterials in amplitude and phase by white-light interferometry*. *J. Opt. Soc. Am. B* **27** (4), 660 (2010)
- [175] J. Zhou, T. Koschny, M. Kafesaki, E.N. Economou, J.B. Pendry, and C.M. Soukoulis: *Saturation of the Magnetic Response of Split-Ring Resonators at Optical Frequencies*. *Phys. Rev. Lett.* **95** (22), 223902 (2005)
- [176] V.M. Shalaev: *Optical negative-index metamaterials*. *Nature Photon.* **1**, 41 (2007)
- [177] G. Dolling, M. Wegener, C.M. Soukoulis, and S. Linden: *Design-related losses of double-fishnet negative-index photonic metamaterials*. *Opt. Express* **15** (18), 11536 (2007)
- [178] G. Dolling, C. Enkrich, M. Wegener, C.M. Soukoulis, and S. Linden: *Simultaneous Negative Phase and Group Velocity of Light in a Metamaterial*. *Science* **312**, 892 (2006)
- [179] J.B. Pendry, A.J. Holden, W.J. Stewart, and I. Youngs: *Extremely low frequency plasmons in metallic mesostructures*. *Phys. Rev. Lett.* **76** (25), 4773 (1996)
- [180] V.A. Podolskiy, A.K. Sarychev, and V.M. Shalaev: *Plasmon modes in metal nanowires and left-handed materials*. *J. Nonlinear Opt. Phys. Mater.* **11** (1), 65 (2002)

- [181] G. Dolling, C. Enkrich, M. Wegener, C.M. Soukoulis, and S. Linden: *Low-loss negative-index metamaterial at telecommunication wavelengths*. Opt. Lett. **31** (12), 1800 (2006)
- [182] S. Zhang, W. Fan, K.J. Malloy, S.R.J. Brueck, N.C. Panoiu, and R.M. Osgood: *Demonstration of metal-dielectric negative-index metamaterials with improved performance at optical frequencies*. J. Opt. Soc. Am. B **23** (3), 434 (2006)
- [183] G. Dolling, M. Wegener, C.M. Soukoulis, and S. Linden: *Negative-index metamaterial at 780 nm wavelength*. Opt. Lett. **32** (1), 53 (2007)
- [184] C. Helgert, C. Menzel, C. Rockstuhl, E. Pshenay-Severin, E.-B. Kley, A. Chipouline, A. Tünnermann, F. Lederer, and T. Pertsch: *Polarization independent negative-index metamaterial in the near-infrared*. Opt. Lett. **34** (5), 704 (2009)
- [185] M. Kafesaki, I. Tsiapa, N. Katsarakis, T. Koschny, C.M. Soukoulis, and E.N. Economou: *Left-handed metamaterials: The fishnet structure and its variations*. Phys. Rev. B **75** (23), 235114 (2007)
- [186] P. Ding, E.J. Liang, W.Q. Hu, L. Zhang, Q. Zhou, and Q.Z. Xue: *Numerical simulations of terahertz double-negative metamaterial with isotropic-like fishnet structure*. Photon. Nanostruct.: Fundam. Applic. **7** (2), 92 (2009)
- [187] X. Wang, Y.H. Ye, C. Zheng, Y. Qin, and T.J. Cui: *Tunable figure of merit for a negative-index metamaterial with a sandwich configuration*. Opt. Lett. **34** (22), 3568 (2009)
- [188] P. Hahmann, L. Bettin, M. Boettcher, U. Denker, T. Elster, S. Jahr, U.-C. Kirschstein, K.-H. Kliem, and B. Schnabel: *High resolution variable-shaped beam direct write*. Microelectron. Eng. **84**, 774 (2007)
- [189] U.D. Zeitner and E.-B. Kley: *Advanced lithography for micro-optics*. Proc. SPIE **6290**, 629009 (2006)
- [190] W. Zhang, A. Potts, D.M. Bagnall, and B.R. Davidson: *Large area all-dielectric planar chiral metamaterials by electron beam lithography*. J. Vac. Sci. Technol. B **24**, 1455 (2006)
- [191] I. Haller, M. Hatzakis, and R. Srinivasan: *High-resolution positive resists for electron-beam exposure*. IBM Journal of Research and Development **12** (3), 251 (1968)
- [192] D.R.S. Cumming, S. Thoms, S.P. Beaumont, and J.M.R. Weaver: *Fabrication of 3 nm wires using 100 keV electron beam lithography and poly (methyl methacrylate) resist*. Appl. Phys. Lett. **68** (3), 322 (1996)
- [193] K. Fuchsels, U. Schulz, N. Kaiser, and A. Tünnermann: *Optical Properties of ITO Thin Films Produced by Plasma Ion-Assisted Evaporation and Pulsed DC Sputtering*. In *52nd Annual Technical Conference Proc., Santa Clara, CA, May 9 - 14* (2009)

- [194] R. Plontke, L. Bettin, D. Beyer, J. Butschke, M. Irmscher, C. Koepernik, B. Leibold, A.B. Vix, and P. Voehringer: *Avoidance/reduction of charging effects in case of partially insufficient substrate conductivity when using ESPACER 300 Z*. Proc. SPIE **5504**, 188 (2004)
- [195] P.D. Drachev, U.K. Chettiar, A.V. Kildishev, H. Yuan, W. Cai, and V. Shalaev: *The Ag dielectric function in plasmonic metamaterials*. Opt. Express **16** (2), 1186 (2008)
- [196] E. Plum, K. Tanaka, W.T. Chen, V.A. Fedotov, D.P. Tsai, and N.I. Zheludev: *A combinatorial approach to metamaterials discovery*. J. Opt. **13**, 055102 (2011)
- [197] J. Nakamura, K. Deguchi, and H. Ban: *Resist Surface Roughness Calculated using Theoretical Percolation Model*. J. Photopolym. Sci. Technol. **11** (4), 571 (1998)
- [198] A. Mary, S.G. Rodrigo, F.J. Garica-Vidal, and L. Martin-Moreno: *Theory of Negative-Refractive-Index Response of Double-Fishnet Structure*. Phys. Rev. Lett. **101** (4), 103902 (2008)
- [199] C. Rockstuhl, T. Zentgraf, T.P. Meyrath, H. Giessen, and F. Lederer: *Resonances in complementary metamaterials and nanoapertures*. Opt. Express **16** (3), 2080 (2008)
- [200] D.J. Cho, F. Wang, X. Zhang, and R.S. Shen: *Contribution of the electric quadrupole resonance in optical metamaterials*. Phys. Rev. B **78** (12), 121101(R) (2008)
- [201] U.K. Chettiar, A.V. Kildishev, H.K. Yuan, W. Cai, S. Xiao, V.P. Drachev, and V.M. Shalaev: *Dual-Band Negative Index Metamaterial: Double-Negative at 813 nm and Single-Negative at 772 nm*. Opt. Lett. **32** (12), 1671 (2007)
- [202] T. Paul, C. Rockstuhl, C. Menzel, and F. Lederer: *Anomalous refraction, diffraction and imaging metamaterials*. Phys. Rev. B **79** (11), 115430 (2009)
- [203] M. Kuwata-Gonokami, N. Saito, Y. Ino, M. Kauranen, K. Jefimovs, T. Vallius, J. Turunen, and Y. Svirko: *Giant optical activity in quasi-two-dimensional planar nanostructures*. Phys. Rev. Lett. **95** (22), 227401 (2005)
- [204] S.I. Maslovski, D.K. Morits, and S.A. Tretyakov: *Symmetry and reciprocity constraints on diffraction by gratings of quasi-planar particles*. J. Opt. A **11**, 074004 (2009)
- [205] S.N. Volkov, K. Dolgaleva, R.W. Boyd, K. Jefimovs, J. Turunen, Y. Svirko, B.K. Canfield, and M. Kauranen: *Optical activity in diffraction from a planar array of achiral nanoparticles*. Phys. Rev. A **79** (4), 43819 (2009)
- [206] B. Bai, J. Laukkanen, A. Lehmuskero, and J. Turunen: *Simultaneously enhanced transmission and artificial optical activity in gold film perforated with chiral hole array*. Phys. Rev. B **81** (11), 115424 (2010)

- [207] S.R. Deng, B.R. Lu, B.Q. Dong, J. Wan, Z. Shu, J. Xue, Y. Chen, E. Huq, R. Liu, and X.P. Qu: *Effective polarization control of metallic planar chiral metamaterials with complementary rosette pattern fabricated by nanoimprint lithography*. *Microelectron. Eng.* **87**, 985 (2010)
- [208] S.V. Zhukovsky, A.V. Novitsky, and V.M. Galynsky: *Elliptical dichroism: operating principle of planar chiral metamaterials*. *Opt. Lett.* **34** (13), 1988 (2009)
- [209] A.V. Rogachewa, V.A. Fedotov, A.S. Schwanecke, and N.I. Zheludev: *Giant gyrotropy due to electromagnetic-field coupling in a bilayered chiral structure*. *Phys. Rev. Lett.* **97** (17), 177401 (2006)
- [210] E. Plum, V.A. Fedotov, A.S. Schwanecke, N.I. Zheludev, and Y. Chen: *Giant optical gyrotropy due to electromagnetic coupling*. *Appl. Phys. Lett.* **90** (22), 223113 (2007)
- [211] M. Decker, M.W. Klein, M. Wegener, and S. Linden: *Circular dichroism of planar chiral magnetic metamaterials*. *Opt. Lett.* **32** (7), 856 (2007)
- [212] E. Plum, J. Zhou, J. Dong, VA Fedotov, T. Koschny, CM Soukoulis, and NI Zheludev: *Metamaterial with negative index due to chirality*. *Phys. Rev. B* **79** (3), 035407 (2009)
- [213] M. Decker, M. Ruther, C.E. Kriegler, J. Zhou, C.M. Soukoulis, S. Linden, and M. Wegener: *Strong optical activity from twisted-cross photonic metamaterials*. *Opt. Lett.* **34** (16), 2501 (2009)
- [214] J. Zhou, J. Dong, B. Wang, T. Koschny, M. Kafesaki, and C.M. Soukoulis: *Negative refractive index due to chirality*. *Phys. Rev. B* **79** (12), 121104 (2009)
- [215] M. Decker, R. Zhao, C.M. Soukoulis, S. Linden, and M. Wegener: *Twisted split-ring-resonator photonic metamaterial with huge optical activity*. *Opt. Lett.* **35** (10), 1593 (2010)
- [216] R. Zhao, L. Zhang, J. Zhou, T. Koschny, and C.M. Soukoulis: *Conjugated swastika chiral metamaterial with uniaxial optical activity and negative refractive index*. *Phys. Rev. B* **83**, 035105 (2011)
- [217] H.S. Oh, S. Liu, H.S. Jee, A. Baev, M.T. Swihart, and P.N. Prasad: *Chiral Poly (fluorene-alt-benzothiadiazole)(PFBT) and Nanocomposites with Gold Nanoparticles: Plasmonically and Structurally Enhanced Chirality*. *J. Am. Chem. Soc.* **132** (49), 17346 (2010)
- [218] Z. Fan and A.O. Govorov: *Plasmonic Circular Dichroism of Chiral Metal Nanoparticle Assemblies*. *Nano Lett.* **10**, 2580 (2010)
- [219] D.R. Smith, D.C. Vier, W. Padilla, S.C. Nemat-Nasser, and S. Schultz: *Loop-wire medium for investigating plasmons at microwave frequencies*. *Appl. Phys. Lett.* **75** (10), 1425 (1999)

-
- [220] C. Rockstuhl, C. Menzel, T. Paul, and F. Lederer: *Optical activity in chiral media composed of three-dimensional metallic meta-atoms*. Phys. Rev. B **79** (3), 035321 (2009)
- [221] D.L. Jaggard, A.R. Mickelson, and C.H. Papas: *On electromagnetic waves in chiral media*. Appl. Phys. A **18** (2), 211 (1979)
- [222] C. Rockstuhl, T. Zentgraf, E. Pshenay-Severin, J. Petschulat, A. Chipouline, J. Kuhl, T. Pertsch, H. Giessen, and F. Lederer: *The origin of magnetic polarizability in metamaterials at optical frequencies - an electrodynamic approach*. Opt. Express **15** (14), 8871 (2007)
- [223] C. Drezet, A. Genet, J.-Y. Laluet, and T.W. Ebbesen: *Optical chirality without optical activity: How surface plasmons give a twist to light*. Opt. Express **16** (17), 12559 (2008)
- [224] E. Plum: *Chirality and metamaterials*. Ph.D. thesis, University of Southampton (2010)
- [225] P. Yeh: *Optical waves in layered media*, vol. 95. Wiley New York (1988)
- [226] N.O. Young and J. Kowal: *Optically active fluorite films*. Nature **183**, 104 (1959)
- [227] P.G. de Gennes and J. Prost: *The Physics of Liquid Crystals*. Oxford University Press (1995)
- [228] I. Hodgkinson, Q. hong Wu, B. Knight, A. Lakhtakia, and K. Robbie: *Vacuum deposition of chiral sculptured thin films with high optical activity*. Appl. Opt **39** (4), 642 (2000)
- [229] E. Plum, V.A. Fedotov, and N.I. Zheludev: *Asymmetric transmission: a generic property of lossy periodic interfaces*. J. Opt. **13**, 024006 (2011)
- [230] A.S. Schwanecke, V.A. Fedotov, V.V. Khardikov, S.L. Prosvirnin, Y. Chen, and N.I. Zheludev: *Nanostructured metal film with asymmetric optical transmission*. Nano Lett. **8** (9), 2940 (2008)
- [231] R. Singh, E. Plum, C. Menzel, C. Rockstuhl, A.K. Azad, R.A. Cheville, F. Lederer, W. Zhang, and N. Zheludev: *Terahertz metamaterial with asymmetric transmission*. Phys. Rev. B **80**, 153104 (2009)
- [232] B. Bai, Y. Svirko, J. Turunen, and T. Vallius: *Optical activity in planar chiral metamaterials: Theoretical study*. Phys. Rev. A **76** (2), 023811 (2007)
- [233] D.A. Powell and Y.S. Kivshar: *Substrate-induced bianisotropy in metamaterials*. Appl. Phys. Lett. **97** (9), 091106 (2010)

- [234] D. Nau, A. Schönhardt, C. Bauer, A. Christ, T. Zentgraf, J. Kuhl, M.W. Klein, and H. Giessen: *Correlation Effects in Disordered Metallic Photonic Crystal Slabs*. Phys. Rev. Lett. **98** (13), 133902 (2007)
- [235] K. Aydin, K. Guven, N. Katsarakis, C. Soukoulis, and E. Ozbay: *Effect of disorder on magnetic resonance band gap of split-ring resonator structures*. Opt. Express **12** (24), 5896 (2004)
- [236] N. Papasimakis, V.A. Fedotov, Y.H. Fu, D.P. Tsai, and N.I. Zheludev: *Coherent and incoherent metamaterials and the order-disorder transitions*. Phys. Rev. B **80** (4), 041102(R) (2009)
- [237] R. Singh, X. Lu, Z. Tian, and W. Zhang: *Random terahertz metamaterials*. J. Opt. **12**, 015101 (2010)
- [238] S.M. Allen, E.L. Thomas, and R.A.L. Jones: *The structure of materials*. Wiley New York (1999)
- [239] R. Rengarajan, D. Mittleman, C. Rich, and V. Colvin: *Effect of disorder on the optical properties of colloidal crystals*. Phys. Rev. E **71** (1), 016615 (2005)
- [240] E. Prodan, C. Radloff, N.J. Halas, and P. Nordlander: *A Hybridization Model for the Plasmon Response of Complex Nanostructures*. Science **302**, 419 (2003)
- [241] C.L. Haynes, A.D. McFarland, L. Zhao, R.P. Van Duyne, G.C. Schatz, L. Gunnarsson, J. Prikulis, B. Kasemo, and M. Käll: *Nanoparticle Optics: The Importance of Radiative Dipole Coupling in Two-Dimensional Nanoparticle Arrays*. J. Phys. Chem. B **107** (30), 7337 (2003)
- [242] C. Rockstuhl, C. Menzel, S. Mühlig, J. Petschulat, C. Helgert, C. Etrich, A. Chipouline, T. Pertsch, and F. Lederer: *Scattering properties of metaatoms*. submitted to Phys. Rev. B
- [243] C.R. Simovski: *Analytical modelling of double-negative composites*. Metamaterials **2** (4), 169 (2008)
- [244] C.R. Simovski: *Material parameters of metamaterials (a Review)*. Opt. Spectrosc. **107** (5), 726 (2009)
- [245] B.J. Seo, T. Ueda, T. Itoh, and H. Fetterman: *Isotropic left handed material at optical frequency with dielectric spheres embedded in negative permittivity medium*. Appl. Phys. Lett. **88** (16), 161122 (2006)
- [246] A.G. Kussow, A. Akyurtlu, and N. Angkawisittpan: *Optically isotropic negative index of refraction metamaterial*. Phys. Status Solidi B **245** (5), 992 (2008)
- [247] P. Mühlischlegel, H.J. Eisler, O.J.F. Martin, B. Hecht, and D.W. Pohl: *Resonant Optical Antennas*. Science **308**, 1607 (2005)

B List of Abbreviations

ALD	Atomic layer deposition
CVD	Chemical vapor deposition
EBL	Electron beam lithography
EUV	Extreme ultraviolet
Eq.	Equation
FDTD	Finite-difference time-domain
FIB	Focused ion beam
Fig.	Figure
FOM	Figure of merit
FMM	Fourier modal method
HSQ	Hydrogen silsesquioxane
IAP	Institute of Applied Physics
IBE	Ion beam etching
ICP	Inductively coupled plasma
IFTO	Institute of Condensed Matter Theory and Solid State Optics
IL	Interference lithography
IOF	Fraunhofer Institute for Applied Optics and Precision Engineering
ITO	Indium tin oxide
LCP	Left-handed circular polarization
NIL	Nanoimprint lithography
OL	Optical lithography
RCP	Right-handed circular polarization
RCWA	Rigorous coupled wave analysis
RIBE	Reactive ion beam etching
RIE	Reactive ion etching
rpm	Revolutions per minute
Sec.	Section
SEM	Scanning electron microscopy
SPP	Surface plasmon polariton

C List of symbols and conventions

a_i	Absorbance for i -polarized light $i = x, y$
c_0	Speed of light in vacuum; $c_0 = 2.9979 \times 10^8 \text{m/s}$
d_i	Semiaxes of an ellipsoidal particle ($i = x, y, z$)
d_{\min}	Minimum interparticle separation between adjacent metaatoms
da	Area segment of a circle to calculate $g(r)$
dr	Radial segment of a circle to calculate $g(r)$
e	Charge of an electron
\mathbf{e}_i	Normalized base vector ($i = x, y$)
f	Area filling fraction of a planar metamaterial
$g(r)$	Pair correlation function for two dimensions; dependent on radial distance r
$\mathbf{j}_0(\mathbf{r}, t)$	Free electric current density; $\mathbf{j}_0(\mathbf{r}, t) = \mathbf{j}_{\text{ext}}(\mathbf{r}, t) + \mathbf{j}_{\text{cond}}(\mathbf{r}, t)$
$\mathbf{j}_{\text{ext}}(\mathbf{r}, t)$	External electric current density
$\mathbf{j}_{\text{cond}}(\mathbf{r}, t)$	Conduction electric current density; $\mathbf{j}_{\text{cond}}(\mathbf{r}, t) = f(\mathbf{E}(\mathbf{r}, t))$
$\mathbf{k}(n, \omega)$	Wave vector
$k(n, \omega)$	Modulus of the wave vector $\mathbf{k}(n, \omega)$
k_x, k_y	Transverse components of the wave vector $\mathbf{k}(n, \omega)$
k_z	Longitudinal component of the wave vector $\mathbf{k}(n, \omega)$
m_e^*	Effective electron mass
$n(\omega)$	Refractive index
$n_{\text{eff}}(\omega)$	Effective refractive index
n_e	Electron density in Drude model
p	Period in both lateral directions of a planar metamaterial
p_i	Period in i -direction of a planar metamaterial ($i = x, y$)
\mathbf{r}	Spatial coordinates (x, y, z)
r	Normalized interparticle distance between adjacent metaatoms; also used as the radius of a circle to calculate $g(r)$
r_i	Reflectance for i -polarized light ($i = x, y$)
s	Thickness of a homogeneous slab
s_i	Side length in i -direction of a cut-wire pair metaatom ($i = x, y$)
t	Time

t_i	Transmittance for i -polarized light ($i = x, y$)
$\hat{\alpha}(\omega)$	Polarizability tensor
$\chi_{\text{el}}(\omega)$	Electric susceptibility
$\chi_{\text{mag}}(\omega)$	Magnetic susceptibility
δ	Circular dichroism
ϵ_0	Vacuum electric permittivity constant; $\epsilon_0 = 8.8542 \times 10^{-12} \text{As/Vm}$
ϵ_{m}	Electric permittivity constant of a dielectric medium
$\epsilon(\omega)$	Electric permittivity
$\epsilon_{\text{eff}}(\omega)$	Effective electric permittivity
$\epsilon_{\text{Drude}}(\omega)$	Electric permittivity from Drude model
γ_0	Damping constant in Drude model
λ	Wavelength
$\mu(\omega)$	Magnetic permeability
μ_0	Vacuum magnetic permeability constant; $\mu_0 = 4\pi \times 10^{-7} \text{Vs/Am}$
$\mu_{\text{eff}}(\omega)$	Effective magnetic permeability
$\rho_0(\mathbf{r}, t)$	Free charge density
$\rho_{\text{ext}}(\mathbf{r}, t)$	Density of external charges
$\langle \rho \rangle$	Average particle number density to calculate $g(r)$
ω_{pl}	Plasma frequency in Drude model
$\mathbf{B}(\mathbf{r}, t)$	Magnetic induction
$C_{n,i}$	n -fold rotational symmetry with respect to the i -axis ($i = x, y, z$)
D	Dimensionless disorder parameter
$\mathbf{D}(\mathbf{r}, t)$	Dielectric displacement
E_i	Electric field coefficient for i -polarization (complex-valued; $i = x, y$ in linear base; $i = +, -$ in circular base)
$\mathbf{E}(\mathbf{r}, t)$	Electric field strength
$\mathbf{E}_{\text{inc}}(\mathbf{r}, t)$	Electric field strength incoming onto a medium
$\mathbf{E}_{\text{trans}}(\mathbf{r}, t)$	Electric field strength transmitted through a medium
$\bar{\mathbf{E}}(\mathbf{r}, \omega)$	Fourier transform of $\mathbf{E}(\mathbf{r}, t)$ with respect to t [likewise: $\bar{\mathbf{P}}(\mathbf{r}, \omega), \bar{\mathbf{M}}(\mathbf{r}, \omega), \bar{\mathbf{H}}(\mathbf{r}, \omega)$]
$\mathbf{H}(\mathbf{r}, t)$	Magnetic field strength
L_i	Geometrical depolarization factor of an ellipsoidal particle ($i = x, y, z$)
$\mathbf{M}(\mathbf{r}, t)$	Magnetization
M_{ij}	Mirror symmetry with respect to the ij -plane ($i = x, y, z$)
R	Reflection coefficient (complex-valued)
$\mathbf{P}(\mathbf{r}, t)$	Dielectric polarization
T	Transmission coefficient (complex-valued)
T_i	Transmission coefficient for i -polarization (complex-valued;

	$i = x, y$ in linear base; $i = +, -$ in circular base)
$\mathbf{T}_{\text{lin,circ}}^{\text{f,b}}$	Total transmission (complex-valued) for forward/backward direction in linear/circular base
$\hat{T}_{\text{lin,circ}}^{\text{f,b}}$	Jones matrix for forward/backward direction in linear/circular base
T_{ij}	Entries of the Jones Matrix \hat{T} ($i, j = x, y$ in linear base; $i, j = +, -$ in circular base)
$Z(\omega)$	Wave impedance
$Z_{\text{eff}}(\omega)$	Effective wave impedance
$\Delta_{\text{lin,circ}}^{i,j}$	Asymmetric transmission for a base vector i, j in linear/circular base
Δx	Random displacement of a metaatom in x -direction
Δy	Random displacement of a metaatom in y -direction
Φ	Azimuth angle for oblique incidence measurements
Θ	Angle of incidence for oblique incidence measurements
Σ	Circular birefringence
$\Psi_{\text{lin}}^{(i)}$	Linear polarization conversion dichroism for i -polarized light ($i = x, y$)

D Publications

D.1 Patents

- H. Lochbihler, E.-B. Kley, J. Petschulat, T. Pertsch, and C. Helgert: *Safety element with multicoloured image*. German Patent Application DE102009012300A1 (2009) and European Patent Application EP2228672A1 (2010)

D.2 Peer-reviewed Journals

- B. Walther, C. Helgert, C. Rockstuhl, and T. Pertsch: *Diffraction optical elements based on plasmonic metamaterials*. Appl. Phys. Lett., accepted
- C. Helgert, C. Rockstuhl, C. Etrich, E.-B. Kley, A. Tünnermann, F. Lederer, and T. Pertsch: *Effects of anisotropic disorder in an optical metamaterial*. Appl. Phys. A., DOI 10.1007/s00339-010-6190-2, in press
- J. Petschulat, C. Helgert, M. Steinert, N. Bergner, C. Rockstuhl, A. Tünnermann, F. Lederer, T. Pertsch, and E.-B. Kley: *Plasmonic modes of extreme subwavelength nanocavities*. Opt. Lett. **35**, 2693-2695 (2010)
- C. Menzel, C. Helgert, C. Rockstuhl, E.-B. Kley, A. Tünnermann, T. Pertsch, and F. Lederer: *Asymmetric transmission of linearly polarized light at optical metamaterials*. Phys. Rev. Lett. **104**, 253902 (2010)
- E. Pshenay-Severin, F. Setzpfandt, C. Helgert, U. Hübner, C. Menzel, C. Rockstuhl, A. Tünnermann, F. Lederer, and T. Pertsch: *Experimental determination of the dispersion relation of light in metamaterials by white-light interferometry*. J. Opt. Soc. Am. B **27**, 660 (2010)
- C. Menzel, C. Helgert, J. Üpping, C. Rockstuhl, E.-B. Kley, R. Wehrspohn, T. Pertsch, and F. Lederer: *Angular resolved effective optical properties of a Swiss cross metamaterial*. Appl. Phys. Lett. **95**, 131104 (2009)
- C. Helgert, C. Rockstuhl, C. Etrich, E.-B. Kley, A. Tünnermann, F. Lederer, and T. Pertsch: *Effective properties of amorphous metamaterials*. Phys. Rev. B **79**, 233107 (2009)

- E. Pshenay-Severin, U. Hübner, C. Menzel, C. Helgert, A. Chipouline, C. Rockstuhl, A. Tünnermann, F. Lederer, and T. Pertsch: *A Double-Element Metamaterial with a Negative Index at Near Infrared Wavelengths*. Opt. Lett. **34**, 1678-1680 (2009)
- C. Helgert, C. Menzel, C. Rockstuhl, E. Pshenay-Severin, E.-B. Kley, A. Chipouline, A. Tünnermann, F. Lederer, and T. Pertsch: *Polarization independent negative-index metamaterial in the near-infrared*. Opt. Lett. **34**, 704-706 (2009)
- M. Kroll, S. Fahr, C. Helgert, C. Rockstuhl, F. Lederer, and T. Pertsch: *Employing dielectric diffractive structures in solar cells: A numerical study*. Phys. Status Solidi A **205**, 2777-2795 (2008)

D.3 Submitted

- C. Helgert, E. Pshenay-Severin, M. Falkner, C. Menzel, E.-B. Kley, C. Rockstuhl, F. Lederer, and T. Pertsch: *Comprehensive characterization of a three-dimensional chiral metamaterial with giant optical activity*. Submitted for publication, under review
- C. Rockstuhl, C. Menzel, S. Mühlig, J. Petschulat, C. Helgert, A. Chipouline, T. Pertsch, and F. Lederer: *Scattering properties of metaatoms*. Submitted for publication, under review

D.4 Conference Proceedings

- J. Üpping, C. Ulbrich, C. Helgert, M. Peters, L. Steidl, R. Zentel, T. Pertsch, U. Rau, R. Zentel, and R.B. Wehrspohn: *Inverted-opal photonic crystals for ultra light-trapping in solar cells*. Proc. SPIE 7725, 772519 (2010)
- C. Rockstuhl, C. Etrich, C. Helgert, C. Menzel, T. Paul, S. Fahr, T. Pertsch, J. Dorfmueller, R. Esteban, W. Khunshin, R. Vogelgesang, A. Dmitriev, K. Bittkau, T. Beckers, R. Carius, and F. Lederer: *Large scale simulations in the realm of nanooptics*. Proc. SPIE 7604, 76040D (2010)
- C. Helgert, T. Pertsch, C. Rockstuhl, E. Pshenay-Severin, C. Menzel, E.-B. Kley, A. Chipouline, C. Etrich, U. Hübner, A. Tünnermann, and F. Lederer: *Tailoring the Properties of Optical Metamaterials*. Chinese Journal of Optics and Applied Optics 3, 1 (2010)
- P. Voisin, M. Peters, C. Helgert, H. Hauser, E.-B. Kley, T. Pertsch, B. Bläsi, M. Hermle, and S.W. Glunz: *Nanostructured back side silicon solar cells*. Proc. of the 24th European Photovoltaic Solar Energy Conference, p. 1529 (2009)

- C. Rockstuhl, C. Menzel, T. Paul, C. Helgert, E. Pshenay-Severin, J. Petschulat, A. Chipouline, T. Pertsch, and F. Lederer: *Bulk properties of metamaterials*. Proc. SPIE 6987, 698710 (2008)

D.5 Invited Talks

- C. Rockstuhl¹, C. Menzel, T. Paul, F. Lederer, E. Pshenay-Severin, M. Falkner, C. Helgert, A. Chipouline, T. Pertsch, W. Smigaj, J. Yang, and P. Lalanne: *Effective properties of metamaterials*. SPIE Optics & Photonics, 21st to 25th August 2011, San Diego, California, USA.
- T. Pertsch, E. Pshenay-Severin, C. Helgert, A. Chipouline, E.-B. Kley, C. Menzel, C. Rockstuhl, and F. Lederer: *Characterization of the complex transfer matrix of metamaterials*. 3rd European Topical Meeting on Nanophotonics and Metamaterials, 3rd to 6th January 2011, Seefeld in Tirol, Austria.
- C. Rockstuhl, C. Menzel, S. Mühlig, C. Helgert, B. Walther, A. Chipouline, C. Etrich, A. Cunningham, T. Bürgi, E.-B. Kley, T. Pertsch, and F. Lederer: *Amorphous metamaterials*. EOS Annual Meeting, 26th to 29th October 2010, Paris, France.
- C. Rockstuhl, C. Menzel, S. Mühlig, C. Helgert, B. Walther, A. Chipouline, C. Etrich, A. Cunningham, T. Bürgi, E.-B. Kley, T. Pertsch, and F. Lederer: *Amorphous metamaterials*. 3rd Mediterranean Conference on Nanophotonics, 18th to 19th October 2010, Belgrade, Serbia.
- C. Rockstuhl, C. Menzel, S. Mühlig, C. Helgert, B. Walther, A. Chipouline, C. Etrich, E.-B. Kley, T. Pertsch, and F. Lederer: *Amorphous bulk metamaterials*. 4th International Congress on Advanced Electromagnetic Materials in Microwaves and Optics, 13th to 16th September 2010, Karlsruhe, Germany.
- R. Geiss, C. Helgert, H. Hartung, E.-B. Kley, C. Rockstuhl, F. Schrempel, F. Lederer, A. Tünnermann, W. Wesch, and T. Pertsch: *Optical metamaterials and photonic crystals: Aspects of large-scale micro- and nanofabrication*. PIERS 2010, The 27th Progress in Electromagnetics Research Symposium, 22nd to 26th March 2010, Xi'an, China.
- C. Rockstuhl, C. Etrich, C. Helgert, C. Menzel, T. Paul, S. Fahr, T. Pertsch, and F. Lederer: *Large scale simulations in the realm of nanooptics*. SPIE Photonics West, 23rd to 28th January 2010, San Francisco, California, USA.
- C. Helgert, C. Rockstuhl, E. Pshenay-Severin, C. Menzel, E.-B. Kley, A. Chipouline, C. Etrich, U. Hübner, J. Üpping, A. Tünnermann, F. Lederer, and T. Pertsch: *Tailoring*

¹The underlined name corresponds to the presenting author.

the Properties of Optical Metamaterials. OSA-COS Topical Meeting on Applications of Optical Metamaterials, 22th to 25th June 2009, Tianjin, China.

- C. Rockstuhl, C. Menzel, T. Paul, F. Lederer, J. Petschulat, E. Pshenay-Severin, C. Helgert, A. Chipouline, T. Pertsch, and A. Tünnermann: *Properties of bulk metamaterials*. SPIE Photonics Europe, 7th to 11th April 2008, Strassbourg, France.
- T. Pertsch, C. Helgert, E.-B. Kley, and A. Tünnermann: *Micro- and nanostructured optical surfaces and their potential for photon control in solar cells*. Heräus-Seminary on Photon Management in Solar Cells, 29th October to 1st November 2007, Bad Honnef, Germany.

D.6 International Conference Contributions

- (oral) T. Kaiser, C. Helgert, T. Paul, S. Bin Hasan, F. Lederer, C. Rockstuhl, and T. Pertsch: *Resonant coupling of dielectric waveguides with plasmonic metaatoms*. SPIE Optics & Photonics, 21st to 25th August 2011, San Diego, California, USA.
- (oral) C. Helgert, E. Pshenay-Severin, M. Falkner, C. Menzel, E.-B. Kley, A. Chipouline, C. Rockstuhl, F. Lederer, and T. Pertsch: *Observation of Giant Optical Activity from Three-dimensional Loop-wire Metaatoms*. International Conference on Materials for Advanced Technologies, 26th June to 1st July 2011, Singapore.
- (oral) C. Helgert, C. Menzel, C. Rockstuhl, E.-B. Kley, A. Tünnermann, F. Lederer, and T. Pertsch: *Directional Asymmetry in the Transmission of Linearly Polarized Light Through a Metamaterial*. International Conference on Materials for Advanced Technologies, 26th June to 1st July 2011, Singapore.
- (poster) M. Falkner, E. Pshenay-Severin, C. Helgert, and T. Pertsch: *Interferometric method for the characterization of optically active metamaterials*. CLEO/EQEC Conference, 22th to 26th May 2011, Munich, Germany.
- (poster) T. Kaiser, C. Helgert, T. Paul, R. Wolf, C. Rockstuhl, F. Lederer, and T. Pertsch: *Metamaterials in waveguide geometries*. CLEO/EQEC Conference, 22th to 26th May 2011, Munich, Germany.
- (poster) A. Chipouline, S. Sugavanam, C. Helgert, J. Petschulat, A. Tünnermann, and T. Pertsch: *A new route toward the description of disordered metamaterials: Merging statistical methods and the multipole expansion*. 3rd European Topical Meeting on Nanophotonics and Metamaterials, 3rd to 6th January 2011, Seefeld in Tirol, Austria.
- (poster) J. Petschulat, C. Helgert, M. Steinert, N. Bergner, A. Chipouline, A. Tünnermann, T. Pertsch, E.-B. Kley, and F. Lederer: *Sub-wavelength field localization in multimode MIM nanocavities*. 3rd European Topical Meeting on Nanophotonics and Metamaterials, 3rd to 6th January 2011, Seefeld in Tirol, Austria.

- (oral) C. Helgert, C. Menzel, C. Rockstuhl, E.-B. Kley, A. Tünnermann, F. Lederer, and T. Pertsch: *3D chiral metamaterials enabling asymmetric transmission of linearly polarized light*. 4th International Congress on Advanced Electromagnetic Materials in Microwaves and Optics, 13th to 16th September 2010, Karlsruhe, Germany.
- (poster) A. Chipouline, S. Sugavanam, C. Helgert, J. Petschulat, and T. Pertsch: *Application of multipole model for analytical description of disorder in metamaterials*. 4th International Congress on Advanced Electromagnetic Materials in Microwaves and Optics, 13th to 16th September 2010, Karlsruhe, Germany.
- (poster) M.L. Miranda, B. Dastmalchi, C. Helgert, H. Schmidt, E.-B. Kley, I. Bergmair, and K. Hingerl: *Spectroscopic Ellipsometry Study of a Swiss Cross Metamaterial*. 4th International Congress on Advanced Electromagnetic Materials in Microwaves and Optics, 13th to 16th September 2010, Karlsruhe, Germany.
- (poster) E. Pshenay-Severin, M. Falkner, B. Walther, C. Helgert, A. Chipouline, A. Tünnermann, and T. Pertsch: *Experimental method for the characterization of the optical properties of metamaterials in the optical spectral domain*. 4th International Congress on Advanced Electromagnetic Materials in Microwaves and Optics, 13th to 16th September 2010, Karlsruhe, Germany.
- (oral) S. Bin Hasan, J. Reinhold, T. Paul, C. Helgert, A. Chipouline, C. Rockstuhl, and T. Pertsch: *Intrinsic and Extrinsic Nonlinearities of Nanooptical Systems*. 2nd International Workshop on Ultrafast Nanooptics, 27th to 30th June 2010, Bad Dürkheim, Germany.
- (oral) C. Menzel, C. Rockstuhl, T. Paul, C. Helgert, J. Petschulat, E.-B. Kley, F. Setzpfandt, T. Pertsch, and F. Lederer: *Asymmetric Transmission of Linearly Polarized Light through Low Symmetry Metamaterials*. CLEO/IQEC Conference USA, 16th to 21st May 2010, San Jose, California, USA.
- (oral) J. Üpping, R.B. Wehrspohn, C. Helgert, T. Pertsch, C. Ulbrich, T. Kirchhartz, U. Rau, L. Steidl, and R. Zentel: *Inverted opal structures for ultra light trapping in solar cells*. SPIE Photonics Europe, 12th to 16th April 2010, Brussels, Belgium.
- (poster) C. Helgert, E. Pshenay-Severin, C. Menzel, J. Petschulat, C. Rockstuhl, E.-B. Kley, F. Lederer, and T. Pertsch: *Experimental demonstration of nanostructured metamaterials in the optical regime*. International Workshop on Photonic Nanomaterials, 24th to 25th March 2010, Jena, Germany.
- (poster) S. Fahr, T. Paul, S. Mühlig, C. Rockstuhl, C. Helgert, M. Kroll, T. Pertsch, and F. Lederer: *Absorption enhancement in thin-film solar cells by nanophotonic structures*. International Workshop on Photonic Nanomaterials, 24th to 25th March 2010, Jena, Germany.
- (poster) T. Kaiser, C. Helgert, C. Rockstuhl, F. Lederer, M. Arens, and T. Pertsch:

Metamaterials in waveguide geometry. International Workshop on Photonic Nanomaterials, 24th to 25th March 2010, Jena, Germany.

- (poster) E. Pshenay-Severin, M. Falkner, F. Setzpfandt, C. Helgert, U. Hübner, C. Menzel, A. Chipouline, C. Rockstuhl, E.-B. Kley, A. Tünnermann, F. Lederer, and T. Pertsch: *Direct experimental optical characterization of metamaterials.* International Workshop on Photonic Nanomaterials, 24th to 25th March 2010, Jena, Germany.
- (poster) J. Reinhold, T. Paul, C. Helgert, J. Petschulat, C. Rockstuhl, E.-B. Kley, F. Lederer, and T. Pertsch: *Enhancing nonlinear effects in lithium niobate exploiting plasmonic resonances in metallic nanostructures.* International Workshop on Photonic Nanomaterials, 24th to 25th March 2010, Jena, Germany.
- (oral) C. Helgert, C. Rockstuhl, B. Walther, A. Chipouline, C. Etrich, E.-B. Kley, F. Lederer, and T. Pertsch: *Anisotropic disorder in optical metamaterials.* META'10, 2nd International Conference on Metamaterials, Photonic Crystals and Plasmonics, 22nd to 25th February 2010, Cairo, Egypt.
- (oral) E. Pshenay-Severin, F. Setzpfandt, C. Helgert, U. Hübner, C. Menzel, C. Rockstuhl, A. Tünnermann, F. Lederer, and T. Pertsch: *Direct experimental optical characterization of metamaterials.* META'10, 2nd International Conference on Metamaterials, Photonic Crystals and Plasmonics, 22nd to 25th February 2010, Cairo, Egypt.
- (poster) S. Fahr, C. Rockstuhl, M. Kroll, C. Helgert, F. Lederer, and T. Pertsch: *Photon Management in Silicon Based Thin Film Solar Cells.* The 12th Euregional Workshop on Novel Concepts for Future Thin-Film Silicon Solar Cells, 28th to 29th January 2010, Delft, The Netherlands.
- (poster) P. Voisin, M. Peters, C. Helgert, H. Hauser, E.-B. Kley, T. Pertsch, B. Bläsi, M. Hermle, and S.W. Glunz: *Nanostructured back side silicon solar cells.* 24th European Photovoltaic Solar Energy Conference, 21st to 25th September 2009, Hamburg, Germany.
- (oral) C. Helgert, C. Rockstuhl, C. Etrich, E.-B. Kley, A. Tünnermann, F. Lederer, and T. Pertsch: *Effective properties of periodic, partially disordered, and amorphous metamaterials.* 3rd International Congress on Advanced Electromagnetic Materials in Microwaves and Optics, 1st to 4th September 2009, London, UK.
- (poster) C. Menzel, C. Helgert, J. Üpping, C. Rockstuhl, T. Paul, E.-B. Kley, T. Pertsch, R.B. Wehrspohn, and F. Lederer: *Effective optical properties of a Swiss cross metamaterial beyond normal incidence.* 3rd International Congress on Advanced Electromagnetic Materials in Microwaves and Optics, 1st to 4th September 2009, London, UK.
- (oral) C. Helgert, C. Menzel, C. Rockstuhl, E. Pshenay-Severin, E.-B. Kley, A. Chipouline, A. Tünnermann, and T. Pertsch: *Polarization independent negative-*

index metamaterials. 18th International Laser Physics Workshop (LPHYS'09), 13th to 17th July 2009, Barcelona, Spain.

- (oral) C. Helgert, C. Menzel, C. Rockstuhl, E. Pshenay-Severin, J. Üpping, E.-B. Kley, F. Lederer, and T. Pertsch: *Measuring Angular Dependent Effective Properties Of Metamaterials*. CLEO/IQEC Conference USA, 31st May to 5th June 2009, Baltimore, Maryland, USA.
- (poster) C. Helgert, E. Pshenay-Severin, E.-B. Kley, A. Chipouline, A. Tünnermann, T. Pertsch, C. Menzel, C. Rockstuhl, and F. Lederer: *Demonstration of a polarization-independent optical negative-index metamaterial*. 2nd European Topical Meeting on Nanophotonics and Metamaterials, 5th to 8th January 2009, Seefeld in Tirol, Austria.
- (poster) T. Paul, C. Helgert, J. Reinhold, E.-B. Kley, J. Petschulat, T. Pertsch, C. Rockstuhl, and F. Lederer: *Enhancing nonlinear effects in lithium niobate exploiting plasmonic resonances in metallic nanostructures*. Heräus-Seminary on Ultrafast Nanooptics, 2nd to 4th June 2008, Bad Honnef, Germany.
- (poster) C. Helgert, R. Geiss, E. Pshenay-Severin, T. Pertsch, E.-B. Kley, and A. Tünnermann: *Fabrication of large-area negative-index metamaterial by Electron-Beam-Lithography*. EIPBN International Conference on Electron, Ion, and Photon Beam Technology and Nanofabrication, 27th to 30th May 2008, Portland, Oregon, USA.
- (oral) C. Helgert, E.-B. Kley, T. Pertsch, C. Rockstuhl, and A. Tünnermann: *Second order nonlinear response from gold nanostructures on lithium niobate*. CLEO/EQEC Conference, 17th to 22th June 2007, Munich, Germany.
- (oral) E. Pshenay-Severin, T. Pertsch, F. Garwe, J. Petschulat, C. Rockstuhl, F. Lederer, E.-B. Kley, C. Helgert, U. Hübner, and A. Tünnermann: *A double cell metamaterial for independent tuning of the magnetic and electric response*. CLEO/EQEC Conference, 17th to 22th June 2007, Munich, Germany.

E Acknowledgements

At this point the author usually states that his or her thesis would have never been possible without the help of many people. Without any exaggeration, this statement holds particularly for me. Over the past years, I have been working in a strongly connected community of colleagues, who have all contributed their specific parts, both personally and scientifically, to the overall success of this work. I will attempt, at least, to satisfy the barest demands of decency by taking the chance to thank

- my supervisor Prof. Thomas Pertsch, for his scientific guidance and vision during my diploma and PhD time; for his efforts and willingness to create such a pleasant working environment; for the opportunities to participate in international conferences and workshops; for his trust and open-mindedness to share information and responsibility with his employees even at a PhD-student level.
- Prof. Carsten Rockstuhl, for his creativity; his fascinating ideas about nanooptics; his precise solution proposals when it came down to how to solve a specific problem; his efforts in teaching me how to write scientific texts; his constant and uncomplicated availability to young academics (quite uncommon for somebody with a high scientific reputation) and his empathy to transfer motivation to young researchers like myself.
- Ernst-Bernhard Kley, for his never-ending inspiration and for his supervision of the technological aspects of my thesis which could always compete with the latest standard in nanostructure technology. I also thank him for allowing me enough freedom to pursue my own ideas.
- Prof. Andreas Tünnermann and Prof. Falk Lederer, for creating a dense network of excellently equipped research facilities here at Jena, that pushed me to accomplish my work with reference to high standards in optics.
- Prof. Stefan Linden and Prof. Costas Soukoulis, for providing critical referee reports of this thesis. The former is thanked for being a member of my jury.
- the German Federal Ministry of Education and Research and the Thuringian State Government, for the financial support during the working period of this thesis.
- Waltraud Gräf, Thomas Käsebier, Detlef Schelle, Holger Schmidt, Hans-Jörg Fuchs, Christiane Fuchs, Christiane Otto and all the members of the Microstructure Technology group, for their constant support regarding the fabrication of samples.

- Michael Banasch, for introducing me into the fine details of electron beam lithography and the very practical aspects associated with this field.
- Christoph Menzel and Thomas Paul, for their endurance to accomplish the cumbersome transfer of theoretical optics to an experimental physicist. A huge part of this work results from our close cooperation, many many thanks!
- Thomas Kämpfe, Stephan Fahr, Reinhard Geiss, Michael Steinert, Jörg Reinhold and all the numerous colleagues I shared office 210 at the IAP Jena with. Each of them contributed with his very own style to create an open and vivid atmosphere which made me go to work with joy almost every day.
- my collaborators Ekaterina Pshenay-Severin, Jörg Petschulat, Norik Janunts, Benny Walther, Thomas Kaiser, Matthias Falkner and all the members of the Nanooptics group, for creating an open-minded and fruitful atmosphere, in which we together explored the realms of nanooptics.
- Christoph Etrich for the computationally demanding FDTD simulations.
- Bodo Martin and Holger Hartung, for keeping the computers running and for fulfilling individual computational requests.
- Uwe Hübner, Birger Steinbach, Kevin Füchsel and Maria Oliva, for providing thin film layers and AFM inspections. The former is thanked for his good advice during my first trials in nanostructure technology.
- all volunteers for their awesome proofreading of this document ☺ . Thanks a lot!
- my dear wife Alexandra and my parents, for their unconditional love and support during my studies.
- my son Jannik, who equilibrated my work-life balance sustainably.
- anybody I may have forgotten unintentionally.

Short Curriculum Vitae

Personal data

Name Christian Helgert
Date of birth 06/29/1980
Place of birth Gera, Germany
Marital status Married, one child



Academic career

02/2011 Submittance of doctoral thesis entitled
“Symmetry-related effects of optical metamaterials”
12/2006 - current Scientific employee and PhD student at the Institute of Applied
Physics at the Friedrich-Schiller-Universität Jena, Germany

Occupation

08/1999 - 10/2000 Civil service at nursing home, Zeitz, Germany

Education

11/2006 Diploma degree in Physics from the Friedrich-Schiller-Universität
Jena, Germany
10/2006 Diploma thesis entitled “Quadratisch nichtlinear optische Eigen-
schaften von metallischen Nanostrukturen auf Lithiumniobat”
10/2004 - 09/2006 Study of Physics at the Friedrich-Schiller-Universität Jena, Germany
08/2003 - 09/2004 Study of Physics at the Università degli Studi di Roma
“Tor Vergata”, Rome, Italy
10/2000 - 08/2003 Study of Physics at the Friedrich-Schiller-Universität Jena, Germany
08/1991 - 07/1999 State-approved private secondary school, Droyßig, Germany

Jena, 04/28/2011

Signature

Ehrenwörtliche Erklärung

Hiermit erkläre ich ehrenwörtlich, dass ich die vorliegende Arbeit selbständig, ohne unzulässige Hilfe Dritter und ohne Benutzung anderer als der angegebenen Hilfsmittel und Literatur angefertigt habe. Die aus anderen Quellen direkt oder indirekt übernommenen Daten und Konzepte sind unter Angabe der Quelle gekennzeichnet.

Weitere Personen waren an der inhaltlich-materiellen Erstellung der vorliegenden Arbeit nicht beteiligt. Insbesondere habe ich hierfür nicht die entgeltliche Hilfe von Vermittlungs- bzw. Beratungsdiensten (Promotionsberater oder andere Personen) in Anspruch genommen. Niemand hat von mir unmittelbar oder mittelbar geldwerte Leistungen für Arbeiten erhalten, die im Zusammenhang mit dem Inhalt der vorgelegten Dissertation stehen.

Die Arbeit wurde bisher weder im In- noch im Ausland in gleicher oder ähnlicher Form einer anderen Prüfungsbehörde vorgelegt.

Die geltende Promotionsordnung der Physikalisch-Astronomischen Fakultät ist mir bekannt.

Ich versichere ehrenwörtlich, dass ich nach bestem Wissen die reine Wahrheit gesagt und nichts verschwiegen habe.

Jena, 28. April 2011

Unterschrift